12-3-2013 12:00 AM

Cyclic and Post-Cyclic Response of Silt and Sandy Silt Soils

Ali El Takch
The University of Western Ontario

Supervisor
Dr. Hesham El Naggar
The University of Western Ontario Joint Supervisor
Dr. Abouzar Sadrekarimi
The University of Western Ontario

Graduate Program in Civil and Environmental Engineering
A thesis submitted in partial fulfillment of the requirements for the degree in Master of Engineering Science

CYCLIC AND POST-CYCLIC RESPONSE OF SILT AND SANDY SILT SOILS

(Thesis format: Integrated Article)

by

Ali El Takch

Graduate Program in Engineering Science
Department of Civil and Environmental Engineering

A thesis submitted in partial fulfillment
of the requirements for the degree of
Master of Engineering Science

The School of Graduate and Postdoctoral Studies
The University of Western Ontario
London, Ontario, Canada

Abstract

A series of cyclic and monotonic constant-volume ring shear tests were carried out to determine the cyclic and post-cyclic response of silts and sandy silts with 25% and 50% sand. The elastic soil behavior at very small shear strain ($\gamma < 10^{-4}\%$) was investigated through shear wave velocity (Vs) measurements using bender elements at vertical stresses ranging from 50 to 300 kPa, while strain-controlled constant volume cyclic ring shear tests were conducted to establish shear modulus (G) and damping ratio (D) at larger shear strain amplitudes ($\gamma > 0.01\%$). Liquefaction and strain-softening occurred at excess pore water pressure ratios (r_u) between 0.6 and 0.7 associated with cumulative shear strains (γ) of 4% to 6%, after which cyclic mobility failure ensued with very large shear strains and excess pore water pressure ratio ($r_u > 0.9$). The test data indicated that existing field CRR-V_{s1} correlations could underestimate the liquefaction resistance of soils with fine content (FC) $\geq$ 50%. It is found that V_s and the maximum shear modulus (G_o) significantly decrease with increasing void ratio. V_s is also found to vary with the effective overburden stress to the power of 0.31 - 0.34 for all silt and sandy silt mixes. The results show that while G decreases with increasing γ, D increases with increasing γ only up to $\gamma < 1\%$, beyond which it exhibits a decreasing trend. The test results further show that dense samples showed higher post-liquefaction undrained shear strength. In addition, silt and sandy silts exhibit strain hardening behaviour during post-liquefaction monotonic shearing. However, the same soil exhibits strain-softening behavior under monotonic shear loading when the pre-cyclic initial stress condition is re-established.

Keywords

Ring shear tests; soil liquefaction; earthquakes; cyclic resistance; silt; sandy silt; critical state; shear wave velocity; shear modulus; critical shear strength.

Co-Authorship Statement

This thesis has been prepared in accordance with the regulations for an Integrated-Article format thesis stipulated by the School of Graduate and Postdoctoral Studies at the University of Western Ontario and has been co-authored as:

Chapter 2: Cyclic Resistance and Liquefaction Behaviour of Silts and Sandy Silts

All the experimental work was conducted by Ali El Takch under close supervision of Dr. Hesham El Naggar and Dr. Abouzar Sadrekarimi. A paper co-authored by Ali El Takch, Abouzar Sadrekarimi and Hesham El Naggar has been submitted to the Journal of *The Soil Dynamics and Earthquake Engineering.*

Chapter 3: Dynamic Behavior of Non-plastic Silts and Sandy Silts in Cyclic Ring Shear Tests

All the experimental work was conducted by Ali El Takch under close supervision of Dr. Hesham El Naggar and Dr. Abouzar Sadrekarimi. A paper co-authored by Ali El Takch, Hesham El Naggar and Abouzar Sadrekarimi. The abstract of this paper has been submitted to *The Geotechnique Symposium in Print 2015.*

Chapter 4: Post-Cyclic Monotonic Response of Non-Plastic Silts and Sandy Silts

All the experimental work was conducted by Ali El Takch under close supervision of Dr. Hesham El Naggar and Dr. Abouzar Sadrekarimi. A paper co-authored by Ali El Takch, Abouzar Sadrekarimi and Hesham El Naggar. A paper co-authored by Ali El Takch, Abouzar Sadrekarimi and Hesham El Naggar will be submitted to the Journal of *Soils and Foundations.*

Acknowledgments

First, I would like to express my sincere gratitude and appreciation to my supervisors Dr. Hesham EL Naggar and Dr. Abouzar Sadrekarimi for their consistent support, advice, and encouragement throughout this research program. It has been a privilege to work under their supervision.

I would like to thank the administrative and laboratory staff at Western University. Special thanks to Melodie Richards, Wilbert Logan, Whitney Barrett and Stephanie Laurence.

Many thanks to my friends and colleagues for their helpful discussion and encouragement through this research, particular thanks to Mohamad Diab, Ekrima Hassan, Botrous Sawaya, Ghalib Abdelsater, Osama Drbe, Naemeh Naghavi, Ahmed Fahmi, and Tarek Omar.

Finally, I can't find the suitable words to express my gratitude for my parents for their love, support, and sacrifices. I am indebted to them for everything I have. Especial thanks to my sister and my brothers for their continuous support and encouragement.

Table of Contents

List of Tables

List of Figures

List of Symbols

CSL	Critical state line
CSR	Cyclic stress ratio
CRR	Cyclic resistance ratio
$\mathbf{C_u}$	Coefficient of uniformity
$\mathbf{C_c}$	Coefficient of curvature
$\mathbf{D_{rc}}$	Relative density at the end of consolidation, [%]
$\mathbf{D_{50}}$	Particle size corresponding to 50% finer soil-size particles, [mm]
$\mathbf{d_{sr}}$	Tip-to-Tip distance between bender elements, [mm]
D	Damping ratio
DA	Double amplitude shear strain, [%]
$\mathbf{e_{max}}$	Maximum void ratio
$\mathbf{e_{min}}$	Minimum void ratio
e	Void ratio
$\mathbf{e_c}$	Void ratio at the end of consolidation
FC	Fines content
F (e)	Void ratio function
f	Frequency, [Hz]
$\mathbf{G_o}$	Small-strain shear modulus, [MPa]
G	Shear Modulus, [MPa]
h	Height of specimen, [mm]
IL	Instability line
$\mathbf{K_o}$	Coefficient of lateral earth pressure at rest
$\mathbf{M_w}$	Earthquake magnitude
N	Number of cycles
NCL	Normal compression line
$\mathbf{N_L}$	Number of cycles to trigger liquefaction
NC	Normally consolidated
n	Stress exponent

OCR	Overconsolidation ratio
P_a	Atmospheric pressure, [kPa]
R_o	Outer radius of the annular confining ring, [mm]
R_i	Inner radius of the annular confining ring, [mm]
r_u	Excess pore water pressure ratio
$r_{u,th}$	Threshold excess pore water pressure ratio
s_u(liq)	Liquefied undrained shear strength, [kPa]
$s_{u,cs}$	critical undrained shear strength, [kPa]
T	Shearing torque force, [N.m]
t	Time, [s]
u_a	Pore-air pressure, [kPa]
u_w	Pore-water pressure, [kPa]
V_s	Shear wave velocity, [m/s]
V_{s1}	Shear wave velocity at overburden pressure of 100 kPa, [m/s]
W_D	Energy dissipated from soil, [J]
W_S	Maximum strain energy stored in soil, [J]
σ_v	Total vertical (normal) stress, [kPa]
σ'_v	Vertical effective stress, [kPa]
σ'_{vc}	Vertical Effective stress at consolidation, [kPa]
σ'_m	Mean effective stress, [kPa]
σ'_{cs}	Vertical effective stress at critical state, [kPa]
ψ	Critical state parameter
ϕ'_{cs}	Critical state friction angle, [degree]
ϕ'	Effective friction angle, [degree]
γ_{DA}	Double amplitude shear strain, [%]
γ	Shear Strain, [%]
γ_{max}	Maximum shear Strain, [%]
γ_{min}	Minimum shear Strain, [%]
δ	Shear displacement, [mm]
θ	Angular rotation, [degree]
Δu	Excess pore water pressure, [kPa]
τ	Shear stress, [kPa]

τ_{cyc}	Cyclic shear stress, [kPa]
τ_{o}	Static shear stress, [kPa]
τ_{max}	Maximum shear stress, [kPa]
τ_{min}	Minimum shear stress, [kPa]
λ_{cs}	Slope of CSL
Γ_{cs}	Critical state void ratio at p′=1 kPa
ε_{a}	Axial strain, [%]

Chapter 1

1 Introduction

1.1 Research Need and Objective

Liquefaction is defined as a significant loss of strength and stiffness in saturated soils under dynamic shear loading in particular seismic loading. It is considered as one of the most important and interesting topics in geotechnical earthquake engineering that can cause serious damage to foundations and structures. Liquefaction mainly happens due to an increase in pore water pressure and a decrease in the effective stress associated with the development of significant shear strain during earthquake loading.

Liquefaction behavior has been extensively studied for clean sands and sandy soils with less than 30% silt content, and the existing relationships for liquefaction analysis and the estimation of cyclic resistance of non-plastic soils are only applicable up to 30% silt content. However, very little work has been conducted on the liquefaction potential and cyclic behaviour of non-plastic silts and sandy silts. Recent observations from previous earthquakes such as the Idaho Earthquake (1983) in United States, Chibaken-Tohooki (1987) in Japan, Loma Prietra Earthquake (1989) in United States, Marmara Earthquake (1999) in Turkey, all showed evidence of fine-grained soil liquefaction during ground shaking. Considering the above, there is urgent need for additional experimental work in order to better understand the cyclic behaviour of non-plastic silts to develop new practical guidelines for evaluating liquefaction susceptibility of primarily silty soils.

In order to fill this gap, the goal of this research is to advance the understanding of the behavior of non-plastic silt under cyclic and post-cyclic conditions, and to develop a comprehensive study of the liquefaction potential of silts and sandy silts (with fines content > 50%) based on shear wave velocity (Vs) measurements. Accomplishment of these objectives will improve the understanding of the behaviour of non-plastic fine-grained soils during earthquake shaking and allow the development of mitigation measures to reduce the influence of liquefaction to civil structures. In recognition of this, a laboratory element testing program was carried out to examine the cyclic and post-cyclic behaviour of non-plastic silt and sandy silt materials using a constant-volume cyclic ring shear machine equipped with piezoelectric bender elements for measuring shear wave velocity.

1.2 Thesis Outline

This thesis has been prepared in "Integrated-Article" format. It is organized into 5 chapters. A brief description of the following four chapters is as follows:

Chapter 2 evaluates the cyclic response and cyclic shear resistance of reconstituted samples of silt and sandy silt soils using a constant volume ring shear testing. In this chapter, a correlation between the cyclic resistance ratio (CRR) and shear wave velocity (Vs) for soils with a fine content (FC) greater than or equal to 50% is established.

Chapter 3 investigates the elastic properties of silt and sandy silt soils at very small strain ($\gamma < 10^{-4}\%$) and at vertical stresses ranging from 50 and 300 kPa. Moreover, this

chapter presents the shear modulus (G) and damping ratio (D) for silts and sandy silts at large shear strain amplitudes ($\gamma > 0.01\%$) and shows the influence of silt content and shear strain on those parameters.

Chapter 4 presents the post-cyclic monotonic response and liquefied shear strength of silt and sandy silt soils. In this chapter, the liquefied undrained strength ratio is correlated with the shear wave velocity and the state parameter (ψ) for each soil mix. Moreover, correlations are developed between the cyclic resistance ratio (CRR) and the state parameter for silts and sandy silts.

Chapter 5 is a summary of the research work carried out and the conclusions drawn.

Chapter 2

2 Cyclic Resistance and Liquefaction Behaviour of Silts and Sandy Silts

2.1 Introduction

Following the extensive damage that occurred as a result of soil failure in the 1964 Alaska and Niigata earthquakes (Fukuoka 1966; Kramer 1996), cyclic liquefaction has become one of the most investigated phenomenon in geotechnical earthquake engineering. This has become even more critical with the increased occurrence of mega-earthquakes around the world. For example, significant liquefaction-related damage occurred following the recent 2011 Tohoku earthquake (Ashford et al. 2011; Boulanger 2012; Tokimatsu and Katsumata 2012; Wakamatsu 2012), 2010 Chilean earthquake (Yasuda et al. 2010; Villalobos et al. 2011), and the 2010 Haitian earthquake at Port-au-Prince (Olson et al. 2011).

Cyclic liquefaction behavior of cohesionless soils has been studied for both level-ground and sloping-ground conditions. As there is no appreciable level of initial static shear stress, τ_o under level ground conditions, most experimental studies of level ground behavior have been conducted using isotropic-consolidation triaxial tests with $\tau_o = 0$. Large excess pore water pressure accumulates in these tests by repeated cycles of shear stress or strain and drives the effective stress path to nearly zero effective stresses (“initial

liquefaction"). On the other hand, cyclic liquefaction under sloping ground occurs by a completely different mechanism. Liquefaction is triggered under sloping ground conditions when the effective stress path reaches the instability line (Lade 1992) established by connecting the peak (yield) strengths of the corresponding undrained monotonic effective stress paths, after which the soil undergoes significant undrained strain softening and reaches an undrained critical shear strength, s_u(critical) (Figure 2.1). This could result in a liquefaction flow failure if τ_o of the sloping ground is sufficiently bigger than s_u(critical).

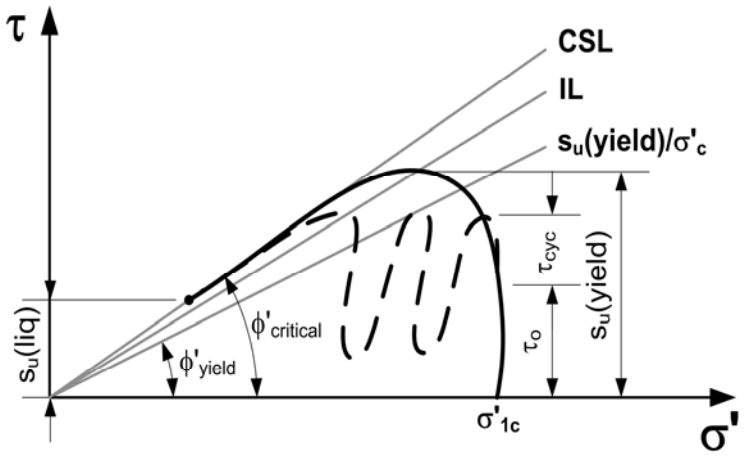

Figure 2.1: Initiation of liquefaction at sloping ground conditions by cyclic or monotonic loading.

Both level-ground and sloping-ground liquefaction behaviors have been extensively studied for clean sands (Boulanger 2003; Yoshimine and Koike 2005; Yoshimiet al. 1989) and sandy soils with less than 30% silt content (Xenaki and Athanasopoulos 2003;

Carraro et al. 2003; Stamatopolous 2010; Polito and Martin 2001), and the existing relationships for liquefaction analysis and the estimation of cyclic resistance of non-plastic soils are only applicable for silty sands with less than 30% silt content (Idriss and Boulanger 2008). Very little work has been conducted on the liquefaction potential and cyclic shearing behaviour of non-plastic silts and sandy silts partly due to the biased perception that fine-grained soils have lower potential to develop excess pore water pressure compared to sands (Kramer 1996; Jurko et al. 2006). Nonetheless, non-plastic silts exhibit similar physical and structural characteristics (e.g. mineralogy, gradation, fabric) to clean sands. In fact, silt materials are known to liquefy (Adachi 1996; Yamamuro and Lade 1997; Sanin and Wijewickreme 2006; Baxter et al. 2008; Singh 1996; Hyde et al. 2006) and liquefaction of silts has been extensively observed in past earthquakes (Seed et al. 1989; Youd et al. 1985; Ishihara 1984; Boulanger et al. 1999; Sancio et al. 2002; Cox et al. 2013; Tokimastu and Katsumata 2012; Orense et al. 2012). For example, boiling of silt occurred widely following the 1987 Chibaken-Tohooki (Japan) and the 1989 Loma Prieta (United States) earthquakes, and liquefaction of silt vastly occurred extensively following the 1995 Kobe earthquake in the reclaimed coastal areas of Port Island, Japan (Hyde et al. 2006). Accordingly, there is an urgent need for additional experimental work in order to better understand the liquefaction potential and cyclic behaviour of silts in order to develop new practical guidelines for evaluating liquefaction susceptibility of primarily silty soils.

2.1.1 Relationship between Cyclic Resistance Ratio (CRR) and Shear Wave Velocity (V_s)

Several soil parameters affect its cyclic resistance including: soil fabric, composition, void ratio, and stress level and they also affect shear wave velocity (V_s) (Richart et al. 1970). Several investigators have studied the relationship between the capacity of soil to resist cyclic loading, described by cyclic resistance ratio (CRR), and its V_s (Andrus and Stokoe 2000, Baxter et al. 2008; Zhou and Chen 2007; Youd and Idriss 2001; Liu and Mitchell 2006; Zhou et al. 2010; Yunmin et al. 2005; Askari 2010; Zhang 2010). For example, Figure 2.1 presents empirical relationships of CRR and V_s developed by Andrus and Stokoe (2000) at an earthquake of moment magnitude (Mw) equal to 7.5 and based on the field observations of liquefaction during past earthquakes. Figure 2.1 shows that for a particular fines content (FC), CRR increases with increasing V_s; and for the same V_s, CRR increases with increasing the amount of fines up to FC $\leq$ 35%. The relationships presented in Figure 2.2 only cover the range 5% $\leq$ FC $\leq$ 35%, and the effect of FC > 35% on CRR-V_s relationship is largely unknown and therefore the existing correlations for the estimation of CRR from V_s are not applicable to silts and sandy silts.

One of the major drawbacks of field-based empirical relationships, similar to those presented in Figure 2.2, is that the in-situ V_s is often measured after the occurrence of liquefaction and describes the state of the post-liquefied soil. Therefore, these relationships do not represent the initial state of the soil prior to liquefaction and would involve some degree of uncertainty for assessing the liquefaction potential. Accordingly, laboratory shear tests on loose cohesionless soils have been used to develop CRR – V_s

relationships. Most of these studies have been conducted on sands and silty sands often with FC ≤ 35% (Ishihara et al. 1975; Alba et al. 1984; Rauch et al. 2000; Huang et al. 2004; Chen et al. 2005; Liu and Mitchell 2006; Zhou and Chen 2007). Only a few studies investigated higher FC and pure silts (e.g. Baxter et al. 2008; Che et. al 2008; Askari 2010), whereas several catastrophic liquefaction failures have occurred in sandy silts or even silts. For example, the liquefaction flow failures of Lower San Fernando Dam (Stark and Mesri, 1992) and the Merriespruit Tailings Dam (Fourie and Tshabalala, 2005) involved soils with average FC about 50% and 60%, respectively.

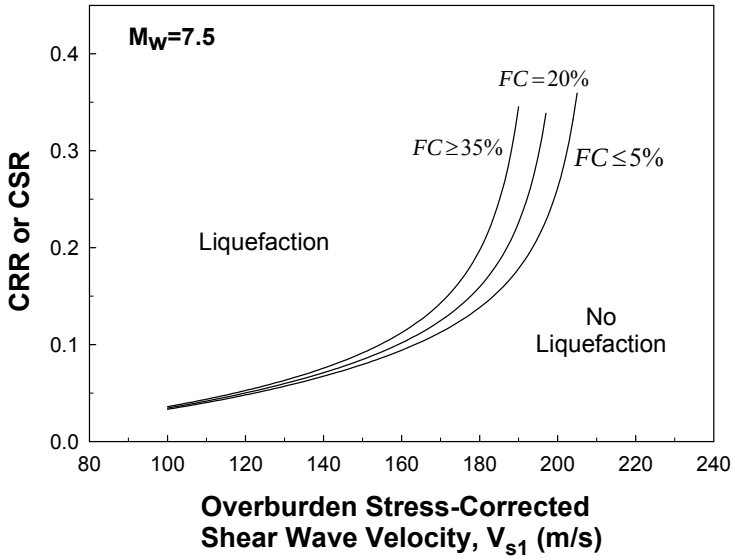

Figure 2.2: Empirical CRR - V_s relationships for silty sands (5% ≤ FC ≤ 35%) suggested by Andrus and Stokoe (2000).

In the present study, a comprehensive laboratory testing program was conducted in order to characterize the cyclic behaviors of silts and sandy silts (with FC > 50%) based on CRR and V_s measurements. A series of cyclic and monotonic constant-volume ring shear tests along with bender element shear wave velocity measurements are conducted on silt and sandy silt specimens with different amounts of sand (25% and 50%). This paper presents the details of the testing program, as well as the main results and outcomes.

2.2 Materials Tested and Specimen Preparation

Reconstituted specimens of silt and sandy silts with 50% and 75% silt content were prepared and tested in the experimental program. The silt used in this study (MIN-U-SIL 40) was produced from the grinding of silica sand by US Silica Company in Berkeley Springs, West Virginia. The silt is mainly composed of white-colored quartz particles. Scanning electron microscopic images of the particles indicate very angular and irregular particle shapes. The added sand is a quartz Ottawa sand with round to subrounded particle shapes. Similar mixes of particles shapes have been also observed in some natural sands from Mississippi river (Sadrekarimi 2009). Figure 2.3 and Table 2.1 present the particle size distributions and the index properties of these materials.

Because of large bulking potential, the ASTM (2006a, 2006b) standard methods are not applicable for soils with more than 15% fines content and therefore the maximum (e_{max}) and minimum (e_{min}) void ratios were consistently determined using a slurry deposition technique (Bradshaw and Baxter 2007) and the modified proctor procedure ASTM (2012) respectively. As illustrated in Figure 2.4, e_{max} and e_{min} and their difference

increase with increasing silt content which is consistent with similar trends reported by other investigators (Naeini and Baziar 2004; Yamamuro and Covert 2001).

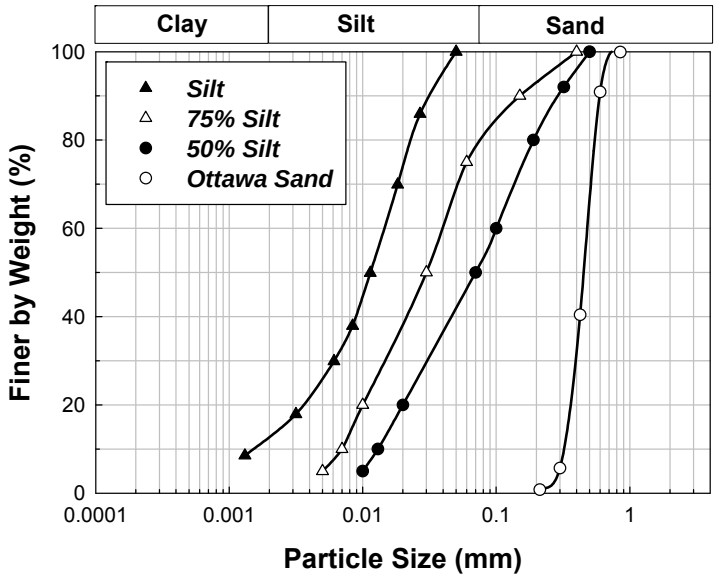

Figure 2.3: Average particle size distributions of the soils used in this study.

Table 2.1: Index properties of the soils used in the first study

Soil	Fine Content (%)	D_{50} (mm)	e_{max}	e_{min}	C_u	C_c
Silt	100	0.012	2.09	0.67	10.28	1.84
Sandy silt	75	0.029	1.48	0.58	5.40	0.82
	50	0.070	1.15	0.46	7.80	0.63
Ottawa Sand	0	0.450	0.74	0.42	1.38	1

C_u and C_c are coefficients of uniformity and curvature, respectively

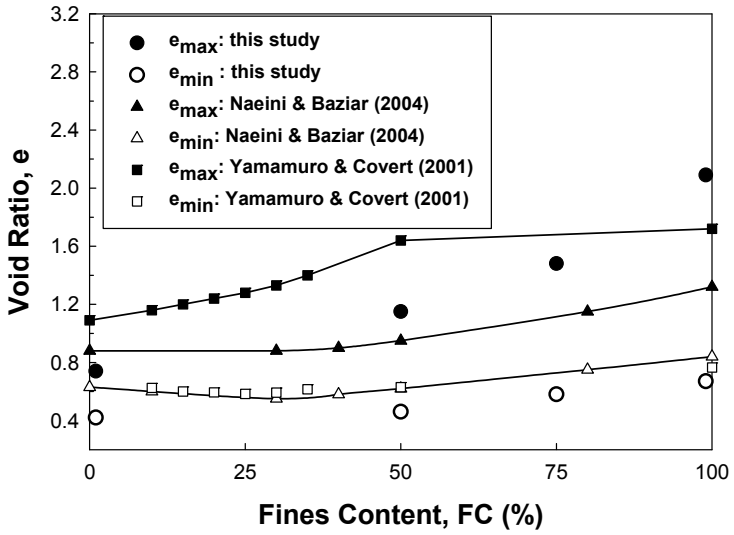

Figure 2.4: Variation of maximum and minimum void ratios with the fines (silt) content.

The moist tamping method was used to prepare all soil specimens in this study, where each specimen was prepared in layers and tamped at a moisture content of 5%. The under compaction technique recommended by Ladd (1978) was used to account for the increased density of the lower layers by compaction and to produce homogenous specimens. All specimens prepared for the cyclic ring shear tests of this study had an annular shape with inner (R_i) and outer (R_o) radii of 48.25 mm, 76.10 mm, respectively, and an initial height (h) of 30 mm.

2.3 Laboratory Testing Procedure

Cyclic and monotonic constant-volume ring shear tests were conducted at the soil mechanics laboratory of Western University using an advanced ring shear testing apparatus (SRS-150) manufactured by GCTS in Arizona, United States. In this apparatus, an annular specimen is confined between inner and outer solid rings with outer and inner diameters of 96.5 mm and 152.2 mm, respectively which can accommodate specimen heights of up to 53.3 mm. This provides an effective specimen area of 108.8 cm^2. The ratio of the inner to outer diameter is 0.63, which conforms with the ASTM (2006c) for ring shear testing. An advanced computer-controlled electro-pneumatic servo-motor applies vertical (σ_v) and shear (τ) stresses of up to 1,000 kPa and 1,300 kPa, respectively at a rate of 0.001^o/min to 360^o/min on the specimen. The amount of vertical force (N) applied on the soil and the shearing torque (T) are measured with a combined force-torque sensor. Cyclic shear and vertical loads are applied through the upper loading platen by the servo motor with zero backlash up to a frequency of 1 Hz. In addition to the vertical and shear stresses, the amount of settlement and angular rotation (θ) of the upper platen are measured by a high resolution LVDT and an angular encoder, respectively. The shear wave velocity of the soil specimen is also measured by piezoelectric bender elements embedded in the upper and lower platens. Figures 2.5 and 2.6 present photos and the schematic diagram of the shearing mode in our cyclic ring shear tests.

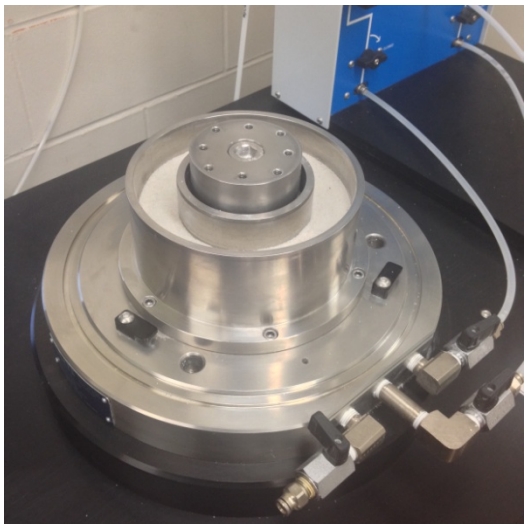

(a)

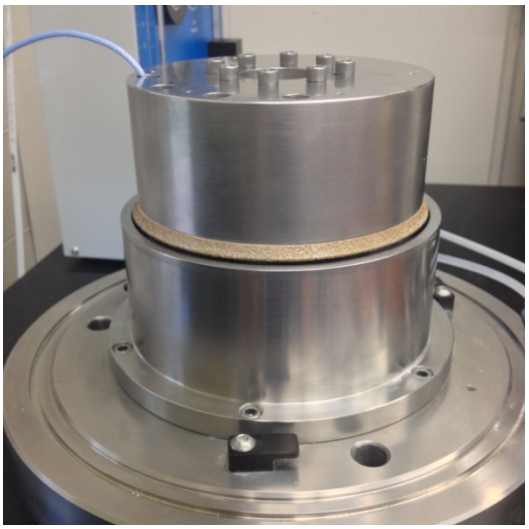

(b)

Figure 2.5: Photos of the cyclic ring shear apparatus at Western University (a) Ring shear chamber filled with sand (b) Complete ring shear testing configuration.

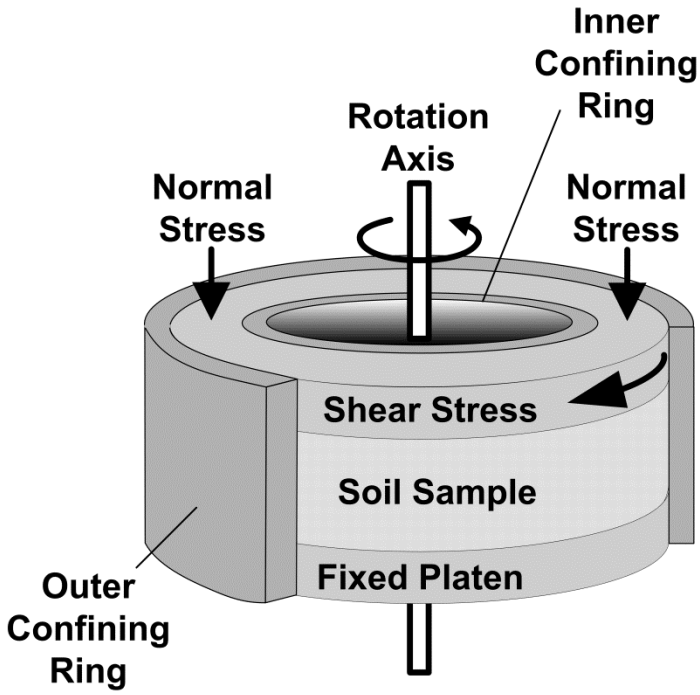

Figure 2.6: Schematic of the mode of shear in the cyclic ring shear tests.

The cyclic ring shear apparatus used in this study was also equipped with a suction control and measurement panel which included dual pressure air regulators, and fine and coarse gauges for the measurement of a wide range of matric suction (Appendix A). Six saturated high air entry ceramic discs separate two water-filled piezometers from the bottom of the specimen and act as an interface for transferring the specimen's air pressure to water. These ceramic discs remain saturated throughout a test as long as the air entry value of the discs is not exceeded. A change in the water level of these piezometers indicates the accumulation of air pressure on the high air entry ceramic discs. To control

or measure matric suction, air pressure is applied through the top of the ring shear specimen until equilibrium is reached in these piezometers.

2.3.1 Data Reduction

The uniformly distributed average vertical (σ_v) and shear (τ) stresses on a horizontal failure plane are calculated using the following equations (La Gatta 1970) in the ring shear tests:

$$\tau = \frac{3T}{2\pi\left(R_o^3 - R_i^3\right)} \tag{2.1}$$

$$\sigma_v = \frac{N}{\pi\left(R_o^2 - R_i^2\right)} \tag{2.2}$$

The average shear displacement (δ) and shear strain (γ) at the mid-radius of the specimen are calculated as below:

$$\delta = \frac{\pi}{180}\left(\frac{R_o + R_i}{2}\right)\theta(^\circ) \tag{2.3}$$

$$\gamma = \frac{\delta}{h} \tag{2.4}$$

2.3.2 Limitations of Ring Shear Tests

Ring shear tests are primarily used to determine the residual shear strength of cohesive soil because of their ability to shear samples to virtually unlimited shear displacements. Recently, a new ring shear apparatus was developed and designed by Sadrekarimi and

Olson (2009) to investigate the large displacement liquefaction behavior (Sadrekarimi and Olson 2011), shear banding (Sadrekarimi and Olson 2010a), and particle crushing (Sadrekarimi and Olson 2010b) of sands and silty sands. Ring shear tests are also used to investigate the cyclic behaviour of soils (Jurko et al. 2006; Sassa et al. 2007; Wang et al. 1998). For example, Jurko et al. (2006) carried out cyclic ring shear tests to study soil behavior associated with slope instability and large displacements following cyclic earthquake loads.

As outlined by Sadrekarimi and Olson (2009), the major limitations and challenges associated with ring shear tests include soil extrusion, wall friction, non-uniform shear stress and strain distributions across the specimen width, and undrained shearing. These limitations are reviewed and addressed for the ring shear tests of this study in the following paragraphs.

The effect of wall friction between the soil specimen and the confining rings is negligible in the ring shear apparatus used in this study as the shear load is applied and measured simultaneously at the upper loading platen, similar to the Bromhead ring shear device (Bromhead 1979; Stark and Vettel 1992).

Soil extrusion is another chronic problem in most ring shear tests, particularly when testing fine-grained soils to large shear displacements, which can significantly affect the measurement of soil shear resistance. However, the very small clearance between the upper loading disc and the annular confining rings and the relatively small shear

displacements applied in our ring shear tests, minimized the amount of soil extrusion as we did not observe any soil extrusion in our experiments. In addition, the upper loading disc was specially designed with tapered upper edges and therefore even if a few silt particles escaped the specimen chamber, they would collected in the cuneal space of the top loading disc and they would not affect the measured shear resistance.

The actual distribution of σ_v and τ across the width of a ring shear specimen is not uniform because of the differences in the amount of shear displacements at the inner and outer radii of the specimen. In order to investigate the inaccuracies resulting from the assumption of uniform stress distribution in Equations (2.1) and (2.2), the Duguet-Ludwig-Prandtl graphical differentiation of the moment-twist curve is extended to a ring-shaped specimen of this study for calculating the shear stress across the width of a specimen (Hvorslev 1939). Figure 2.7 presents the results of this analysis for a typical ring shear tests of this study. As indicated in Figure 2.7, Equations (2.1) and (2.2) would produce only up to 1.5% error in the measurement of soil shear resistance at the peak shear stress (Hvorslev 1939) mobilized in this apparatus compared to the actual stresses across the specimen width. Note that at large shear displacements where a critical state is reached, the effect of stress non-uniformity disappears and the shear stresses mobilized at the inner (τ_i) and outer (τ_o) radii of the specimen become very close to the average shear stress (τ) calculated from Equation (2.1).

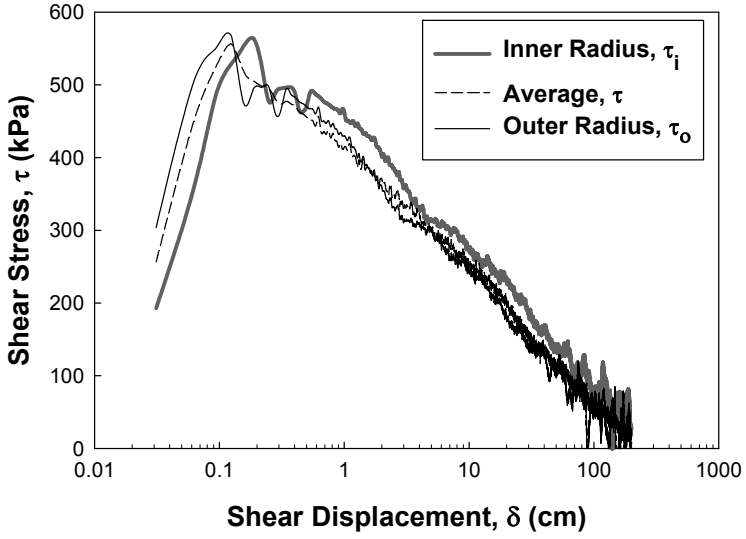

Figure 2.7: Comparison of the average shear stress (τ) calculated from Equation (1) with those mobilized at the inner (τ_i) and outer (τ_o) radii of the ring shear specimens in this study.

The cyclic ring shear apparatus does not allow undrained shear tests or measurement of pore water pressure. Accordingly, constant volume ring shear tests were performed to replicate undrained soil behavior. In these tests, the vertical displacement of the upper loading platen was carefully monitored to prevent specimen volume changes of the specimen. Many researchers have demonstrated that constant volume testing can simulate undrained conditions where the decease or increase in σ_v is equal to the increase or decrease in the excess pore water pressure (Δu) in an equivalent undrained shear test, respectively (e.g. Sadrekarimi and Olson 2009, Finn et al. 1994; Dyvick et al. 1987; Taylor 1952). This is particularly advantageous for undrained cyclic shear tests of silts.

Because of the low permeability and the slow rate of excess pore water pressure equalization in silts, the water pressure measured at the boundaries of the specimen in undrained cyclic shear tests may not represent the overall pore water pressure of the specimen and particularly the pore water pressure developed in the shear zone.

2.3.3 Ring Shear Testing Procedure

Stages of the ring shear testing procedure adopted in this study are briefly described below.

2.3.3.1 Consolidation Stage

All the ring shear specimens were consolidated to a vertical stress of σ_{vc} = 100 kPa. The amount of vertical deformation and thus the volume change of the specimen were carefully measured during the application of the consolidation stress and the specimen void ratio (e_c) was calculated at the end of consolidation.

2.3.3.2 Constant-volume Monotonic Shear

The undrained monotonic shear behaviour of different soil mixes was investigated by carrying out constant-volume monotonic shear tests. In these tests after the application of σ_{vc} = 100 kPa, the monotonic shear load was applied at a shear strain rate of 3.3% /sec while the upper loading platen was locked to prevent specimen volume change. Shearing was continued until a critical state – characterized by constant τ and σ_v – was achieved.

2.3.3.3 Constant-Volume Cyclic Shear

Constant-volume cyclic shear tests were performed by subjecting the specimens to different amplitudes of uniform sinusoidal cyclic shear stresses (τ_{cyc}) at a frequency of 0.1 Hz while in common to the monotonic shear tests, while the upper loading platen was locked to prevent specimen volume change. The ring shear machine was fine-tuned at different cyclic shearing frequencies and it was found that the cyclic shearing frequency of 0.1 Hz provided the most consistent sinusoidal harmonic feedback with better control of the loading system. A cyclic shearing frequency of 0.1 Hz has been also used in many other studies of cyclic soil behavior (e.g. Erken and Ulker 2007; James et al. 2011; Sitharam and Dash 2008; Wijewickreme et al. 2005; Sanin and Wijewickreme 2006; Vaid and Sivathayalan 1996). Uniform cyclic shear stress ratios, CSR = τ_{cyc}/σ'_{vc} of 0.075 to 0.225 were applied in the ring shear tests of this study until large excess pore water pressure ratios, $r_u = \Delta u/\sigma_{vc} > 0.9$ were developed. The total number of cycles and the cumulative amount of the loading and unloading shear strains (double-amplitude total shear strain, γ_{DA}) incurred to develop this condition were recorded. Figure 2.8 illustrates a typical time history of τ_{cyc} applied in our ring shear tests and Tables 2.2 to 2.4 present the details of the ring shear testing program conducted in this study.

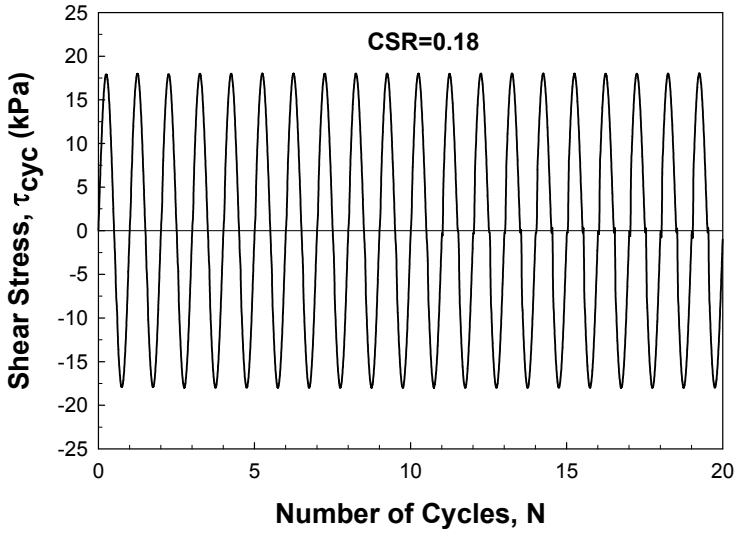

Figure 2.8: Typical time-history of τ_{cyc} applied in the cyclic ring shear tests.

2.3.3.4 Shear Wave Velocity Measurements

The shear wave velocity (V_s) traveling through the soil specimen was measured before the application of the cyclic shear loading by a pair of piezoelectric bender elements embedded in the upper and lower platens of the specimen chamber. A pulse of shear wave is generated by applying an electrical voltage to the source bender element, which is transmitted through the soil to the receiving element and subsequently converted into an output electrical voltage signal. V_s of the specimen is calculated from the travel time (t) of the pulse and the tip-to-tip distance (d_{sr}) between the source and receiver bender elements as below:

$$V_s = \frac{d_{sr}}{t} \tag{2.5}$$

As suggested by several investigators (Kawagushi et al. 2001; Lee and Santamarina 2005; Baxter et al. 2008), it was found that the initial zero-crossing of the first major signal provided a reasonable estimate of V_s for the silt and sand mixes of this study. Accordingly, as illustrated in Figure 2.9 the time of the initial zero-crossing of the first major electrical signal captured by the receiving bender element was used in this study for the measurement of propagation time and V_s. Appendix C provides the complete details and results of shear wave velocity measurements.

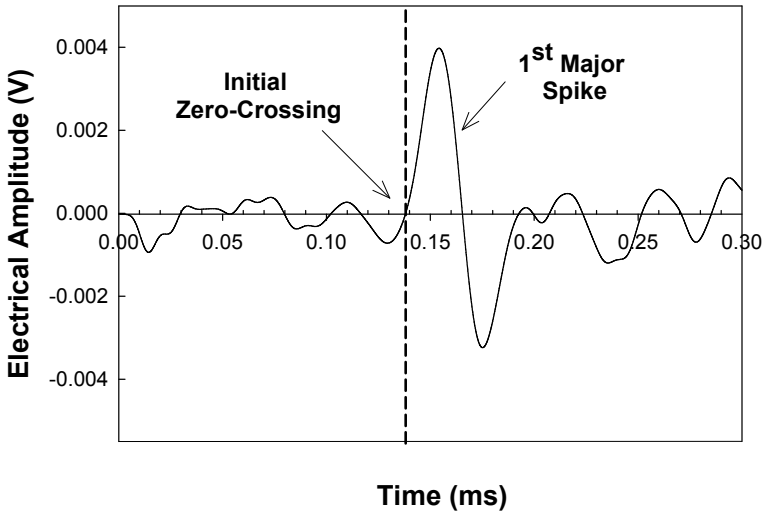

Figure 2.9: Typical electrical signal received by the bender element and the interpretation of shear wave arrival time in this study (Specimen of silt content 75%, D_{rc} = 37% and at σ'_{vc} = 100kPa).

2.4 Test Results and Analysis

Typical examples of the cyclic ring shear tests are presented in Figures 2.10 to 2.12. Tables 2.2 to 2.4 and Appendix B provide the complete details and results of these experiments.

Figures 2.10 to 2.12 show vertical stress reduction reflecting excess pore water pressure generation during constant-volume cyclic shear and demonstrate significant stiffness degradation with the number of shear cycles. Figures 2.10 to 2.12 further indicate threshold values of $\gamma_{DA} \approx 5\%$ and $r_{u,th} = 0.6 - 0.7$ after a certain number of shear stress cycles (N_L), where the specimen becomes unstable and r_u and γ_{DA} exhibit a dramatic rise.

For example, according to Figure 2.10 r_u progressively increases with γ_{DA} and the number of shear cycles for a pure silt specimen at a relative density, $D_{rc} = 35\%$. This continues until at the 10^{th} shear stress cycle (N_L) the average r_u rapidly increases from about 0.6 to 0.9, and the specimen experiences a significant increase in γ_{DA} from slightly over 5% to about 7.5%. All other specimens exhibited similar behavior at different N_L and Tables 2.2 to 2.4 summarize the threshold, N_L, $r_{u,th}$, and γ_{DA} which triggered instability in the cyclic ring shear experiments of this study.

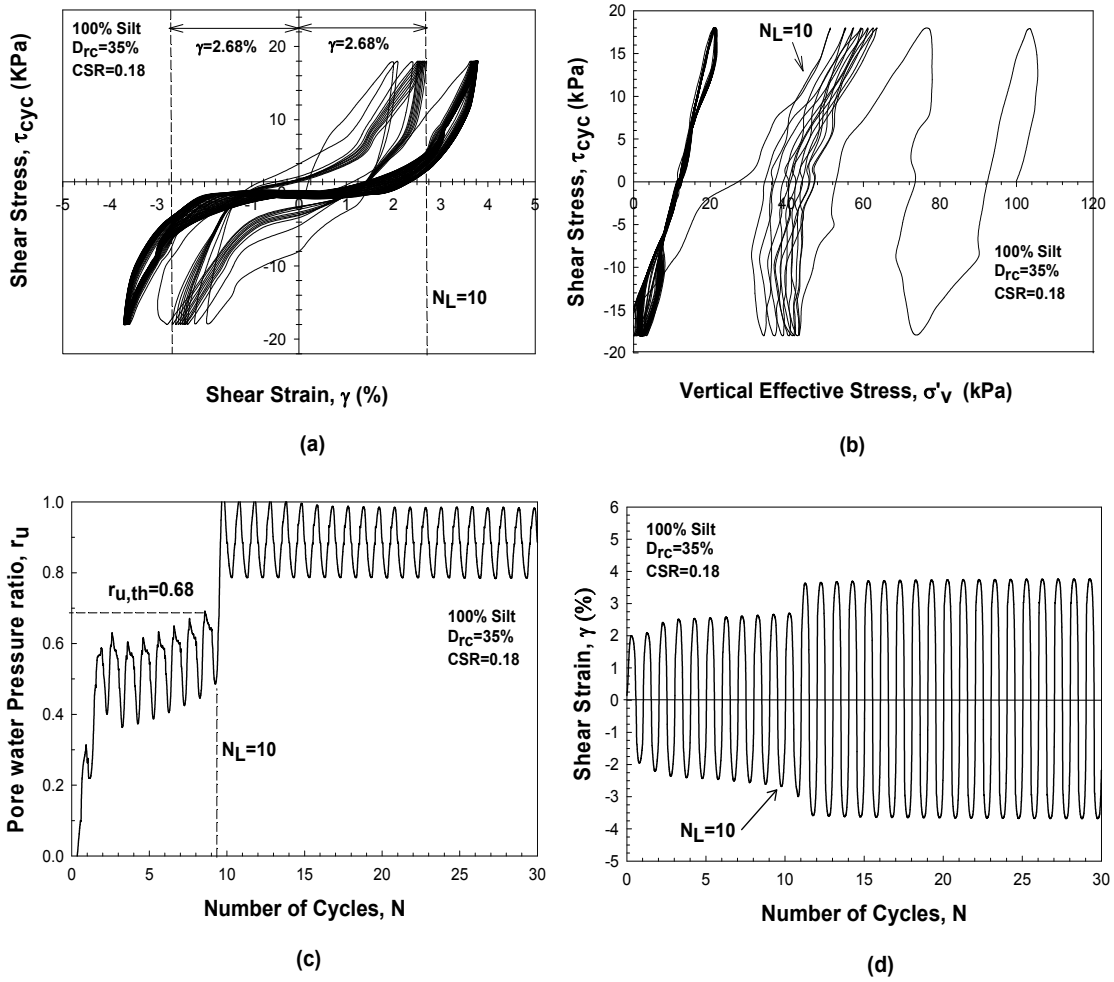

Figure 2.10: Response of a pure silt specimen in a constant volume cyclic ring shear test(D_{rc} = 35%, CSR = 0.18, σ'_{vc} = 100 kPa): (a) cyclic stress-strain response, (b) cyclic effective stress path, (c) excess pore water pressure ratio versus number of cycles, (d) shear strain versus number of cycles.

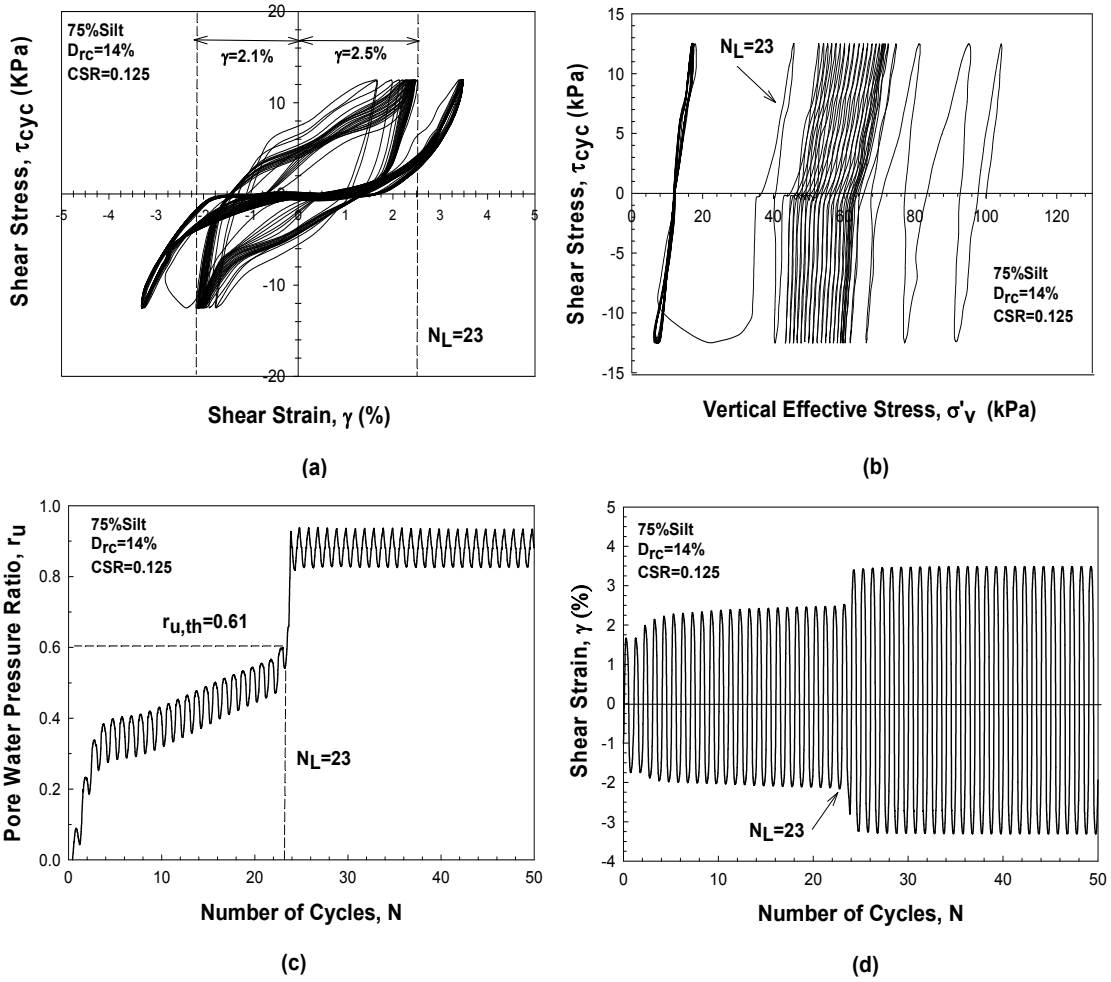

Figure 2.11: Response of a sandy silt specimen with 75% silt a content in constant volume cyclic ring shear test (D_{rc} = 14%, CSR = 0.125, σ'_{vc} = 100 kPa): (a) cyclic stress-strain response, (b) cyclic effective stress path, (c) excess pore water pressure ratio versus number of cycles, (d) shear strain versus number of cycles.

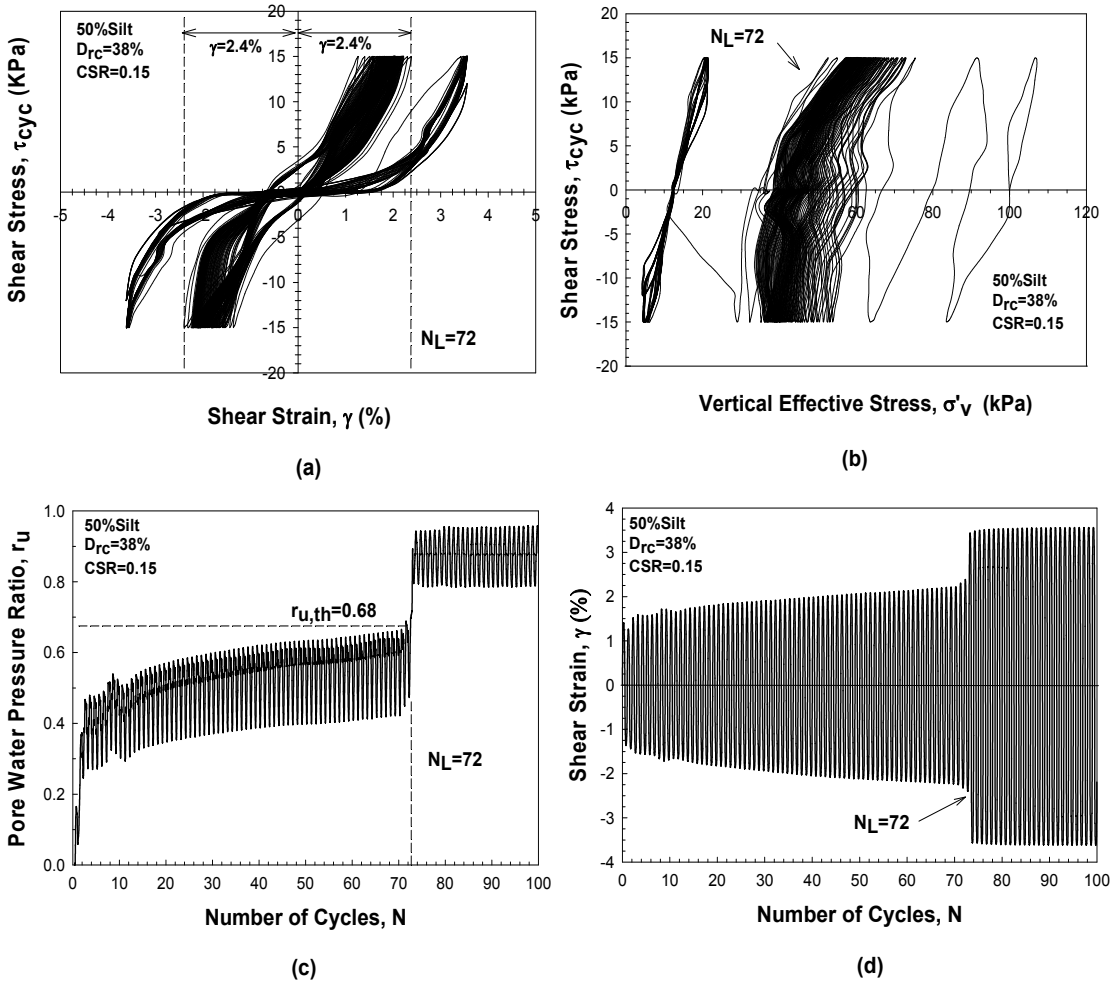

Figure 2.12: Response of a sandy silt specimen with 50% silt a content in constant volume cyclic ring shear test (D_{rc} = 14%, CSR = 0.125, σ'_{vc} = 100 kPa): (a) cyclic stress-strain response, (b) cyclic effective stress path, (c) excess pore water pressure ratio versus number of cycles, (d) shear strain versus number of cycles.

Table 2.2: Summary of the constant volume cyclic ring shear tests on pure silt specimens.

Test#	e_c	D_{rc}	CSR	N_L	γ_{DA} (%)	$r_{u,th}$
S100D35-1	1.60	35	0.125	86	4.3	0.68
S100D35-2	1.60	35	0.125	88	4.3	0.62
S100D35-3	1.60	35	0.125	83	4	0.61
S100D35-4	1.60	35	0.150	39	4.2	0.64
S100D35-5	1.60	35	0.150	45	4.1	0.67
S100D35-6	1.60	35	0.150	44	4.3	0.73
S100D35-7	1.60	35	0.180	12	5.7	0.67
S100D35-8	1.60	35	0.180	10	5.4	0.68
S100D35-9	1.60	35	0.180	11	5.7	0.69
S100D45-10	1.45	45	0.150	58	4.5	0.69
S100D45-11	1.45	45	0.150	62	4.5	0.68
S100D45-12	1.45	45	0.150	54	4.4	0.64
S100D45-13	1.45	45	0.180	29	5.4	0.7
S100D45-14	1.45	45	0.180	32	4.5	0.72
S100D45-15	1.45	45	0.180	33	5.2	0.7
S100D45-16	1.45	45	0.200	12	5.3	0.71
S100D45-17	1.45	45	0.200	11	5.8	0.71
S100D45-18	1.45	45	0.200	9	5.5	0.69
S100D55-19	1.31	55	0.180	58	4.5	0.69
S100D55-20	1.31	55	0.180	66	4.8	0.7
S100D55-21	1.31	55	0.180	62	5.5	0.7
S100D55-22	1.31	55	0.200	24	4.6	0.69
S100D55-23	1.31	55	0.200	21	5.3	0.71
S100D55-24	1.31	55	0.200	20	4.8	0.69
S100D55-25	1.31	55	0.225	12	4.7	0.71
S100D55-26	1.31	55	0.225	15	5.3	0.7
S100D55-27	1.31	55	0.225	14	5.2	0.7

Table 2.3: Summary of the constant volume cyclic ring shear tests on sandy silt specimens with 75% silt content.

Test#	e_c	D_{rc}	CSR	N_L	γ_{DA} (%)	$r_{u,th}$
S75D14-1	1.36	14	0.100	68	3.0	0.64
S75D14-2	1.36	14	0.125	23	4.2	0.61
S75D14-3	1.36	14	0.150	16	5.2	0.63
S75D14-4	1.36	14	0.180	6	5.6	0.63
S75D31-5	1.20	31	0.100	75	3.8	0.64
S75D31-6	1.20	31	0.125	45	6.1	0.65
S75D31-7	1.20	31	0.150	27	6.9	0.64
S75D31-8	1.20	31	0.180	8	6.7	0.63
S75D37-9	1.15	37	0.125	97	4.5	0.65
S75D37-10	1.15	37	0.150	84	5.3	0.65
S75D37-11	1.15	37	0.180	31	6.2	0.67
S75D37-12	1.15	37	0.200	9	5.9	0.68

Table 2.4: Summary of the constant volume cyclic ring shear tests on sandy silt specimens with 50% silt content.

Test#	e_c	D_{rc}	CSR	N_L	γ_{DA} (%)	$r_{u,th}$
S50D13-1	1.06	13	0.100	102	5.2	0.65
S50D13-2	1.06	13	0.125	80	3.9	0.64
S50D13-3	1.06	13	0.150	29	4.9	0.62
S50D13-4	1.06	13	0.180	12	5.6	0.64
S50D25-5	0.98	25	0.125	85	5.3	0.66
S50D25-6	0.98	25	0.150	36	5.8	0.64
S50D25-7	0.98	25	0.180	17	6.1	0.64
S50D25-8	0.98	25	0.200	10	6.2	0.68
S50D38-9	0.89	38	0.150	72	4.8	0.68
S50D38-10	0.89	38	0.180	63	6.6	0.67
S50D38-11	0.89	38	0.200	33	4.2	0.67
S50D38-12	0.89	38	0.225	5	3.8	0.68

2.4.1 Effect of Soil Moisture

The moist tamped specimens prepared for in this experimental program were not saturated and the sand and silt particles were at a moisture content of 5%. Soil suction could be significant in unsaturated fine-grained soils at low moisture content, resulting in large changes in effective stress and soil shear resistance (Lu et al. 2007; Toan et al. 2013). Using the suction control and measurement system of the ring shear device, we measured maximum matric suctions of 100 – 120 kPa in the moist tamped ring shear specimens. Because of the very low saturation ratio (8 – 15%) of our moist tamped specimen, the effective stress parameter which describes the contribution of matric suction on soil effective stress is about 0.05 (Escario and Juca 1989; Khalili et al. 2004; Lu and Likos 2004). Accordingly, soil suction among the moist sand and silt particles merely adds a maximum of about 5 to 6 kPa to σ'_{vc}. We believe that this was further reduced before the application of cyclic shear stress as the soil was open to air and dried during the period of normal compression. Therefore, the impact of soil suction and the low moisture content of the specimens was negligible on the shearing behavior of the soils tested here.

2.5 Interpretation of the Experimental Results

2.5.1 Level-Ground Cyclic Mobility

Cyclic mobility failure happens when the static shear stress (τ_o) is smaller than the critical-state shear strength ($s_{u,cs}$) is mainly initiated by the accumulation of shear strain (deformation) accompanied with a decrease in the effective stresses during cyclic loading (Kramer 2006). As illustrated in Figures 2.10 to 2.12, the liquefaction failure observed in the cyclic ring shear tests closely resembles cyclic mobility failure. Figures 2.13 to 2.15 illustrate typical monotonic and cyclic effective stress paths from the ring shear tests.

Instability occurs during cyclic shear as the effective stress path moves toward the instability line of the monotonic shear test at a similar void ratio as a result of effective stress reduction. The rate of pore water pressure development and shear strain accumulation subsequently increases as the specimen enters the strain-softening region. This led the specimen to undergo cyclic mobility liquefaction failure in Figures 2.13 to 2.15. However, this large increase in pore water pressure generation and shear strain accumulation is soon arrested as the effective stress path quickly reaches the critical state and exhibits strain-hardening by repeated shear stress cycles without further reduction in effective stress or shear strain accumulation. Although this phenomenon would not produce a liquefaction flowslide, the surface manifestations of level-ground cyclic mobility are ground oscillations during the earthquake shaking followed by post-earthquake large settlement and fracturing of nearly level grounds and lateral spreading of gently sloping grounds. In a gently sloping ground, the additional static shear stress

biased towards the slope would be superimposed on $\tau_o + \tau_{cyc}$, leading to ground lateral spreading to occur. Lateral spreading associated with a ground fissures, vertical and horizontal ground displacements has caused extensive damage to infrastructures (buried pipelines, utility lines, and foundations) in many past earthquakes (Hamada et al. 1986; Idriss 1999; Holzer et al. 2004; Forcellini et al. 2013).

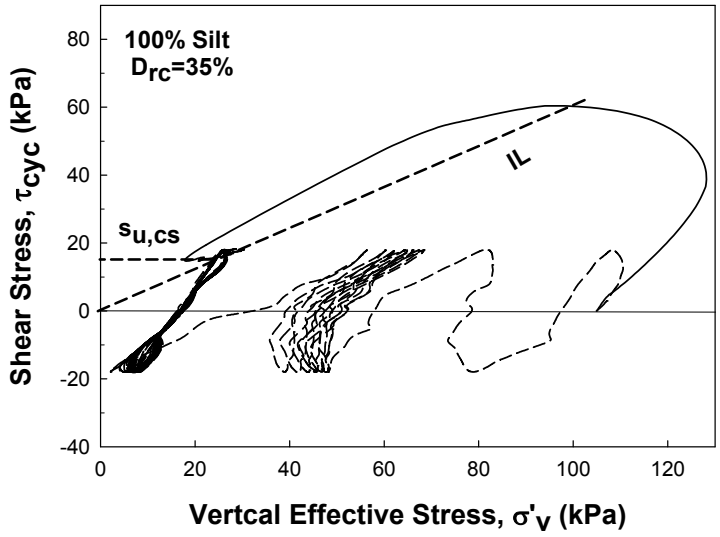

Figure 2.13: Monotonic and cyclic effective stress paths of a pure silt specimen at D_{rc} = 35% (IL is the instability line).

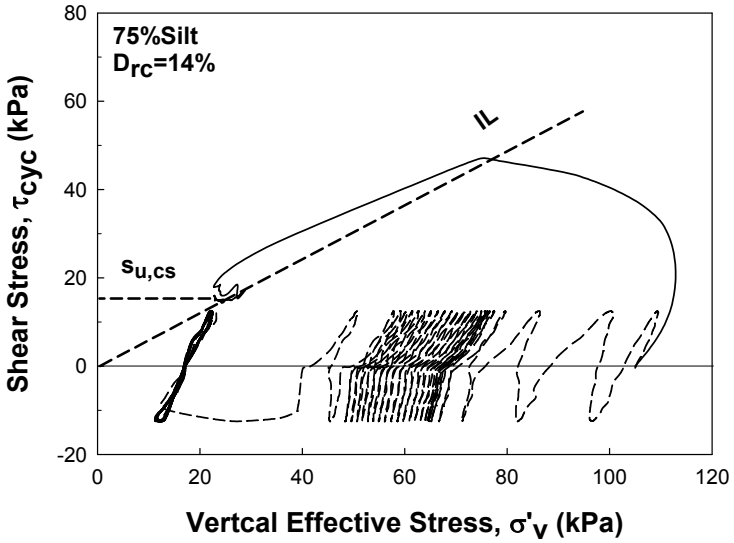

Figure 2.14: Monotonic and cyclic effective stress paths of a sandy silt specimen with 75% silt content at D_{rc}=14% (IL is the instability line).

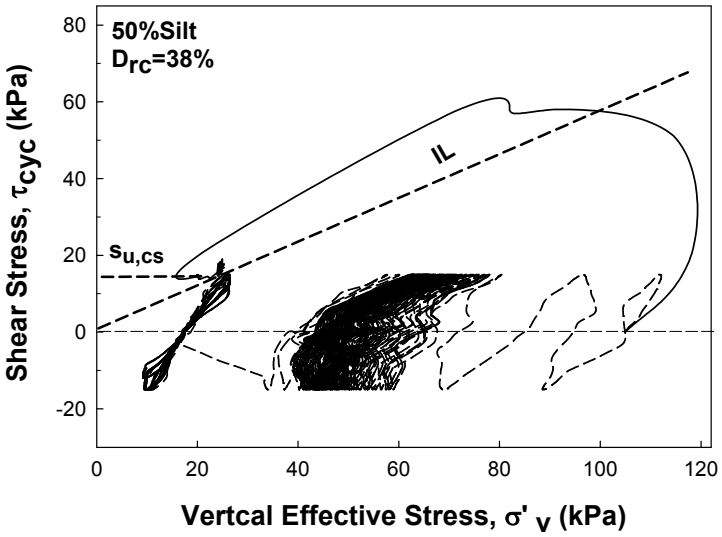

Figure 2.15: Monotonic and cyclic effective stress paths of a sandy silt specimen with 50% silt content at D_{rc} = 38% (IL is the instability line).

2.5.2 Triggering of Level-Ground Cyclic Mobility Liquefaction

It is well known that during cyclic loading, the rise in pore water pressure is accompanied by the accumulation of shear strain until the excess pore water pressure reaches a threshold value, after which a large deformation or shear strain occurs. Based on this definition, excess pore water pressure and shear strain (deformation) are considered as two principal parameters that should be monitored during any experimental program in order to determine whether or not a sample has reached liquefaction. Since in most field investigations ground deformation is used as an evidence to determine liquefaction where pore water pressure is not readily measured, many experimental studies have focused on determining the shear strain values at which liquefaction is triggered (Seed and Lee 1966; Ishihara et al. 1975).

As illustrated in Figures 2.13 to 2.15, cyclic mobility failure was reached in all cyclic ring shear tests at an average threshold pore water pressure ($r_{u,th}$) varied between 0.6 to 0.7, producing γ_{DA} = 7.5% immediately afterwards, irrespective of the applied CSR and specimen D_{rc}. This is practically significant as it implies that contrary to the current perception that r_u = 1.0 is required for level-ground liquefaction (Yegian 1980; Steedman and Sharp 1995), level-ground cyclic mobility liquefaction failure and the associated large shear deformations can be triggered in loose cohesionless soils without necessarily developing r_u = 1.0. Moreover, since the in-situ pore water pressure is seldom measured in field failures, γ_{DA} = 7.5% could be used as a practical strain criterion to identify the soil conditions and the earthquake ground motions which could triggering cyclic mobility

liquefaction failure. This is similar to the double amplitude axial strain of 5% and the single amplitude shear strain of 3.75% reported for triggering liquefaction and achieving large excess pore water pressures in cyclic triaxial (Ishihara et al. 1975; Zhou and Chen 2007; Baxter et al. 2008; Kokusho 2013) and cyclic direct simple shear tests (Boulanger et al. 1991; Sivathayalan and Ha 2004; Wijewickreme et al. 2005; Sanin and Wijewickreme 2006), respectively.

Figures 2.16 to 2.18 further present the number of shear stress cycles (N_L) applied to reach the instability line and trigger cyclic mobility liquefaction failure for the experiments performed in this study. Clearly a larger τ_{cyc} not only accelerates pore water pressure development, but also produces total shear stresses closer to the instability line. Therefore, as illustrated in Figures 2.16 to 2.18, larger N_L is required to reach instability with a smaller CSR at a particular D_{rc} and the CSR required to trigger cyclic mobility liquefaction failure at a certain N_L increases with increasing D_{rc}.

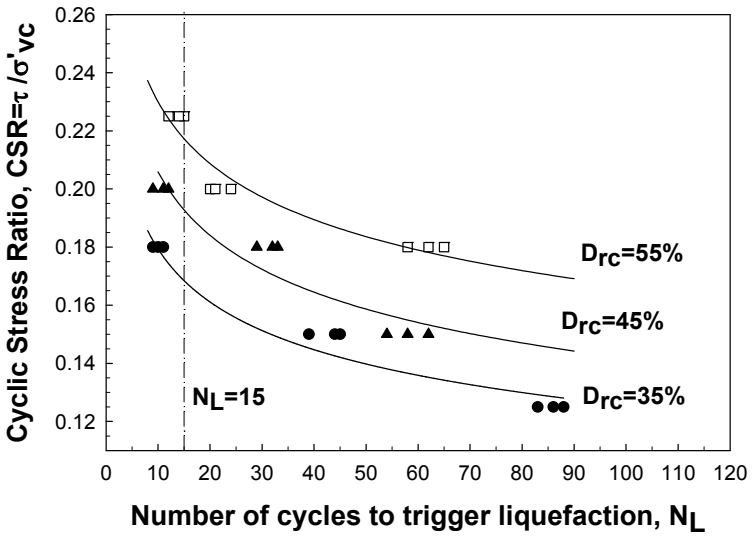

Figure 2.16: N_L versus CSR to trigger cyclic mobility liquefaction failure in pure silt specimens at σ'_{vc} = 100 kPa.

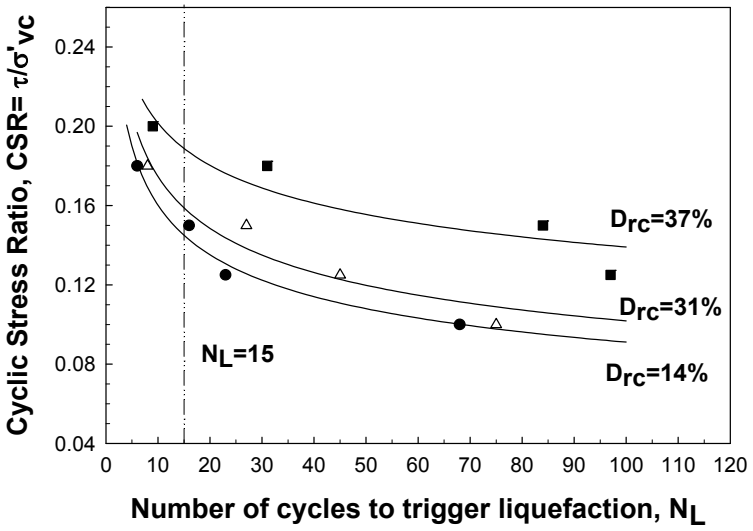

Figure 2.17: N_L versus CSR to trigger cyclic mobility liquefaction failure in sandy silt specimens with 75% silt content at σ'_{vc} = 100 kPa.

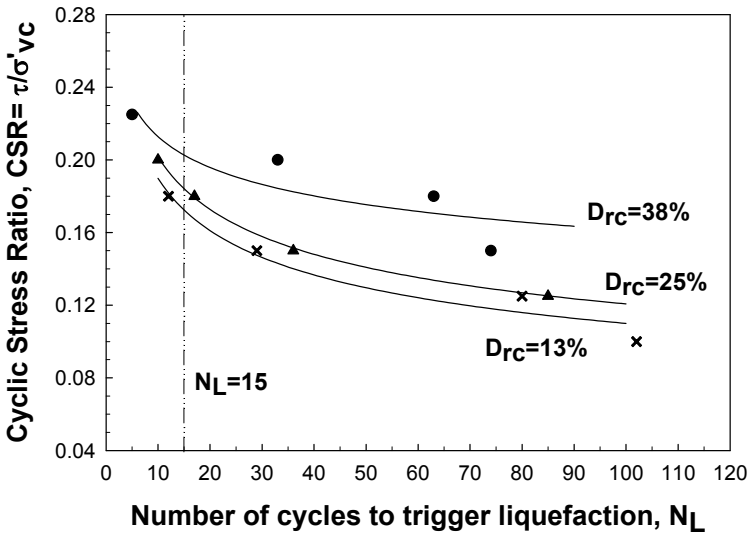

Figure 2.18: N_L versus CSR to trigger cyclic mobility liquefaction failure in sandy silt specimens with 50% silt content at σ'_{vc} = 100 kPa.

2.5.3 Cyclic Shear Resistance

Cyclic shear resistance of a soil is its capacity to resist cyclic loading that is described by the cyclic resistance ratio (CRR). As demonstrated in Figures 2.16 to 2.18, soil cyclic resistance to trigger level-ground cyclic mobility liquefaction failure depends on N_L as well as D_{rc}. The number of shear stress cycles applied by a particular earthquake depends on the earthquake magnitude. As an earthquake with a moment magnitude of 7.5 would produce 15 uniform shear stress cycles (Idriss 1999), past studies have adopted CRR as the cyclic soil resistance mobilized after 15 uniform cycles of shear stress (Andrus and Stokoe 2001, Baxter et al. 2008; Zhou and Chen 2007). Accordingly, in order to preserve the consistency with these studies, CRR is defined here as the CSR that drives the cyclic

effective stress path to the instability line within 15 cycles of shear stress (N_L = 15). CRR determined from the cyclic ring shear tests is reduced by 10% in order to account for the influence of multidirectional cyclic stresses in real earthquake ground motions (Seed 1979). According to Figure 2.19, CRR decreases with increasing e_c at a certain silt content while at a given e_c CRR increases with increasing silt content.

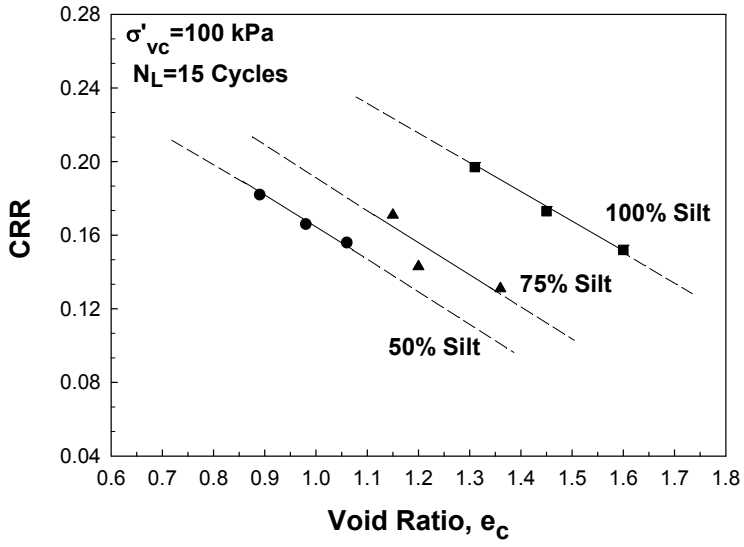

Figure 2.19: Effect of silt content on CRR from the cyclic ring shear tests of this study.

2.5.4 Comparison with Past Laboratory Studies

The experimental work described in this paper and the observations of level-ground cyclic mobility liquefaction failure are among the first ring shear experiments on the cyclic behavior of silts and sandy silts (FC ≥ 50%). The close proximity of CRR data from the cyclic ring shear tests of this study with those from the cyclic triaxial

compression tests on Providence silt specimens (Baxter et al. 2008) demonstrated in Figure 2.20, are because of the very similar N_L developing $r_{u,th}$ and $r_u \approx 1.0$ in the cyclic ring shear tests despite the differences in mode of shear. In fact, Hosono and Yoshimine (2004) demonstrate that the liquefaction resistance under simple shearing condition is 75% to 85% of that from triaxial compression mode of shear, which is consistent with the data presented in Figure 2.20. However, as a result of adopting different liquefaction criteria, CRR from the cyclic direct simple shear tests which are based on a liquefaction criterion of γ_{DA} = 3.75% (Sanin and Wijewickreme 2006) are somewhat smaller than those from the cyclic ring shear tests of this study.

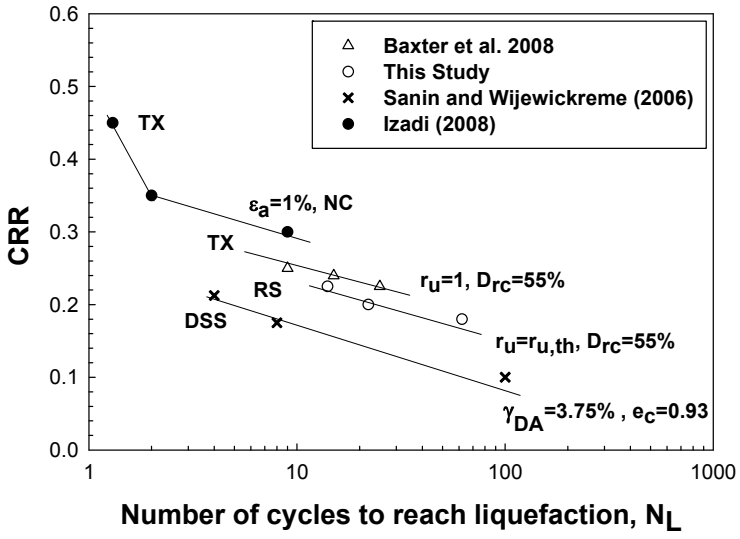

Figure 2.20: Comparison of CRR of silts from the cyclic ring shear tests (RS) of this study and those from cyclic direct simple shear (DSS) (Sanin and Wijewickreme 2006), and cyclic triaxial compression shear tests (TX) (Baxter et al. 2008, Izadi 2008) ($r_{u,th}$ corresponds to the threshold pore water pressure, ε_a corresponds to the axial strain and NC for normally consolidated silts).

2.5.5 CRR-V_s Relationships

Figure 2.21 presents the cyclic resistance ratio (CRR) and shear wave velocity (V_{s1}) data for the non-plastic silt and sandy silts at σ'_{vc} =100 kPa. Figure 2.21 shows that CRR increased as V_{s1} increased for all mixes irrespective of FC and a unique relationship describes the trend of these data with little scatter. The CRR-V_{s1} relationship developed in this study is plotted in Figure 2.21 along with empirical field-based correlations (Andrus and Stokoe, 2000) and laboratory cyclic triaxial shear test results (Baxter et al. 2008; Che et al. 2008). Comparing CRR values obtained in the current study with those reported by Andrus and Stokoe (2000) indicate that CRR is higher for soils with higher FC ratios (i.e. beyond the upper limit FC of 35%). The effect of FC would then diminish at FC $\geq$ 50% where a silt-dominant fabric is formed. In support of our findings, Figure 2.22 shows that the CRR-V_s data obtained by Che et al. (2008) for low plasticity sandy silts with FC varying from 76% and 98% are very close to the CRR-V_s relationships developed in this study. However, the differences with the measurements of Baxter et al. (2008) could be due to the differences in particle composition and mineralogy of the tested materials as well as the differences mode of shear, sample fabrics, and specimen preparation methods.

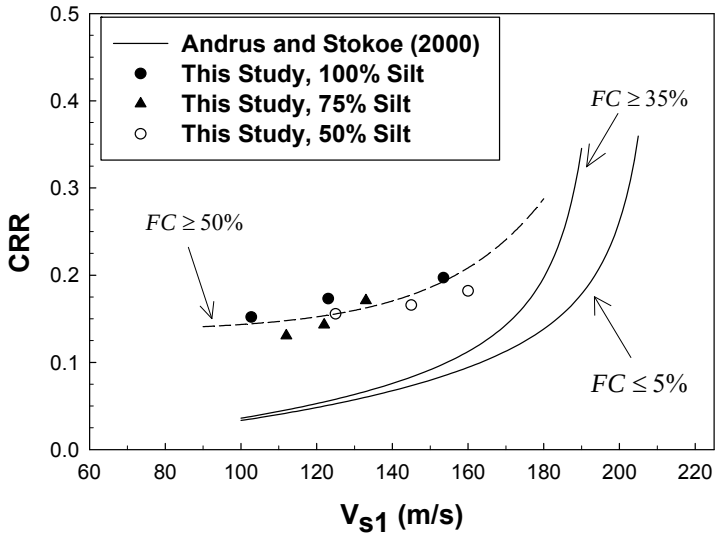

Figure 2.21: Relationships of CRR and V_{s1} from the cyclic ring shear tests of this study (at FC ≥ 50%), and field-based data (Andrus and Stokoe 2000) at M_w=7.5 (N_L=15 cycles).

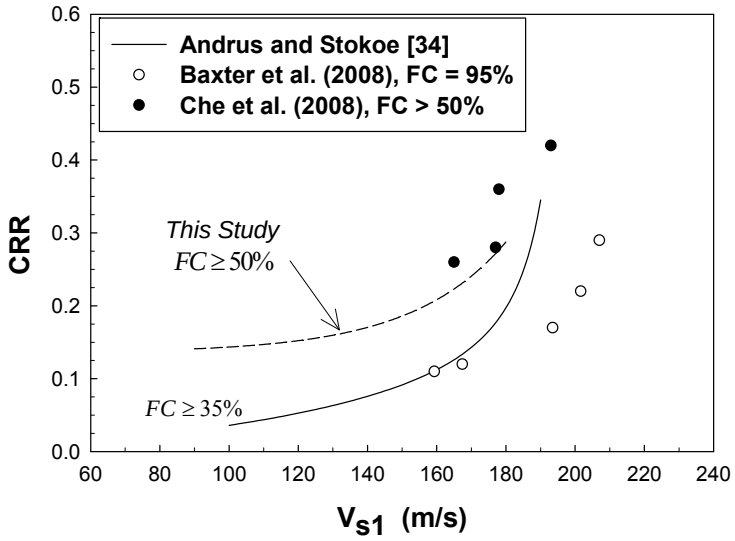

Figure 2.22: : Relationships of CRR and V_{s1} from the cyclic ring shear tests of this study (at FC ≥ 50%), and cyclic triaxial shear tests from Baxter et al. 2008, and Che et al. 2008 at M_w=7.5 (N_L=15 cycles).

2.6 Summary and Conclusion

The cyclic and monotonic behaviour of clean silt and silt with 25% and 50% sand mixes was examined using constant-volume cyclic ring shear testing along with bender element shear wave velocity measurements. Cyclic mobility liquefaction failure was observed to occur for the level ground condition when the cyclic stress path from ring shear tests reaches the instability line (IL). An increase in the cyclic load amplitude accelerated excess pore water pressure development in the samples and decreased the number of cycles needed to reach failure. Liquefaction and strain-softening occurred at excess pore water pressure ratios (r_u) between 0.6 and 0.7 associated with cumulative shear strains (γ) of 4% to 6%, after which cyclic mobility failure ensued with very large shear strains and excess pore water pressure ratio ($r_u > 0.9$). Accordingly, non-plastic silts are found to be susceptible to liquefaction and their cyclic response is very similar to sand in terms of strain and excess pore water pressure development. Cyclic resistance ratio (CRR) was defined as the cyclic stress ratio needed to trigger liquefaction at $r_u = r_{u,th}$ in 15 cycles of uniform shear stress. It was observed that CRR decreased with increasing initial void ratio, while at the same void ratio CRR increased with increasing silt content. The test data further indicate that the existing field CRR-V_{s1} correlations could underestimate the liquefaction resistance of soils with FC $\geq$ 50%.

2.7 References

Adachi, M. (1996). Liquefaction strength and post-liquefaction settlement of finer containing sands. Ph.D. thesis, Ibaraki Univ., Japan.

Alba, P. D., Baldwin, K., Janoo, V., Roe, G., and Celikkol, B. (1984). Elastic-wave velocities and liquefaction potential. Geotechnical Testing Journal 7(2): 77–87.

Andrus, R. and K. Stokoe II (2000). Liquefaction Resistance of Soils from Shear-Wave Velocity. Journal of Geotechnical and Geoenvironmental Engineering 126(11): 1015-1025.

Ashford, S. A., Boulanger, R. W., Donahue, J. L., and Stewart, J. P. (2011). Geotechnical quick report on the Kanto plain region during the March 11, 2011 off pacific coast of Tohoku earthquake, Japan. Geotechnical Extreme Events Reconnaissance (GEER), Report o. GEER No. GEER-025a, April 5, 2011: 1 – 20.

Askari, F., Dabiri, R., Shafiee, A., Jafari, M. K., (2010). Effects of Non-Plastic Fines Content on Cyclic Resistance and Post Liquefaction of Sand-Silt Mixtures Based on Shear Wave Velocity. Journal of seismology and eartquake engineering, 12 (1&2).

ASTM Standards D4253-00 (2006a). Standard Test Methods for Maximum Index Density and Unit Weight of Soils Using a Vibratory Table. ASTM International, West Conshohocken, PA 2006. DOI: 10.1520/D4253-00R06

ASTM Standards D1557-12 (2012). Standard Test Methods for Laboratory Compaction Characteristics of Soil Using Modified Effort ASTM International, West Conshohocken, PA 2012. DOI: 10.1520/D1557-12

ASTM Standards D4254-00 (2006b). Standard Test Methods for Minimum Index Density and Unit Weight of Soils and Calculation of Relative Density. ASTM International, West Conshohocken, PA 2006.

ASTM Standards D6467-06a (2006c). Standard Test Method for Torsional Ring Shear Test to Determine Drained Residual Shear Strength of Cohesive Soils. ASTM International, West Conshohocken, PA 2006. DOI: 10.1520/D6467-06.

Baxter, C., Bradshaw, A., Green, R., and Wang, J. (2008). Correlation between Cyclic Resistance and Shear-Wave Velocity for Providence Silts. Journal of Geotechnical and Geoenvironmental Engineering 134(1): 37-46.

Boulanger, R. W., Seed, R. B., Chan, C. K., Seed, H. B., and Sousa, J. (1991). Liquefaction behavior of saturated sands under uni-directional and bi-directional monotonic and cyclic simple shear loading. Geotechnical Report No. UCB/GT/91-08, Univ. of California, Berkeley, CA.

Boulanger, R. W., Mejia, L. H., Myers, M. W., and Idriss, I. M. (1999). Behavior of a fine-grained soil during the Loma Prieta earthquake: Reply. Canadian Geotechnical Journal 36(3):584-584.

Boulanger, R. (2003). High Overburden Stress Effects in Liquefaction Analyses. Journal of Geotechnical and Geoenvironmental Engineering 129(12): 1071-1082.

Boulanger, R. W. (2012). Liquefactoin in the 2011 great east Japan earthquake: lessons for U.S. practice.Proceedings of the International Symposium on Engineering Lessons Learned from the 2011 Great East Japan Earthquake, March 1- 4, Tokyo, Japan: 655 – 664.

Bradshaw, A.S. and Baxter, C.D.P (2007). Sample Preparation of Silts for Liquefaction Testing, ASTM Geotechnical Testing Journal, 30(40): 324-332.

Bromhead, E. N. (1979). A Simple Ring Shear Apparatus. Ground Engineering 12(5) :40-44.

Carraro, J. A. H., Bandini, P., and Salgado, R. (2003). Liquefaction Resistance of Clean and Silty Sands from Cone Penetration Resistance. Journal of Geotechnical and Geoenvironmental Engineering 129(11): 965-976.

Che, A., Luo, X., QI, J., (2008). Study on correlation between shear wave velocity and ground properties for ground liquefaction investigation of silts. International journal of modern physics b 22(31n32): 5705-5710.

Chen, Y. M., Ke, H., and Chen, R. P. (2005). Correlation of shear wave velocity with liquefaction resistance based on laboratory tests. Soil Dyn. Earthquake Eng., 25 (6): 461–469.

Cox, B. R., Boulanger, R. W., Tokimatsu, K., Wood, C. M., Clinton M., Abe, A., and Ashford, S. (2013). Liquefaction at Strong Motion Stations and in Urayasu City during the 2011 Tohoku-Oki Earthquake. Earthquake Spectra 29(S1): S55-S80.

Dyvick, R., Berre, T., and Lacasse, S., 1987. Comparison of truly undrained and constant volume direct simple shear tests. Geotechnique, 37(1): 3-10.

Erken, A. and Ulker, B. M. C. (2007). Effect of cyclic loading on monotonic shear strength of fine-grained soils, Engineering Geology 89: 243 – 257.

Escario, V. and Juca, J.F.T. (1989) Strength and Deformation of Partly Saturated Soils, Proc. 12th Int. Conf. on Soil Mechanics and Foundation Engineering, Rio de Janeiro, 1: 43-46.

Fukuoka M., (1966). Damage to civil engineering structures. Soils and Foundations, Vol. VI, No. 2, p45-52.

Finn, W. D., R. H. Ledbetter, and G. Wu (1994). Liquefaction in Silty Soils: Design and Analysis. Ground Failures Under Seismic Conditions, ASCE, 44:51-76.

Forcellini, D., Della Bartola, F.,Tarantino, A. (2013). Liquefaction-Induced Lateral Deformations Computational Assessment during Tohoku Earthquake. ISRN Civil Engineering 2013.

Fourie, A. B., and Tshabalala, L. (2005). Initiation of static liquefaction and the role of ko consolidation. Canadian Geotechnical Journal, 42, 892-906.

Hamada, M., Yasuda, S., Isoyama, R., and Emoto, K., 1986. Study on liquefaction induced permanent ground displacement. Report for the Association for the Development of Earthquake Prediction.

Holzer, T. L., Noce, T. E., Bennett, M. J., Tinsley, J. C., III, and Rosenberg, L. I., (2004). Liquefaction-induced lateral spreading in Oceano, California, during the 2003 San Simeon Earthquake, U.S. Geol. Surv. Open-File Rep. 2004-1269.

Hosono, Y. And Yoshimine, M. (2004). Liquefaction of sand in simple shear condition. International Conference on Cyclic Behavior of Soils and Liquefaction Phenomena, Bochum, Germany, 129 – 136, Balkema, Rotterdam, The Netherlands.

Huang, Y.T., Huang, A.B., Kuo, Y.C, Tasi, M.S. (2004). A laboratory study on the undrained strength of a silty sand from Central Western Taiwan. Soil Dynamics and Earthquake Engineering 24(9–10): 733-743.

Hvorslev, M. J. (1939). Torsion shear tests and their place in the determination of shearing ressitance of soils. Proceedings of the American Society of Testing and Materials, Symposium on Shear Testing of Soils, 39: 999 - 1022.

Hyde, A., Higuchi, T., and Yasuhara, K. (2006). Liquefaction, Cyclic Mobility, and Failure of Silt. Journal of Geotechnical and Geoenvironmental Engineering 132(6): 716-735.

Idriss, I. M., and Boulanger, R. W. (2008). Soil Liquefaction During Earthquakes, Earthquake Engineering Research Institute.

Idriss, I. M. (1999). An update to the Seed-Idriss simplified procedure for evaluation liquefaction potential. In proceeding of the TRB workshop on new approaches to liquefaction analysis, Federal Highway Administartion Washington, D.C.

Ishihara, K. (1984). Post Earthquake Failure of a Tailings Dam due to liquefaction of the Pond Deposit. Conf. on Case Histories in Geotechnical Eng.St. Louis, Missouri 3: 1129-1143.

Ishihara, K., Tatsuoka, F., and Yasuda, S. (1975). Undrained deformation and liquefaction of sand under cyclic stresses, Soils and Foundations 15(1): 29-44.

Izadi, A. (2008). Liquefaction and Postliquefaction Behavior of Low Plasticity Silts Using Cyclic Triaxial Tests. A Phd dissertation, Missory University of Science and Technology.

James, M., Aubertin, M., Wijewickreme, D., Wilson, G. W. (2011). A laboratory investigation of the dynamic properties of tailings. Canadian Geotechnical Journal 48(11):1587-1600.

Jurko J., Sassa K. and Fukuoka H. (2006). Dynamic Behavior of Gentle Silty Slopes Based on Undrained Cyclic Shear Test. Universal Academy Press, Inc. Tokyo, Japan (2006): 411–420.

Kawaguchi, T., Mitachi, T., and Shibuya, S. (2001). Evaluation of shear wave travel time in laboratory bender element test. Proc., 15th Int. Conf. on Soil Mechanics and Geotechanics Engineering 155–158.

Khalili, N., Geiser, F., and Blight, G. E. (2004). Effective stress in unsaturated soils: Review with new evidence. International Journal of Geomechanics, 4 (2): 115–126.

Kokusho, T. (2013). Liquefaction potential evaluations: Energy based method versus stress-based method. Canadian Geotechnical Journal.

Kramer, L.K. (1996). Geotechnical Earthquake Engineering. Prentice Hall in Civil Engineering and Engineering Mechanics, Upper Saddle River, NJ.

Lade, P.V. (1992). Static instability and liquefaction of loose fine sandy slopes. Journal of Geotechnical Engineering, ASCE, 103(2): 51-71.

Ladd, R.S. (1978). Preparing Test Specimen Using Undercompacton. Geotechnical Testing Journal 1(1):16-23.

LaGatta, D. P. (1970). Residual Strength of Clay and Clay-Shales by Rotation Shear Tests. Harvard University Cambridge Mass Soil Mechanics Lab 86.

Lee, J., and Santamarina J. (2005). Bender Elements: Performance and Signal Interpretation. Journal of Geotechnical and Geoenvironmental Engineering 131(9): 1063-1070.

Liu, N., and Mitchell, J. (2006). Influence of Nonplastic Fines on Shear Wave Velocity-Based Assessment of Liquefaction. Journal of Geotechnical and Geoenvironmental Engineering 132(8): 1091-1097.

Lu, N., Wu, B., P.Tan, C. (2007). Tensile Strength Characteristics of Unsaturated Sands. Journal of Geotechnical and Geoenvironmental Engineering 133 (2): 144-154.

Lu, N., and Likos, W. J. (2004). Unsaturated soil mechanics, Wiley, NewYork.

Naeini, S.A., Baziar, M.H. (2004). Effect of fine content on steady state of mixed and layered samples of sand. Soil Dynamics and Earthquake Engineering, 24(2004): 181-187.

Olson, S. M., Green, R. A., Lasley, S., Martin, N., Cox, B. R., Rathje, E., Bachhuber, J., and French, J. (2011). “Documenting liquefaction and lateral spreading triggered by the 12 January 2010 Haiti Earthquake.” Earthquake Spectra (2011), 27(S1): S93 – S116.

Orense, R. P. Kiyota, T.,Yamada, S., Cubrinovski, M., Hosono, Y., and Okamura, M. 2011. Comparison of liquefaction Features observed during the 2010 and 2011 Canterbury earthquakes. Seismological Research Letters 82(6): 905-918.

Polito, C. and Martin II, J. (2001). "Effects of Nonplastic Fines on the Liquefaction Resistance of Sands." Journal of Geotechnical and Geoenvironmental Engineering 127(5): 408-415.

Rauch, A., Duffy, M., and Stokoe, II, K. (2000). Laboratory Correlation of Liquefaction Resistance with Shear Wave Velocity. Computer Simulation of Earthquake Effects: 66-80.

Richart, F. E., Hall, J. R., and Woods, R. D. (1970). Vibrations of soils and foundations, Prentice-Hall, Englewood Cliffs, N.J., 152–156.

Sadrekarimi, A. (2009). Development of a new ring shear machine apparatus for investigating the critical state of sands. Phd dissertation, University of Illinois at Urbana-Champaign.

Sadrekarimi, A., and Olson S. M. (2009). A New Ring Shear Device to Measure the Large Displacement Shearing Behavior of Sands. Geotechnical Testing Journal 32(3): 197 - 208.

Sadrekarimi, A., and Olson S. M. (2011). Yield strength ratios, critical strength ratios, and brittleness of sandy soils from laboratory tests. Canadian Geotechnical Gournal 48: 493-510.

Sadrekarimi, A., and Olson, S. M. (2010a). Shear band formation observed in ring shear tests on sandy soils. Journal of Geotechnical and Geoenvironmental Engineering, ASCE, 136(2): 366 - 375.

Sadrekarimi, A., and Olson, S. M. (2010b). Particle damage and crushing observed in ring shear tests on sands. Canadian Geotechnical Journal, 47(5): 497-515.

Sanin, M. V., and Wijewickreme D. (2006). Cyclic shear response of channel-fill Fraser River Delta silt. Soil Dynamics and Earthquake Engineering 26(9):854-869.

Sancio, R. B., Bray, J. D., Stewart, J. P., Youd, T. L., Durgunoglu, H. T., Onalp, A., Seed, R. B., Christensen, C., Baturay, M. B., and Karadayılar, T. (2002). Correlation between ground failure and soil conditions in Adapazari, Turkey. Soil Dynamics and Earthquake Engineering 22(9–12): 1093-1102.

Sassa, K., Fukuoka, H., Wang, G., and Wang, F.(2007).Undrained Stress-controlled Dynamic-loading Ring-shear Test to Simulate Initiation and Post-failure Motion of Landslides. In Progress in Landslide Science. K. Sassa, H. Fukuoka, F. Wang, and G. Wang, eds. Pp. 81-98: Springer Berlin Heidelberg.

Seed H.B, Inc, United States. Army. Corps of Engineers, and U.S. Army Engineer Waterways Experiment Station (1989). Re-evaluation of the Lower San Fernando Dam: Examination of the post-earthquake slide of February 9, 1971. Report 2: U.S. Army Engineer Waterways Experiment Station.

Singh S. (1996). Liquefaction characteristics of silts. Geotechnical and Geological Engineering 14(1): 1-19.

Seed H. B., and Lee K. L., (1966). Liquefaction of saturated sands during cyclic loading. Journal of the Soil Mechanics and Foundations Division, 1966, 92 (6): 105 – 134.

Seed, H.B. (1979). Soil liquefaction and cyclic mobility evaluation for level ground during earthquakes. Journal of the Geotechnical Engineering Division, ASCE, 105(2): 201-255.

Sivathayalan, S. and D. Ha (2011). Effect of static shear stress on the cyclic resistance of sands in simple shear loading. Canadian Geotechnical Journal 48(10): 1471-1484.

Sitharam, T. and Dash, H. (2008). Effect of Non-Plastic Fines on Cyclic Behaviour of Sandy Soils. GeoCongress 2008: 319-326.

Stamatopoulos, C.A. (2010). An experimental study of the liquefaction strength of silty sands in terms of the state parameter. Soil Dynamics and Earthquake Engineering 30(8):662-678.

Stark, T.D. and G. Mesri (1992). Undrained Shear Strength of Liquefied Sands for Stability Analyses. Journal of Geotechnical Engineering, ASCE, 118(11): 1727-1747.

Stark, T.D., and Vettel, J. (1992). Bromhead Ring Shear Test Procedure. Geotechnical Testing Journal (1992), 15(1): 24-32.

Steedman, R. S., and Sharp, M. (1995). Liquefaction of deep saturated sands under high effective confining stress. Proc. 4th International Conference on Earthquake Engineering, G. Duma, Ed., Balkema, Rotterdam: 441 – 446.Taylor, D.W. (1952). A direct shear tests with drainage control, Symposium on Direct Shear Testing of Soils. ASTM International, West Conshohocken, PA:63-74.

Taylor, D.W. 1952. A direct shear tests with drainage control. Symposium on direct shear testing of soils, ASTM STP, 131: 63-74.

Tokimatsu, K., and Katsumata, K. (2012). Liquefaction-induced damage to buildings in Urayasu City during the 2011 Tohoku pacific earthquake. Proceedings of the

International Symposium on Engineering Lessons Learned from the 2011 Great East Japan Earthquake, March 1-4, Tokyo, Japan, pp. 665 – 674.

Toan, D. T., Komine, H., Murakami, S. and Duc, D. M. (2013). Grain size and soil suction effect on hydraulic conductivity and shear strength of simulated red river soil. Geotechnical Society of Singapore (GeoSS).

Vaid, Y.P, and Sivathayalan, S. (1996). Static and cyclic liquefaction potential of Fraser river sand in simple shear and triaxial tests. Canadian Geotechnical Journal, 33: 281-289.

Villalobos, F., Ovando, E., Mendoza, M., and Orostegui, P. (2011). Damages observed in the 2010 Concepcion earthquake related to soil phenomena, 5th International Conference on Earthquake Geotechnical Engineering, January 10 -13, Paper No. DOCVI.

Wakamatsu, K. (2012). Recurrent liquefaction induced by the 2011 great east Japan earthquake compared with the 1987 earthquake, Proceedings of the International Symposium on Engineering Lessons Learned from the 2011 Great East Japan Earthquake, March 1 – 4, 2012, Tokyo, Japan.

Wang, F., Sassa, K., Fukuoka, H. (1998). Cyclic-Loading Ring-Shear Tests to Study High-Mobility of Earthquake-Induced-Landslides. Environmental Forest Science, Springer Netherlands, 54: 575-582.

Wijewickreme, D., Sanin, M., and Greenaway, G., 2005, Cyclic Shear Response of Fine-grained Mine Tailings, Canadian Geotechnical Journal, Vol. 42, No. 5: 1408-1421.

Xenaki, V.C. & Athanasopoulos, G.A., 2003. Liquefaction resistance of sand–silt mixtures: an experimental investigation of the effect of fines. Soil Dynamics and Earthquake Engineering, 23: 183-194.

Yegian, M.K. (1980). Empirical Procedure for Pore Pressure Prediction in Sands. Proceedings of the Seventh World Conference on Earthquake Engineering, Istanbul, September.

Yamamuro, J. A., and Lade, P. V. (1997). Static liquefaction of very loose sands. Canadian Geotechnical. Journal, 34(6): 905–917.

Yamamuro, J. and K. Covert (2001). Monotonic and Cyclic Liquefaction of Very Loose Sands with High Silt Content. Journal of Geotechnical and Geoenvironmental Engineering 127(4): 314-324.Yegian, M. K. (1980). Empirical procedure for pore pressure prediction in sands. Proceedings of the 7th World Conference on Earthquake Engineering, Istanbul.

Yasuda, S., Verdugo, R., Konagai, k., Sugano, T., Villalobos, F., Okamura, M.,Tobita, T., Torres, A., and Towhata, I. (2010). Geotechnical damage caused by the 2010 Maule, Chile earthquake. ISSMGE Bulletin, 4(2): 16-27.

Yoshimine, M., and Koike, R. (2005). Liquefaction of clean sand with stratified structure due to segregation of particle size. Soils and Foundations, 45(4), 89-98.

Yoshimi, Y., K. Tokimatsu, Hosaka, Y. (1989). Evaluation of liquefaction resistance of clean sands based on high-quality undisturbed samples. Soils and Foundations 29(1): 93-104.

Youd, T. L., Harp, E. L., Keefer, D. K., Wilson, R. C. (1985). The Borah Peak, Idaho Earthquake of October 28, 1983-Liquefaction. Earthquake Spectra 2(1): 71-89.

Youd, T. L., Idriss, I. M. (2001). Liquefaction resistance of soils: Summary report from the 1996 NCEER and 1998 NCEER/NSF Workshops on Evaluation of Liquefaction Resistance of Soils. Journal of Geotechnical and Geoenvironmental Engineering 127(10): 817-833.

Yunmin, C., Han, K., Chen, R-P. (2005). Correlation of shear wave velocity with liquefaction resistance based on laboratory tests. Soil Dynamics and Earthquake Engineering 25(6): 461-469.

Zhang, L. (2010). A simple method for evaluating liquefaction potential from shear wave velocity. Frontiers of Architecture and Civil Engineering in China, 4(2): 178-195.

Zhou, Y., and Chen, Y. (2007). Laboratory Investigation on Assessing Liquefaction Resistance of Sandy Soils by Shear Wave Velocity. J. Geotech. Geoenviron. Eng., 133(8), 959–972.

Zhou, Y., Y. Chen, and Shamoto, Y. (2010). Verification of the Soil-Type Specific Correlation between Liquefaction Resistance and Shear-Wave Velocity of Sand by Dynamic Centrifuge Test. Journal of Geotechnical and Geoenvironmental Engineering 136(1): 165-177.

Chapter 3

3 Dynamic Behavior of Silt and Sandy Silt Soils in Cyclic Ring Shear Tests

3.1 Introduction

Shear wave velocity (also called S-wave or secondary wave velocity) is an important parameter used in many geotechnical earthquake engineering applications. It is used particularly for evaluating the liquefaction resistance of soils (Stokoe et al. 1988; Andrus et al. 1999; Youd et al. 2001) as V_s provides a convenient method for determining the small-strain shear modulus (G_o) of soils from the following relationship:

$$G_o = \rho V_s^2 \tag{3.1}$$

Where, G_o is in Pa, V_s in m/s, and ρ is soil density in kg/m^3. The small-strain shear modulus G_o is a useful parameter to characterize the elastic behaviour of soils in many geotechnical engineering applications. It can be used in the deformation analysis of soil (Wang and Lu 2003), in the design of foundations subjected to dynamic loading (Richart et al. 1970, El Naggar and Novak 1996; El Naggar 2004), and also to determine the shear modulus reduction curves of soils employed in seismic site response analysis (Sadrekarimi 2013; Kokusho 1980; Seed et al. 1986; Rollins et al. 1998).

The shear wave velocity can be easily measured in both field and laboratory settings. The in-situ V_s can be measured utilizing many techniques including the down-hole or cross hole seismic test, seismic cone penetration test (SCPT), suspension logging test, and spectral analysis of surface waves (SASW). In the laboratory, V_s is measured mainly through bender elements (Viggiani and Atkinson 1995; Lee and Santamarina 2005; Alvarado and Coop 2012) or resonant column tests (Khan et al. 2008; Khan et al. 2011; Cascante and Santamarina 1997) .

Normalized shear modulus (G/G_o) and material damping (D) relationships have been investigated by many previous researchers (Richart et al. 1970; Hardin and Drnevich 1972; Kokusho et al. 1982; Seed et al. 1986; Vucetic et al. 1998a; Stokoe et al. 1999; Roblee and Chiou 2004; Stokoe et al. 2004; Zhang et al. 2005) and used as inputs for the analysis of soil exposed to dynamic loads (earthquakes, machine loading, traffic vibration, wave loading). The relationship between G/G_o and shear strain (γ) is called the normalized shear modulus reduction curve, where G is the secant shear modulus which is obtained from the slope of the line connecting the tips of a cyclic stress-strain loop as illustrated in Figure 3.1 and using the following equation:

$$G = \frac{\tau_{max} - \tau_{min}}{\gamma_{max} - \gamma_{min}} \tag{3.2}$$

The damping ratio (D) of soils represents the energy dissipated in a soil element during a cycle of loading which is described as below:

$$D = \frac{W_D}{4\pi W_S} \tag{3.3}$$

where W_D is the energy dissipated in one cycle of loading, which is calculated from the area of the hysteresis cyclic loop and W_S is the maximum strain energy stored during the loading cycle which is equivalent to the area of the triangle shown in Figure 3.1.

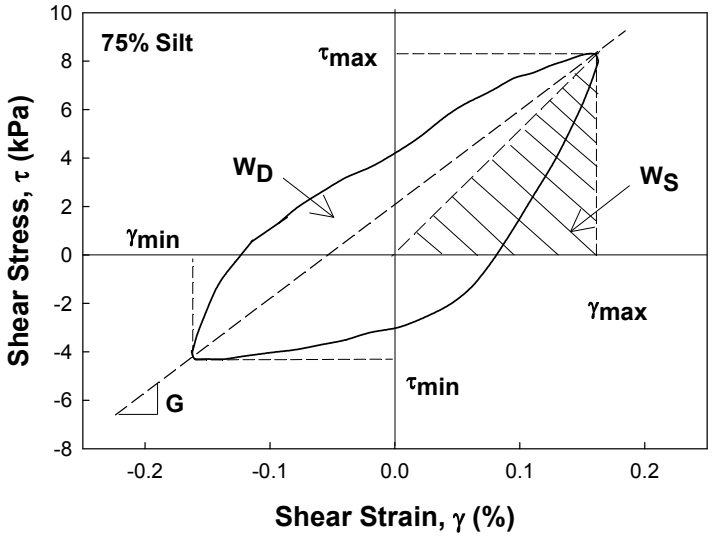

Figure 3.1: A cyclic hysteresis loop from a constant-volume cyclic ring shear test on a specimen with 75% silt content at $\gamma = 0.15\%$ and $\sigma'_{vc} = 100$ kP.

G and D have been investigated mainly by the resonant column tests (Wood 1994), because of the possibility to measure very small strains. On the other hand, cyclic triaxial, cyclic simple shear, and cyclic ring shear have been used to investigate the cyclic response of soils at larger shear strains (Vucetic et al. 1998b).

G/G_o and D are mainly affected by the soil type, shear strain and vertical effective consolidation stress (Stokoe et al. 1999; Roblee and Chiou 2004; Stokoe et al. 2004; Zhang et al. 2005). However other parameters such as void ratio, frequency of loading, degree of saturation, over consolidation ratio have been found to have less significant impact on both G/G_o and D (Darandeli 2001).

Past studies have shown that G/G_o decreases with increasing γ and D exhibits an increase with increasing γ from 0.0001% to 1% for most soil types (Stokoe et al. 2004; Zhang et al. 2005).

In the present study, a comprehensive laboratory testing program was conducted in order to characterize the elastic and cyclic behaviors of silts and sandy silts (with fines content > 50%) at very small and large shear strains. The elastic soil behavior at very small shear strains ($\gamma < 10^{-4}$%) was characterized by V_s measured by bender element tests. Moreover, strain-controlled constant-volume cyclic ring shear tests are conducted to establish shear modulus reduction and damping ratio curves for silts and sandy silts at shear strains, $\gamma >$ 0.01% and to describe the influence of silt content and shear strain amplitude (γ) on G and D.

3.2 Experimental Program

3.2.1 Materials Tested and Specimen Preparation

Reconstituted specimens of pure silica silt and sandy silts with 50% and 75% silt content were prepared and tested in this study. As shown in Figure 3.1, scanning electron microscopic images of the silt particles indicate very angular and irregular particle shapes. Table 3.1 summarizes the results of the index laboratory tests, which were conducted to determine the physical properties of each soil. The undercompaction moist tamping method (Ladd, 1978) was used to prepare homogeneous specimens. In this method, the cohesionless soil was thoroughly mixed with 5% moisture and tamped in 3 layers in the specimen chamber. The void ratio of each layer was adjusted (at an undercompaction ratio of 10%) in order to account for the densification of the lower layers by the compaction of the upper soil layers. The ring shear specimens had an annular shape with inner (R_i) and outer (R_o) radii of 48.3 mm, 76.1 mm, respectively, and an initial height (h) of 30 mm.

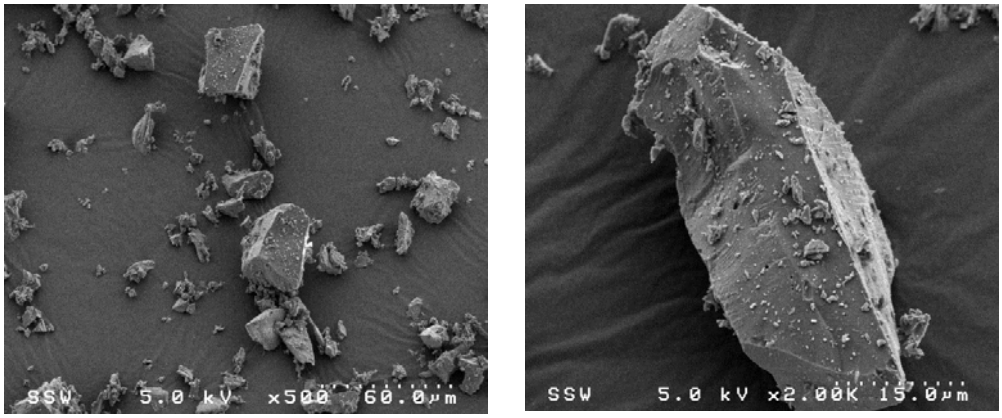

Figure 3.2: SEM images for the pure non-plastic silt (MIN-U-SIL 40) captured at Surface Science Western, Western University.

Table 3.1: Index properties of the soils used in the second study

Soil	Fines Content (%)	D_{50} (mm)	e_{max}	e_{min}	C_u	C_c
Silt	100	0.012	2.09	0.67	10.28	1.84
Sandy silt	75	0.029	1.48	0.58	5.40	0.82
	50	0.070	1.15	0.46	7.80	0.63
Ottawa Sand	0	0.450	0.74	0.42	1.38	1

C_u and C_c are coefficients of uniformity and curvature, respectively

3.2.2 Shear Wave Velocity Measurement

The shear wave velocity (V_s) traveling through the soil specimen was measured after the application of the consolidation stress by a pair of piezoelectric bender elements embedded in the upper and lower platens of the specimen chamber. These elements are constructed by the bonding of two piezoelectric materials. An electrical voltage applied to the element causes one of the piezoelectric films to expand, while the other film contracts. This leads to the deflection of the entire bender element. Similarly, the bender element produces an electrical voltage when it is bent by an external disturbance. A pulse of shear wave is generated by applying an electrical voltage to the source bender element, which is transmitted through the soil to the receiving element and subsequently converted into an output electrical voltage signal. The received signal is then amplified and recorded to determine the time of propagation of the shear wave between the source and receiver bender elements. The shear wave velocity of the specimen is calculated from the travel time (t) of the pulse and the tip-to-tip distance (d_{sr}) between the source and receiver bender elements, as below:

$$V_s = \frac{d_{sr}}{t} \tag{3.4}$$

Although the measurement of the travel distance (d_{sr}) is relatively straightforward, the detection of time of the first arrival of the shear wave is critical, as the calculation of V_s is very sensitive to the measured propagation time (t). The received shear wave is often distorted by noise, wave reflection from the boundaries, and near field effects which

make the visual detection of the first arrival time challenging and uncertain. Figure 3.3(a) shows that most of the signal was transmitted at frequencies less than 75 kHz and the response signal at higher frequencies was primarily noise. Accordingly, a low-pass filter with a cut-off frequency of 75 kHz was applied to the received signal to eliminate noise, as demonstrated in Figure 3.3.

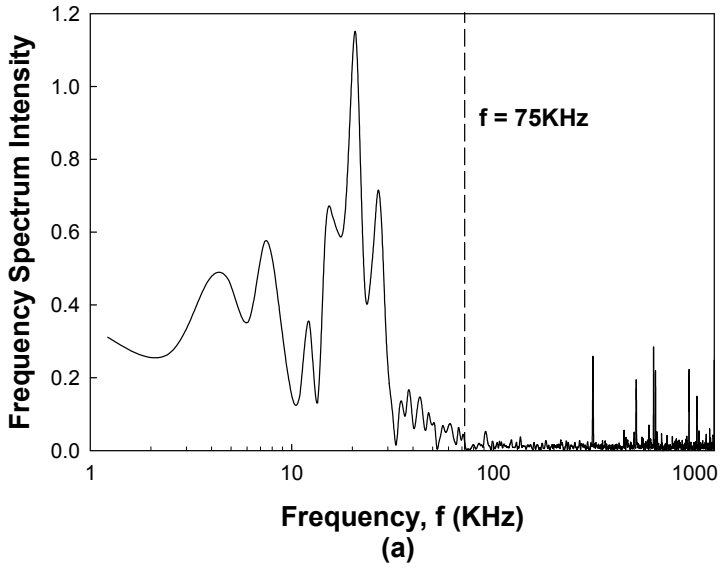

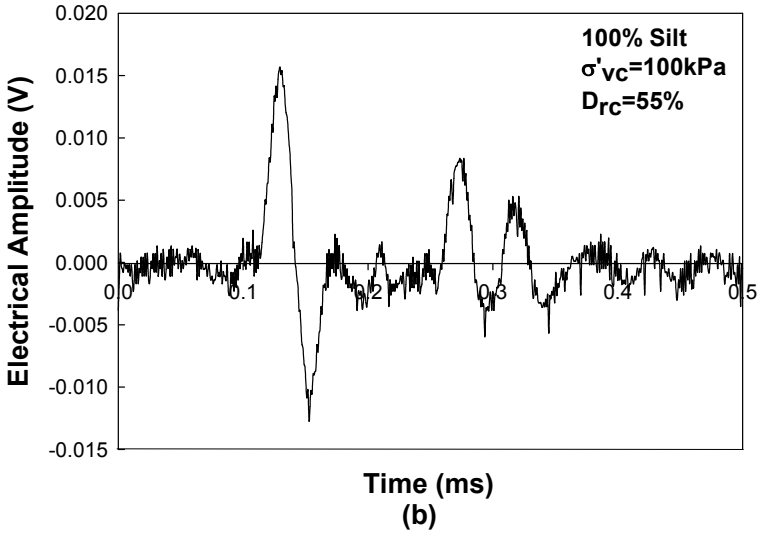

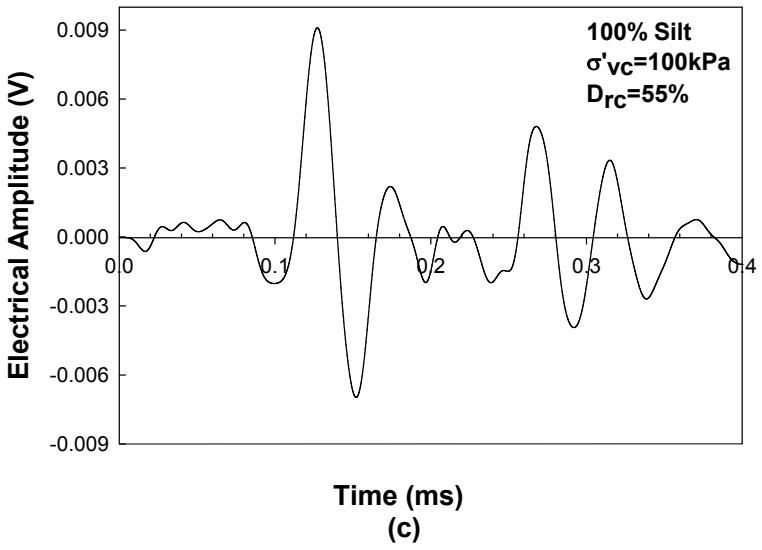

Figure 3.3: Typical electrical signal amplitude received by the bender element (a) in frequency domain, (b) in time-domain, and (c) in time-domain where the response at frequencies greater than 75 kHz has been filtered.

Despite the potential uncertainty, many studies (Viggiani and Atkinson 1995; Jovicic et al. 1996; Kawagushi et al. 2001; Greening 2001, Abbis 1981) show that the first major spike captured by the receiving bender element represents the incipient arrival signal. Several investigators suggest that the initial zero-crossing of the first major signal provides a reasonable estimate of V_s and G_o for silts and sands (e.g. Kawagushi et al. 2001; Lee and Santamarina, 2005; Baxter et al. 2008). This method would provide arrival times very close to the energy-rising interpretation method recently proposed by El Dean et al. (2013) based on dynamic finite difference analyses of bender element tests. Accordingly, as illustrated in Figure 3.4 the time of the initial zero-crossing of the first

major electrical signal captured by the receiving bender element was used in this study for the measurement of propagation time and V_s.

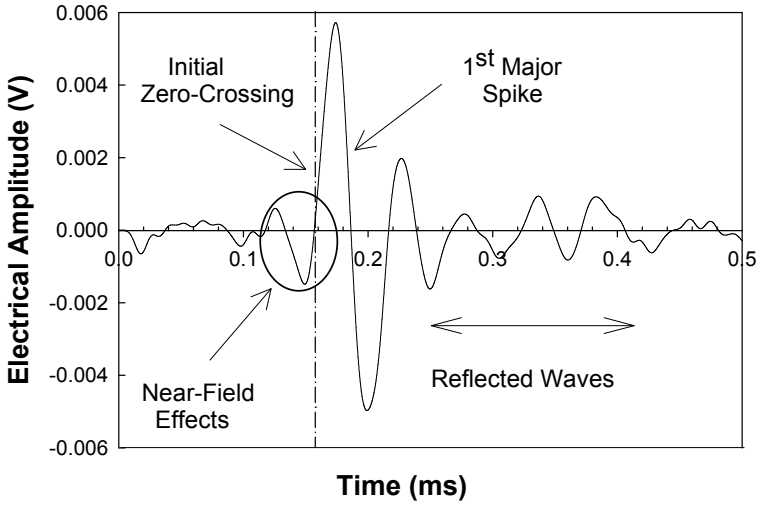

Figure 3.4: Typical electrical signal received by the bender element and the interpretation of shear wave arrival time in this study for a pure silt specimen at D_{rc} = 35% and σ'_{vc} = 100 kPa.

The shear wave velocity of the specimens were measured at σ'_{vc} ranging from 50 to 300 kPa, in 50 kPa increments. Figures 3.5 and 3.6 show typical examples of the shear waves transmitted through pure silt specimens over the range of σ'_{vc}. Because of the large compressibility of silt, the increase in σ'_{vc} was followed by a significant decrease in void ratio and increase in D_{rc} of the tested specimens. Therefore, the reduction in the arrival times and increase in V_s shown in Figures 3.5 and 3.6 reflect the impact of increasing both σ'_{vc} and D_{rc} of the specimens. Figures 3.7 to 3.10 present similar plots for a range of

sand and silt mixtures tested in this study, which demonstrate the increasing of V_s as D_{rc} and σ'_{vc} increase. Appendix B provides the complete details and results of shear wave velocity measurements.

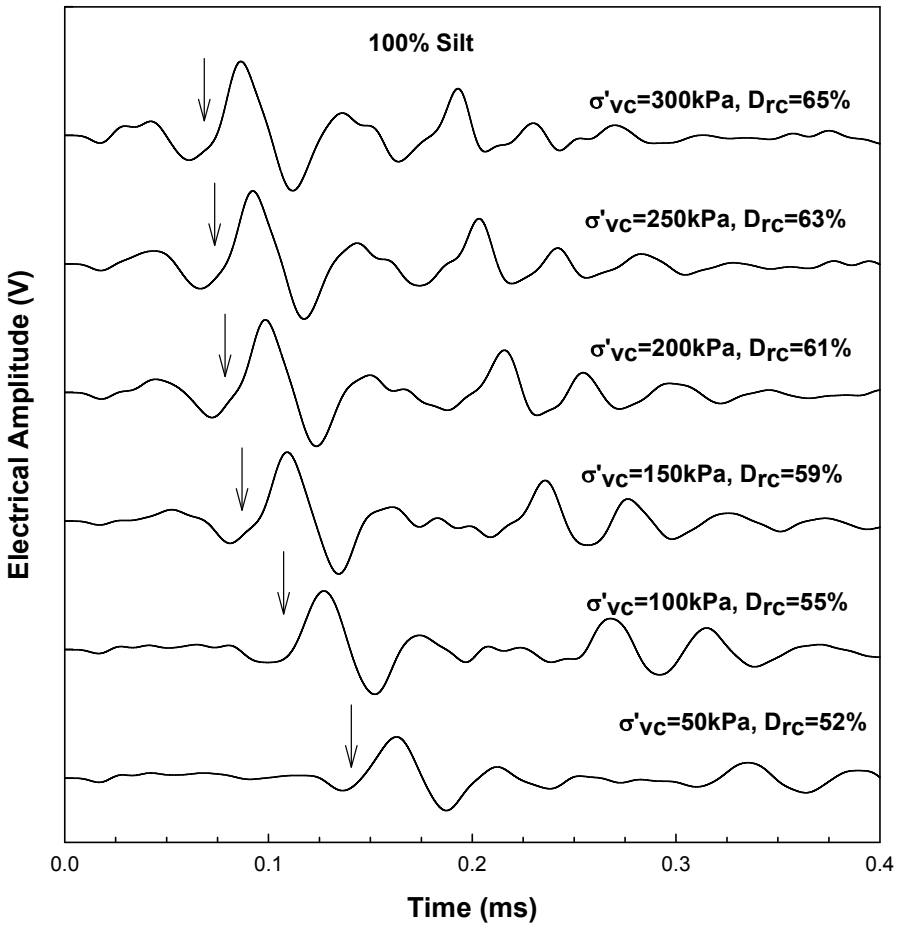

Figure 3.5: Electrical wave signals captured by the bender element over a range of σ'_{vc} = 50 - 300 kPa in pure silt specimens.

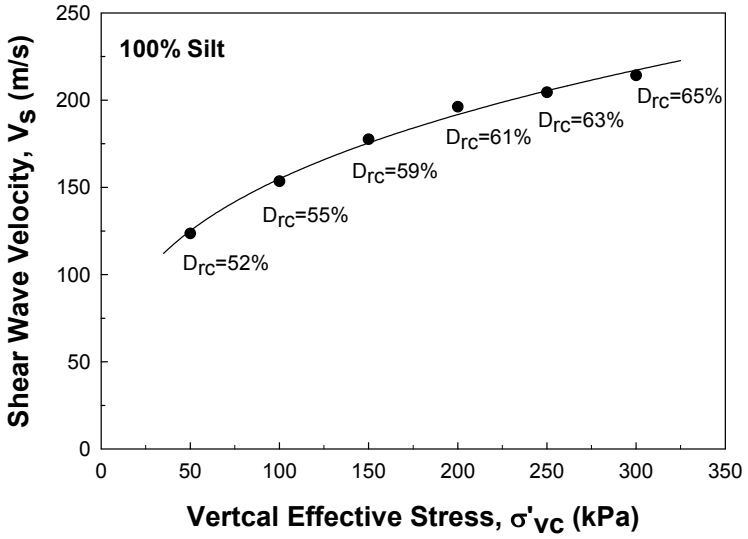

Figure 3.6: Shear wave velocity versus σ'_{vc} over a range of σ'_{vc} = 50 - 300 kPa in pure silt specimens.

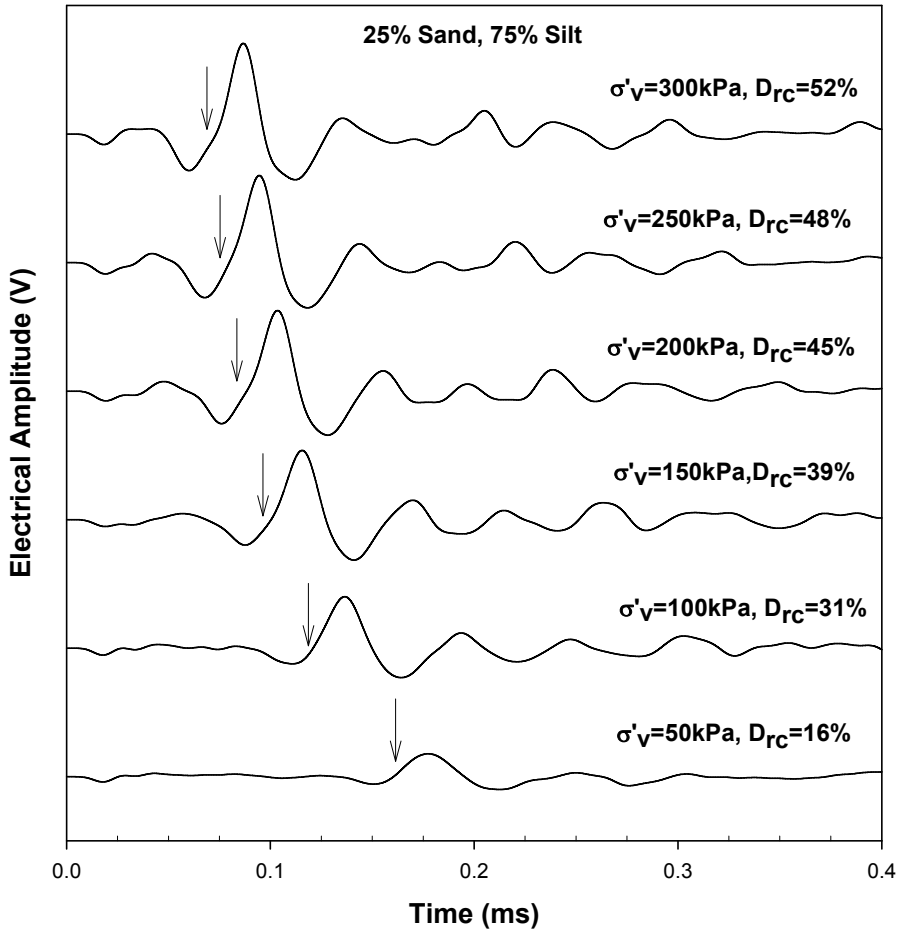

Figure 3.7: Electrical wave signals captured by the bender element and over a range of σ'_{vc} = 50 - 300 kPa in specimens of 75% silt content.

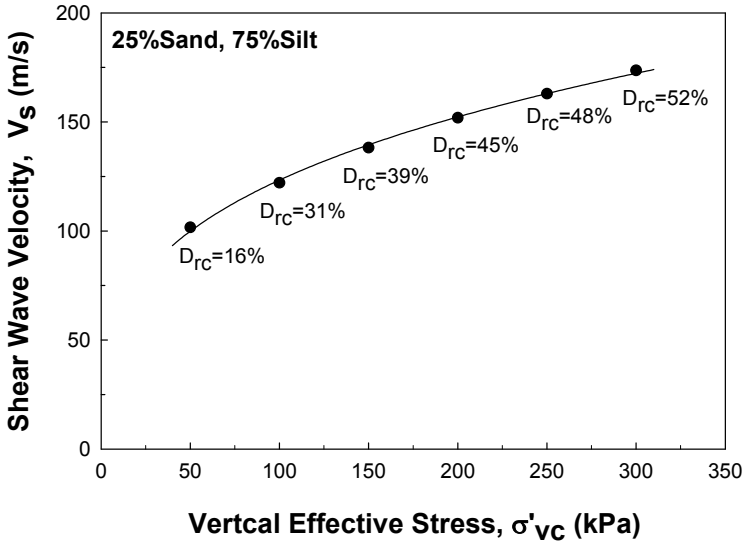

Figure 3.8: Shear wave velocity versus σ'_{vc} over a range of σ'_{vc} = 50 - 300 kPa in specimens of 75% silt content.

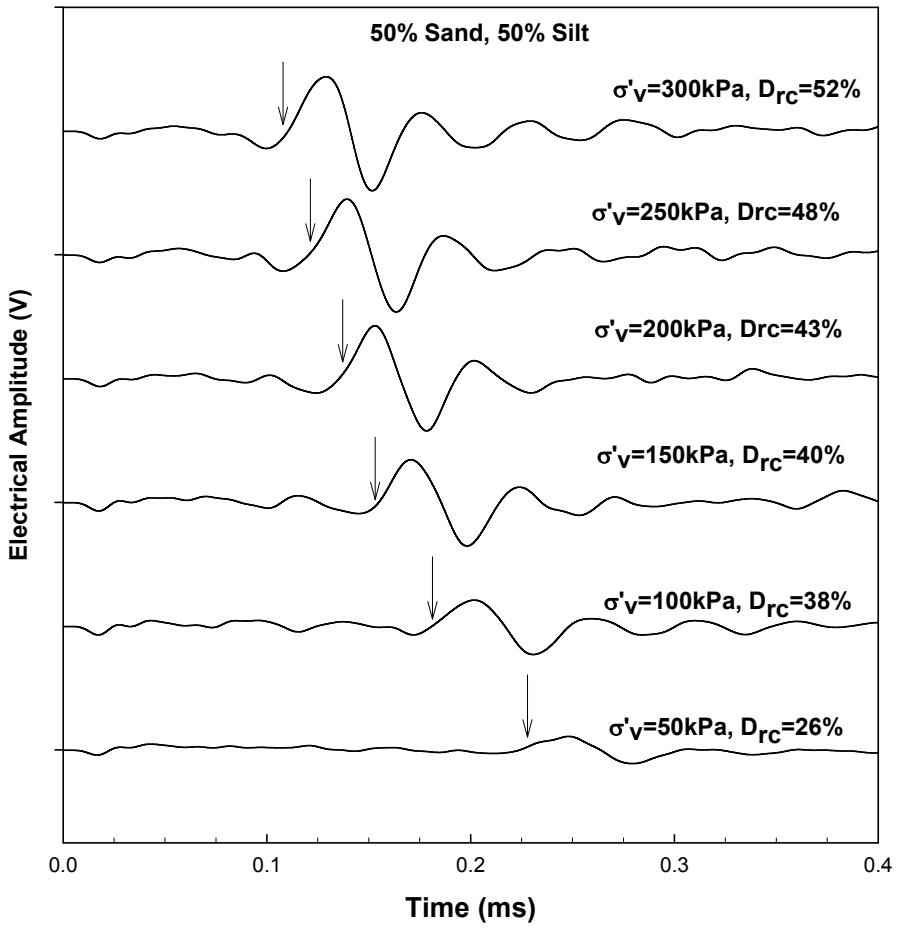

Figure 3.9: Electrical wave signals captured by the bender element over a range of σ'_{vc} = 50 - 300 kPa in specimens of 50% silt content.

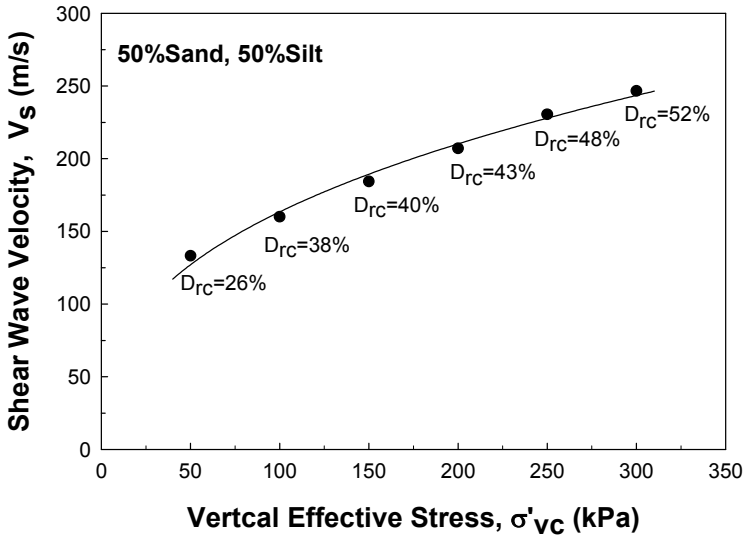

Figure 3.10: Shear wave velocity versus σ'_{vc} over a range of σ'_{vc} = 50 - 300 kPa in specimens of 50% silt content.

3.2.3 Cyclic Ring Shear Testing and Results

To investigate the cyclic behaviour of silts and sandy silts at large strain level ($\gamma > 0.01\%$), a separate series of strain-controlled constant-volume cyclic ring shear tests were carried out. All specimens were first consolidated to σ'_{vc} = 100 kPa and then subjected to increasing levels of cyclic shear strain amplitudes at a frequency 0.1 Hz. Figure 3.11 shows a typical example of the stress-strain loops at different strain levels for a soil specimen of 75% silt content. These results generally show that the cyclic response of the tested soils is a function of shear strain amplitude. According to Figures 3.11(a) to 3.11(c), with the increase in the shear strain amplitude the stress-strain loops change and become more slender (i.e. S-shaped). This change in the shapes of the cyclic stress-strain

loops had a significant impact on the damping behavior of the silt and sandy silt specimens as subsequently explained in this paper.

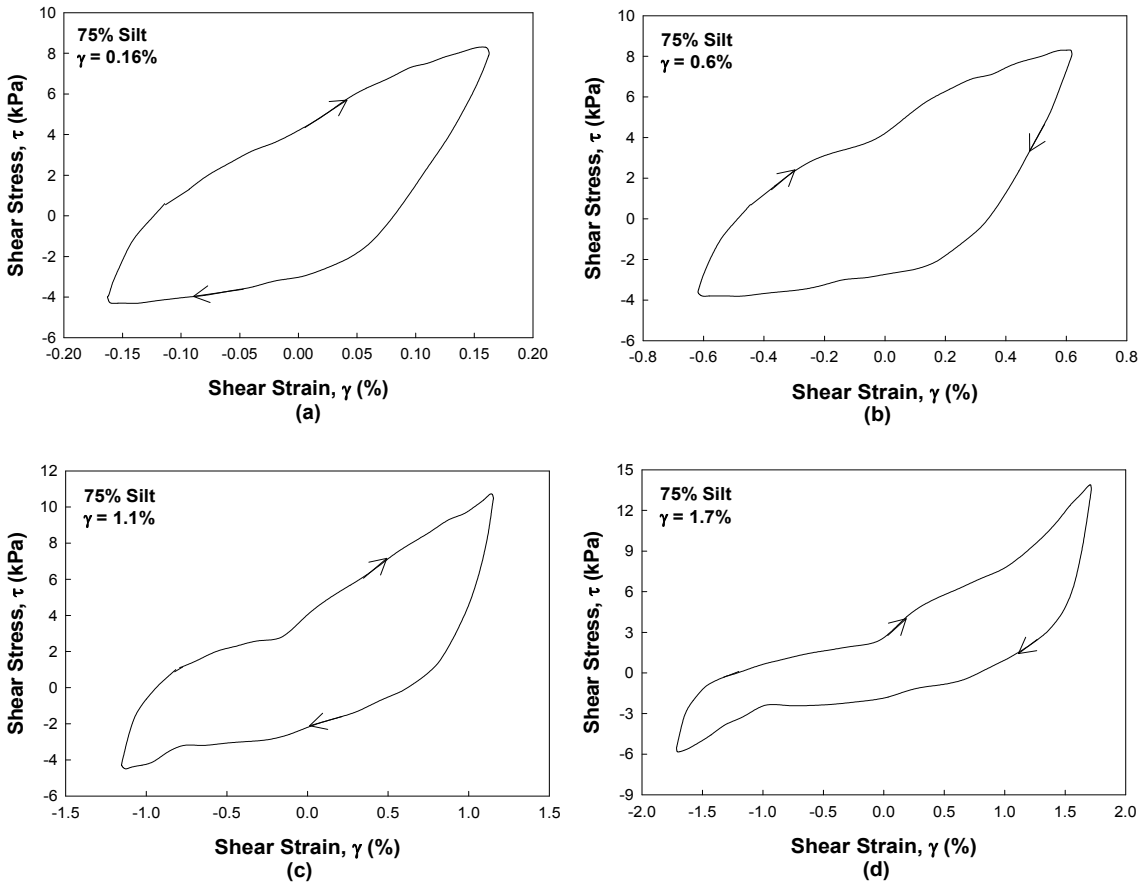

Figure 3.11: Cyclic stress-strain response of a soil specimen at 75% silt content in a constant-volume strain-controlled cyclic ring shear test: (a) at $\gamma = 0.16\%$, (b) at $\gamma = 0.6\%$, (c) at $\gamma = 1.1\%$, and (d) at $\gamma = 1.7\ \%$.

3.3 Discussion

In the following paragraphs, the results of this study are discussed for characterizing soil behavior at increasing shear strain levels (γ). This includes elastic soil behavior at very small shear strains ($\gamma < 10^{-4}\%$) followed by plastic soil behavior at larger shear strains ($\gamma > 0.01\%$).

3.3.1 Elastic Soil Behavior at Small Shear Strains ($\gamma < 10^{-4}\%$)

The small strain soil behavior is characterized by the shear wave velocity transmitted through the soil which is measured from the bender elements response and the small-strain maximum shear modulus (G_o) obtained from Equation (3.1).

Figure 3.12 summarizes G_o of the silt and sand mixtures versus their initial void ratios (e_c). According to this figure, G_o sharply decreases with increasing e_c for each soil mix. G_o also increases with increasing silt content, particularly from FC = 75% to pure silt and at denser void ratios. However, the influence of FC on G_o is not as significant as that of e_c. In fact, with decreasing e_c or increasing silt content, the number of particle contacts increases and, the shear wave is transmitted through a larger number of particle contacts resulting in higher V_s and G_o.

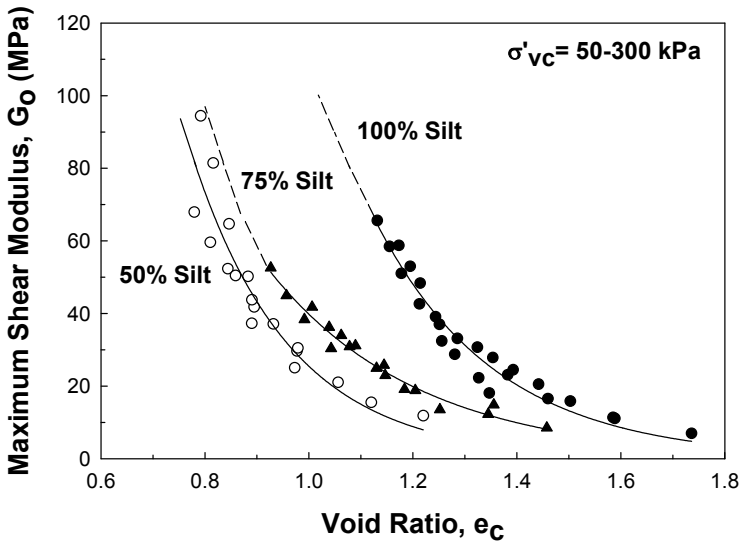

Figure 3.12: Effect of e_c and silt content on maximum shear modulus at small shear strains.

The general relationship between e_c and G_o is provided below (Kramer 1996):

$$G_o = 625F(e)(OCR)^k p_a^{1-n}(\sigma'_m)^n \tag{3.5}$$

In which F(e) is a function of void ratio, OCR is the overconsolidation ratio, k is an OCR exponent, n is a stress exponent (often taken as 0.5 for sands), σ'_m is the effective mean stress, and p_a is the atmospheric pressure (= 101 kPa) with the same unit as σ'_m and G_0. As the specimens tested in this study were all normally consolidated with constrained lateral deformation, OCR = 1 and σ'_m is calculated from $\sigma'_{vc}(1+2K_o)/3$ based on the assumption of $K_o = 1 - \sin(\phi') = 0.42$ corresponding to an average $\phi' = 35^o$ for the silt and sand mixtures of this study.

Different empirical correlations have been proposed for F(e) by different researchers, some of which are summarized below:

Richart (1970): $F(e) = \frac{(2.97-e)^2}{1+e}$ (3.6)

Hardin (1978): $F(e) = \frac{1}{0.3+0.7e^2}$ (3.7)

Jamiolkowski (1991): $F(e) = \frac{1}{e^{1.3}}$ (3.8)

Similar to these studies, the shear wave velocity and G_o measurements of this study are used to determine F(e) for each soil mix. The following correlations are curve-fitted for the pure silt and sandy silt specimens:

For pure silt: $F(e) = \frac{0.53}{e^{2.1}}$ (3.9)

For sandy silts (FC = 75% and 50%): $F(e) = \frac{1.26}{e^{3.52}}$ (3.10)

Figure 3.13 presents the normalized maximum shear modulus, $G_o / 6250(\sigma_m^{'})^{0.5}$ and e_c from the results of this study along with Eqs. 7 and 8.

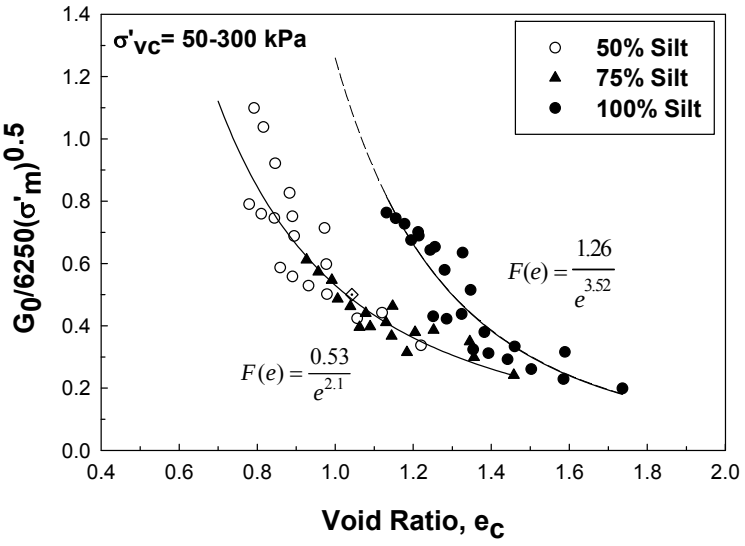

Figure 3.13: Normalized maximum shear modulus ($G_o/6250(\sigma'_m)^{0.5}$) and e_c for the silt and sand mixtures of this study

The V_s measurements at multiple magnitudes of σ'_{vc} are further used to evaluate the existing relationships for the stress normalization of V_s and develop a representative relationship for normalizing V_s at σ'_{vc} = 100 kPa (V_{s1}). As illustrated in Figure 3.14, the relationship between V_{s1}/V_s and σ'_{vc} can be described by a power function for the silts and sandy silt of this study as below:

For pure silt and sandy silts with FC = 75%: $$\frac{V_{s1}}{V_s} = \left(\frac{P_a}{\sigma'_{vc}}\right)^{0.31} \quad (3.11)$$

For sandy silts with FC = 50%: $$\frac{V_{s1}}{V_s} = \left(\frac{P_a}{\sigma'_{vc}}\right)^{0.35} \quad (3.12)$$

Where P_a is the atmospheric pressure. The stress exponent which varies from 0.31 (for 100% and 75% silt contents) to 0.35 (for 50% silt content), is greater than that (0.25) suggested by Idriss and Boulanger (2008).

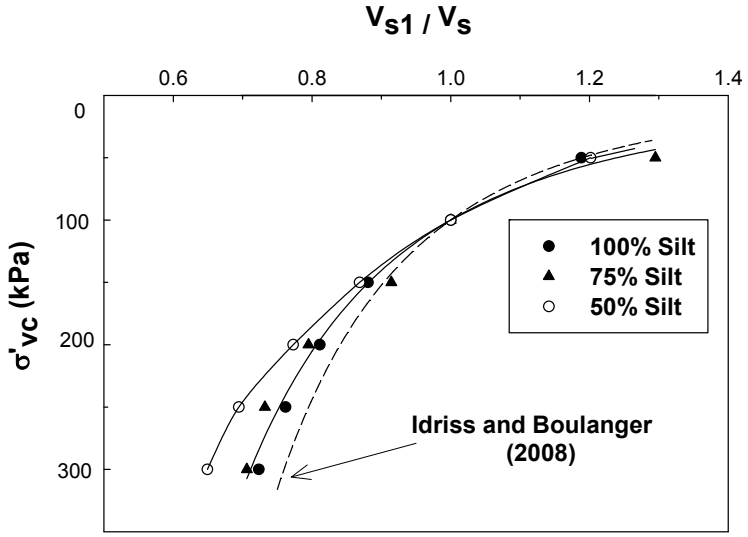

Figure 3.14: Relationship between normalized shear wave velocity (V_{s1}/V_s) and σ'_{vc} for the silt and sand mixtures of this study.

3.3.2 Soil Behavior at Large Shear Strains ($\gamma > 0.01\%$)

Soil behavior at large strains ($\gamma > 0.01\%$) is determined from the results of the cyclic ring shear tests and characterized by shear modulus (G), and damping ratio. These parameters and their relationships with the large strain soil parameters are described below.

3.3.2.1 Shear Modulus at Large Strains (γ > 0.01%)

The shear stiffness of soil decreases with increasing shear strain. Figure 3.15 illustrates a typical shear stress – strain loop from a cyclic ring shear test on pure silt specimen. The secant shear modulus (G) is the slope of the line connecting the tips of the stress-strain loop.

As demonstrated in Figure 3.15, the slope of the stress-strain cyclic loops and thus G progressively decrease with the number of loading cycles and the cyclic shear strain amplitude, γ_{cyc}. The reduction of soil stiffness is presented by the shear modulus reduction curves (G/G_o) in Figure 3.16. This figure shows that G/G_o decreases as γ_{cyc} increases for the pure silt and sandy silt specimens.

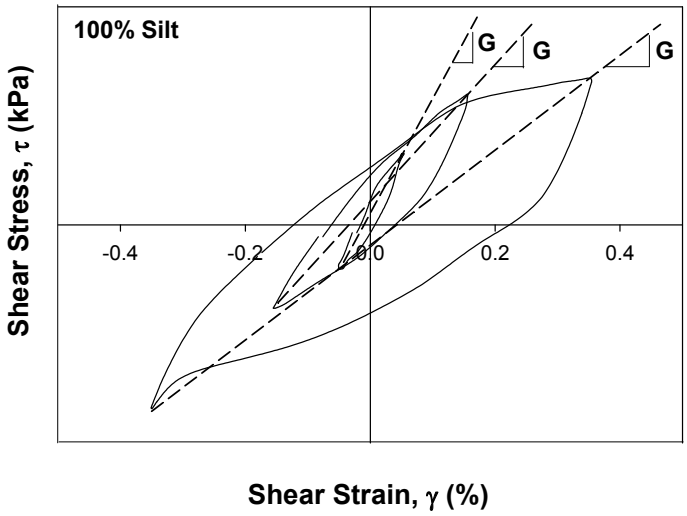

Figure 3.15: Cyclic hysteresis loops for pure silt specimens at σ'_{vc} = 100 kPa.

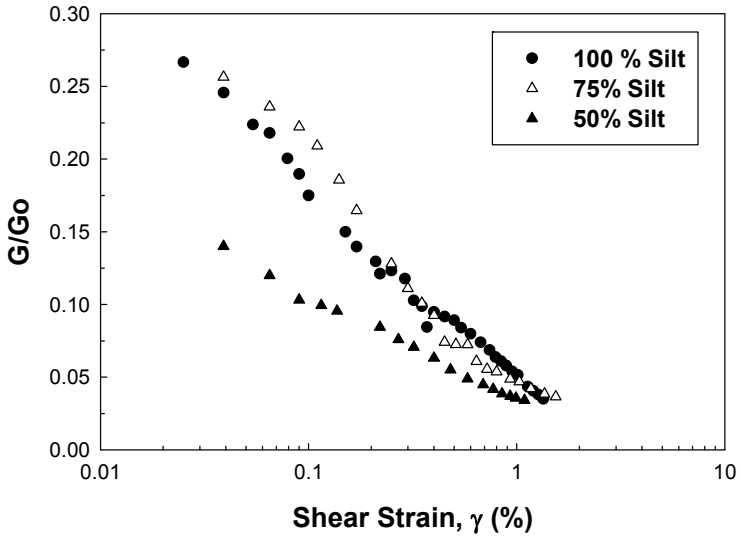

Figure 3.16: Shear modulus reduction curves for pure silt and sandy silt specimens at σ'_{vc} = 100 kPa.

3.3.2.2 Cyclic Damping Ratio at Large Strains (γ > 0.01%)

With increase in the number of cycles and shear strain amplitude, the areas of hysteresis loops (W_D) increase which reflects the increase in the amount of energy dissipated in each cyclic loading with increasing γ_{cyc}. When shear strain reaches a threshold value at around 1%, the area of hysteresis loops start to decrease with increasing shear strain and as illustrated in Figure 3.11 this leads to the reduction of the amount of dissipated energy, W_D. As a result, the damping ratio increases with γ_{cyc} until a threshold strain (1%) after which D starts to decrease as presented in Figure 3.17. Contrary to other studies (e.g., Stokoe et al. 2004; Zhang et al. 2005) that show damping ratio only increases with increasing shear strain, this study shows that the cyclic response and whether the

damping ratio would increase or decrease with γ_{cyc} depends on the level of cyclic shear strain. This would have significant implications on site response analysis and evaluating the amount of energy transferred through silts and sandy silts subjected to large magnitude earthquakes. Figure 3.17 further indicates that the damping ratio tends to decrease with increasing silt content from 50% to 100%.

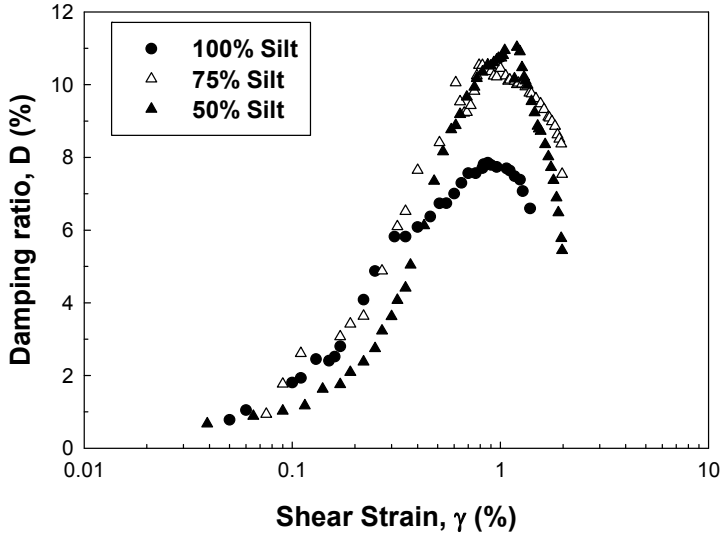

Figure 3.17: Material damping ratio versus γ_{cyc} for pure silt and sandy silt specimens at σ'_{vc} = 100 kPa.

3.4 Summary and Conclusions

A comprehensive laboratory testing program was conducted in this study in order to characterize the dynamic behaviour of silt and sandy silt with 25% and 50% sands at increasing levels of shear strain (γ). The elastic soil behavior at very small shear strains

($\gamma < 10^{-4}\%$) was investigated through shear wave velocity (V_s) measurements using bender elements at vertical stresses ranging from 50 to 300 kPa, while strain-controlled constant-volume cyclic ring shear tests were conducted to establish shear modulus (G) and damping ratio (D) for silts and sandy silts at larger shear strain amplitudes ($\gamma > 0.01\%$). The results demonstrated that V_s and the maximum shear modulus (G_o) significantly decrease with increasing void ratio. V_s was found to increase with increasing effective overburden stress to the power of 0.31 - 0.34 for all silt and sandy silt mixes. The results further showed that while G decreases with increasing γ, D increases with increasing γ only up to $\gamma < 1\%$, beyond which it exhibits a decreasing trend.

3.5 References

Abbiss, C. P. (1981). Shear wave measurements of the elasticity of the ground. Geotechnique, 31(1), 91–104.

Alvarado, G. and Coop, M.R. (2012). On the performance of bender elements in triaxail tests. Geotechnique 62(1):1-17

Andrus, R. D., Stokoe, K. H., II, and Chung, R. M. (1999). Draft guidelines for evaluating liquefaction resistance using shear wave velocity measurements and simplified procedures. NISTIR 6277, National Institute of Standards and Technology, Gaithersburg, Md.

Baxter, C., Bradshaw, A., Green, R., Wang, J. (2008). Correlation between Cyclic Resistance and Shear-Wave Velocity for Providence Silts. Journal of Geotechnical and Geoenvironmental Engineering 134(1): 37-46.

Cascante, G., and Santamarina J., 1997. Low Strain Measurements with a Resonant-Column Apparatus. Geotechnical Testing Journal, 20(1): 29-39.

El Dean, G., Lefebvre, G., and Karray, M. (2013). Wave propagation and interpretation of bender elements pulse tests. Proceedings of the GeoMontreal 2013 conference, Montreal, Canada.

Darendeli, M. B. (2001). Development of a new family of normalized modulus reduction and material damping curves. PhD dissertation, Univ. of Texas at Austin, Austin, Tex.

El Naggar, M.H. and Novak, M. (1996). Nonlinear analysis of dynamic lateral pile response. Soil Dynamics and Earthquake Engineering, 15(4): 233–244

El Naggar, M.H. (2004). The 2002 Colloquium Address: The role of soil-structure interaction in foundation engineering. Canadian Geotechnical Journal, 41(3): 485-509.

Greening, P. D. & Nash, D. F. T. (2004). Frequency domain determination of G_o using bender elements. Geotech. Test. J. 27(3): 288–294.

Hardin, B.O., and Drnevich, V.P (1972). Shear modulus and damping of soils, measurements and parameters effects. Journal of the Soil Mechanics and Foundations Divivon, 98(SM7): 667-692.

Hardin, B.A. (1978). The nature of stress-strain behavior of soils. Proceedings, Earthquake Engineering and Soil Dynamics, ASCE Pasadena, California, Vol. I, pp. 3-89.

Idriss, I. M., Boulanger, R. W. (2008). Soil Liquefaction During Earthquakes, Earthquake Engineering Research Institute.

Jamiolkowski, M., Leroueil, S., And Lopresti, D.C.F. (1991). Theme lecture: Design parameters from theory to practice. Proceedings, Geo-Coast, Yokohama, Japan, pp. 1-41.

Jovicic, V., Coop, M. R., and Simic, M. (1996). Objective criteria for determining Gmax from bender element tests. Geotechnique, 46(2), 357–362.

Kawaguchi, T., Mitachi, T., and Shibuya, S. (2001). Evaluation of shear wave travel time in laboratory bender element test. Proc., 15th Int. Conf. on Soil Mechanics and Geotechanics Engineering 155–158.

Khan, Z., El Naggar, M.H. and Cascante, G. 2011. Frequency dependent dynamic properties from resonant column and cyclic triaxial tests. J. Franklin Institute, 348: 1363-1376.

Khan, Z., Cascante, G., El Naggar, M.H. and Lai, C.G. 2008. Measurement of frequency dependent dynamic properties of soils using the resonant column device. Journal of Geotechnical and Geoenvironmental Engineering, ASCE, 134(9): 1319-1326.

Kokusho, T. (1980). Cyclic triaxial test of dynamic soil properties for wide strain range. Soils and Foundations 20(2): 45–60.

Kokusho, T., Yoshida, Y., and Esashi, Y. (1982). Dynamic properties of soft clay for wide strain range. Soils Found., 22(4): 1–18.

Kramer, L.K. (1996). Geotechnical Earthquake Engineering. Prentice Hall in Civil Engineering and Engineering Mechanics, Upper Saddle River, NJ.

Ladd, R.S. (1978). Preparing Test Specimen Using Undercompacton. Geotechnical Testing Journal 1(1):16-23.

Lee, J., and Santamarina J. (2005). Bender Elements: Performance and Signal Interpretation. Journal of Geotechnical and Geoenvironmental Engineering 131(9): 1063-1070.

Richart, F. E., Hall, J. R., and Woods, R. D. (1970). Vibrations of soils and foundations, Prentice-Hall, Englewood Cliffs, N.J., 152–156.

Rollins, K. M., Evans, M. D., Diehl, N. B., and Daily, W. D. (1998). Shear modulus and damping relationships for gravels. Journal of Geotechnical and Geoenvironmental Engineering, ASCE 124(5), 396–405.

Roblee, C., and Chiou, B. (2004). A proposed geoindex model for design selection of non-linear properties for site response analysis. Proc., NSF/PEER Int. Workshop on Uncertainties in Nonlinear Soil Properties and their Impact on Modeling Dynamic Soil Response, Univ. of California at Berkeley, Berkeley, California.

Sadrekarimi, A. (2013). Dynamic Behavior of Granular Soils at Shallow Depths from 1 g Shaking Table Tests. Journal of Earthquake Engineering 17(2): 227-252.

Seed, H. B., Wong, R. T., Idriss, I. M., and Tokimatsu, K. (1986). Moduli and damping factors for dynamic analyses of cohesionless soils. Journal of Geotechnical Engineering, ASCE 112(11): 1016–1032.

Stokoe, K. H., II, Nazarian, S., Rix, G. J., Sanchez-Salinero, I., Sheu, J.-C., and Mok, Y. J. (1988). In situ seismic testing of hard-to-sample soils by surface wave method. Earthquake engineering and soil dynamics II—Recent advances in ground-motion evaluation, Geotech. Spec. Publ. No. 20, J. L. Von Thun, ed., ASCE, New York, 264–289.

Stokoe, K. H., II, Darendeli, M. B., Andrus, R. D., and Brown, L. T. (1999). Dynamic soil properties: Laboratory, field and correlation studies. Proc., 2nd Int. Conf. on Earthquake Geotechnical Engineering, Vol. 3, Lisbon, Portugal, 811–845.

Stokoe, K. H., II, Darendeli, M. B., Gilbert, R. B., Menq, F.-Y., and Choi, W.-K. (2004). Development of a new family of normalized modulus reduction and material damping curves. Proc., NSF/PEER Int. Workshop on Uncertainties in Nonlinear Soil Properties and their Impact on Modeling Dynamic Soil Response, Univ. of California at Berkeley, Berkeley, California.

Viggiani, G., Atkinson, J.H., 1995. Interpretation of bender element tests. Géotechnique, 45(1):149-154.

Vucetic, M., Lanzo, G., and Doroudian, M. (1998a). Damping at small strains in cyclic simple shear test. Journal Geotech. Geoenviron. Eng., 124(7): 585–594.

Vucetic, M., Lanzo, G., and Doroudian, M., (1998b). Damping at Small Strains in Cyclic Simple Shear Test. Journal of Geotechnical and Geoenvironmental Engineering 124(7): 585-594.

Wang, Z. and Y. Lu (2003). Numerical analysis on dynamic deformation mechanism of soils under blast loading. Soil Dynamics and Earthquake Engineering 23(8): 705-714.

Woods, R. D. (1994). Laboratory measurements of dynamic soil properties. Dynamic Geotechnical Testing II, ASTM STP 1213, ASTM, West Conshohocken, Pa., 165-190.

Youd, T. L., I. M. Idriss, et al. (2001). Liquefaction resistance of soils: Summary report from the 1996 NCEER and 1998 NCEER/NSF Workshops on Evaluation of Liquefaction Resistance of Soils. Journal of Geotechnical and Geoenvironmental Engineering 127(10): 817-833.

Zhang, J. (2004). Characterizing the dynamic properties of South Carolina soils for ground motion evaluation. PhD dissertation, Clemson Univ., Clemson, S.C.

Chapter 4

4 Post-Cyclic Monotonic Response of Silt and Sandy Silt Soils

4.1 Introduction

Field case studies on the post-liquefaction response of liquefied soils show that soils can develop some shear resistance after liquefaction (Castro 1969; Seed 1979; Babbitt et al. 1983; Smart and Von Thun, 1983) which is referred to as the undrained liquefied shear strength, s_u(liq) (Stark and Mesri 1992). The undrained liquefied shear strength is an important parameter required for evaluating the stability of an earth deposit or geotechnical structure against post-liquefaction failure. Accordingly the undrained shear strength properties of liquefied soils for post-liquefaction stability analysis have become an important aspect of liquefaction assessment besides the evaluation of conditions that would trigger liquefaction. The post liquefaction resistance of cohesionless soils has been studied by many researchers (Pillai 1994; Vaid and Thomas 1995; Stark et al. 1998; Olson and Stark 2003a, b; Idriss and Boulanger 2008; Sadrekarimi and Olson 2011). Liquefied shear strength is estimated either from correlations with in-situ field tests (SPT or CPT) or directly measured in laboratory shear tests. Although several correlations have been developed for estimating s_u(liq) from in-situ penetration resistances often based on case histories from past liquefaction events (Seed and Harder 1990; Stark and Mesri 1992; Ishihara 1993; Olson and Stark 2003a; Idriss and Boulanger 2008), there are a

number of limitations associated with these empirical methods including inaccuracies in the back analysis of s_u(liq), limited number of case histories, and uncertainties in identifying liquefied soil zones and representative penetration resistances. Accordingly, although these empirical correlations are still more popular in engineering practice, laboratory triaxial shear (Sadrekarimi and Oslon 2011; Sitharam et al. 2013; Huang et al. 2012), direct simple shear (Wijewickreme and Sanin 2010) or ring shear tests (Sadrekarimi and Olson 2011) on reconstituted or undisturbed samples obtained by ground freezing are also employed for the determination of s_u(liq) of cohesionless soils. Most of the past experimental studies have focused on estimating s_u(liq) of clean sands or silty sands with only up to 30% fines contents (e.g. Ishihara 1993; Sitharam and Dash 2009; Vaid 1994; Yamamuro and Lade 1998; Sitharam et al. 2013), while the effect of fines may continue to increase with increasing fines content (FC) beyond 30%. In particular, the post-liquefaction behavior and s_u(liq) of sandy silts (FC > 50%) and silts is not adequately investigated compared to silty sands and clean sands.

In this paper, the post-cyclic behavior and s_u(liq) of non-plastic silt and sandy silts is investigated in a series of displacement-controlled monotonic ring shear tests following stress-controlled cyclic shearing using an advanced ring shear apparatus.

4.2 Materials Tested and Specimen Preparation

Reconstituted specimens of pure silt and sandy silts with 50% and 75% silt contents were prepared and tested in the experimental program. The index properties of each mix are summarized in Table 4.1. The moist tamping undercompaction method (Ladd 1978) was

used to prepare all specimens. In this method, the soil is mixed at 5% moisture content and subsequently poured and tamped in 3 layers in the specimen mold. In order to ensure specimen uniformity, each layer was tamped slightly looser than the overlying sublayer to account for the additional densification produced by the tamping of the overlying soil layers. The annular ring shear specimens had inner (R_i) and outer (R_o) radii of 48.3 mm and 76.1 mm, respectively with an initial height (h) of 30 mm.

Table 4.1: Index properties of the soils used in the third study

Soil	Fines Content (%)	D_{50} (mm)	e_{max}	e_{min}	C_u	C_c
Silt	100	0.012	2.09	0.67	10.28	1.84
Sandy silt	75	0.029	1.48	0.58	5.40	0.82
	50	0.070	1.15	0.46	7.80	0.63
Ottawa Sand	0	0.450	0.74	0.42	1.38	1

C_u and C_c are coefficients of uniformity and curvature, respectively

4.3 Laboratory Testing Procedure

Cyclic and monotonic constant-volume ring shear tests were conducted on moist (5% moisture content) specimens using an advanced ring shear testing apparatus at the soil mechanics laboratory of Western University. All specimens were consolidated to a vertical stress (σ'_{vc}) of 100 kPa. After consolidation and prior to the application of the cyclic shear load, the upper loading platen was locked in place against any vertical movement to maintain a constant-volume condition. Uniform cyclic stress ratios, CSR = τ_{cyc}/σ'_{vc} of 0.075 to 0.225 were applied in the ring shear test until a large excess pore water pressure ratio, $r_u = \Delta u/\sigma_{vc} > 0.9$ was developed. The total number of cycles

and the cumulative amount of the loading and unloading shear strains (double-amplitude shear strain, γ_{DA}) incurred to develop $r_u > 0.9$ were recorded. After the application of the cyclic shear loads, the specimens were immediately subjected to displacement-controlled constant-volume monotonic shear tests (approach 1), which replicated the conditions of landslide or flow failure following a cyclic loading event (e.g. earthquake). In another set of tests, after cyclic shear loading the upper loading platen was released, and the specimen was allowed to compress and re-established the initial σ'_{vc} = 100 kPa. The upper loading platen was then locked and a constant-volume monotonic shear loading was applied (approach 2) in order to simulate the post-cyclic behavior of soils under level-ground conditions (e.g. beneath building foundations). Figure 1 demonstrates the shear stress patterns applied in these approaches. In both phases of monotonic shear (approaches 1 and 2), the shear load was applied at a shear strain rate of 3.3%/sec until a state of constant shear and effective vertical stress (i.e. critical state) was established. The cyclic ring shear machine was equipped with piezoelectric bender elements for measuring shear wave velocity. Bender elements were installed inside the upper and the lower platen, whereby shear wave velocity readings were made before applying the cyclic load in approach 1 and also before applying the post-cyclic monotonic shear loading in approach 2.

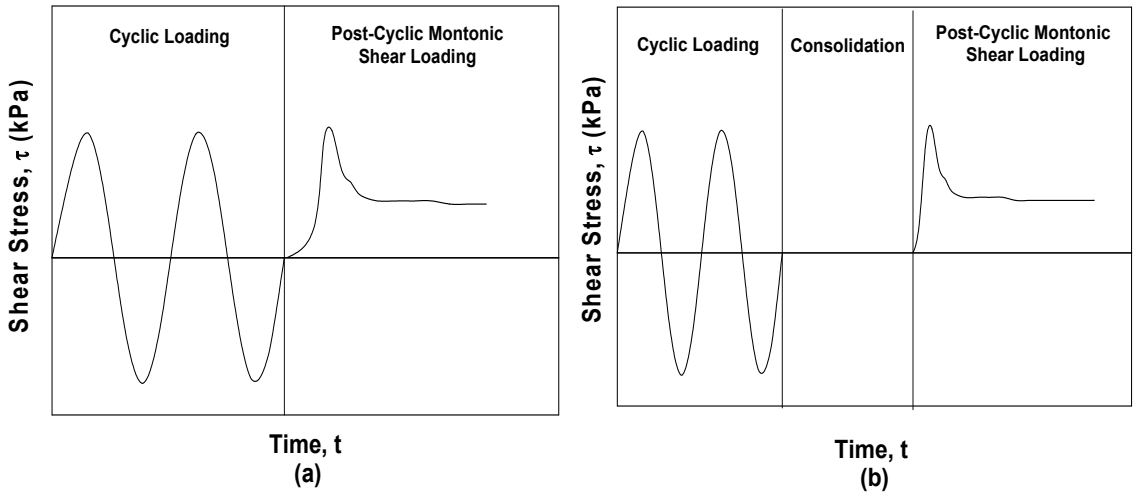

Figure 4.1: Patterns of shear loading applied in (a) approach 1, and (b) approach 2.

Note that the moist tamped specimens prepared in this experimental program were not saturated and the sand and silt particles were merely moistened at 5% moisture content in order to produce the bulky moist tamped soil fabric. Soil suction can be significant in unsaturated fine-grained soils, resulting in large changes in effective stress and soil shear resistance (Lu et al. 2007; Toan et al. 2013). Using the suction control and measurement panel of the ring shear device, we measured a maximum matric suction of 100 – 120 kPa in the moist tamped silt specimens in the ring shear tests. Because of the very low saturation ratios (8 – 15%) of our moist tamped specimens, the effective stress parameter which describes the contribution of matric suction in soil effective stress is about 0.05 (Escario and Juca 1989; Khalili et al. 2004; Lu and Likos 2004). Accordingly, soil

suction among the moist sand and silt particles increased σ'_{vc} only up to 5 - 6 kPa, which is taken into account in the results and discussions presented below.

4.4 Test Results and Discussion

4.4.1 Constant-Volume Cyclic Shear Tests

Because of space limitations, only a typical example of the cyclic shear behavior of a pure silt specimen at $D_{rc} = 35\%$ is presented in Figure 4.2. It can be noted from Figure 4.2 that σ'_{vc} progressively decreases with the number of shear load cycles, which reflects the cumulative development of excess pore water pressure (Δu) with increasing cyclic shear strain (γ_{cyc}). This continues until the excess pore water pressure ratio $r_u = \Delta u/\sigma'_{vc}$ reaches about 0.69, in about 10 shear load cycles, after which failure occurs and the soil accelerates towards initial liquefaction ($r_u \approx 1$). Similar cyclic responses were observed in all other cyclic ring shear experiments, except that the number of shear load cycles required to trigger failure (N_L) varied with the CSR and D_{rc} of each specimen. The soil cyclic shear resistance is its capacity to resist cyclic loading and is often described by the cyclic resistance ratio (CRR). In this study, CRR is defined as the CSR that triggers liquefaction failure in $N_L = 15$.

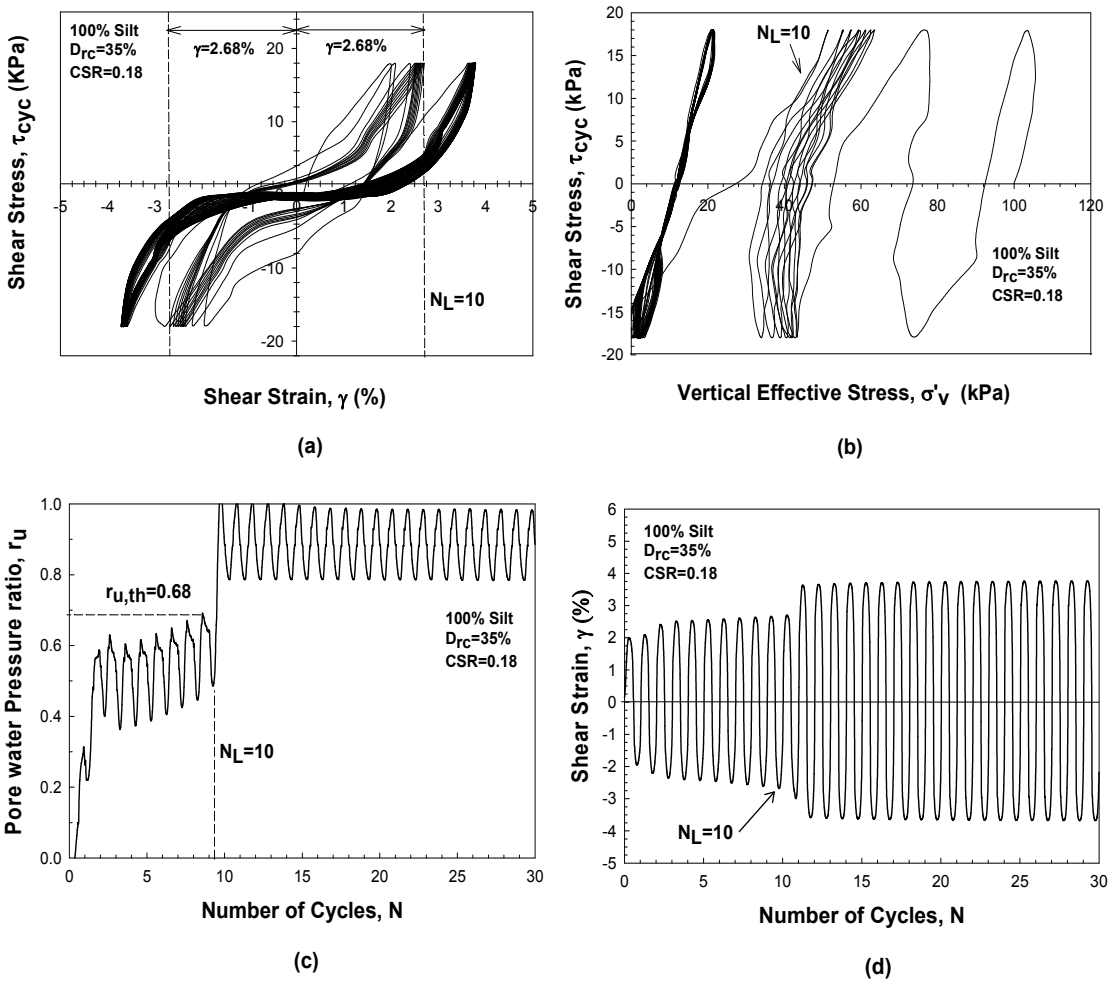

Figure 4.2: Response of pure silt in constant volume cyclic ring shear test (Drc=35%, CSR=0.18, σ'vc = 100 kPa): (a) cyclic stress-strain response, (b) cyclic effective stress path, (c) excess pore water pressure ratio versus number of cycles, (d) cyclic shear strain versus number of cycles.

4.4.2 Results of the Post-Cyclic Constant-Volume Monotonic Shear Tests

Figures 4.3 to 4.8 present the stress paths and stress-strain behaviors obtained from the constant-volume monotonic ring shear tests on silt and sandy silt mixes tested in this study. Figures 4.3, 4.5, and 4.7 demonstrate the post-cyclic soil behaviors immediately after liquefaction (approach 1), and Figures 4.4, 4.6, and 4.8 illustrate the post-cyclic monotonic behavior of the soils after excess pore pressure dissipation, and the re-establishment of σ'_{vc} = 100 kPa (approach 2). Figures 4.3 to 4.8 show that all soil mixes exhibit a strong strain-hardening behavior in monotonic shear immediately after cyclic loading because of the substantially reduced σ'_{vc} (< 30 kPa). Post-liquefaction strain-hardening has been also observed by many other researchers (e.g. Pillai and Saldago 1994; Vaid and Thomas 1995; Ashour 2002; Amini and Trandafir 2008; Sitharam et al. 2013). On the other hand, the specimens undergo strain-softening after the re-application of σ'_{vc} = 100 kPa, reflecting the strong impact of σ'_{vc} on the undrained strain-softening response of silts and sandy silts. In these tests, a critical state is reached after about 100 to 150% of shear strain (based on the entire specimen height), at which the soil samples deform at constant shear stress, constant effective vertical stress, and constant volume conditions. The corresponding shear strength mobilized at this condition is the critical shear strength ($s_{u,cs}$) of the soil, which represents the minimum value of s_u(liq) at the same effective stress and void ratio (Sadrekarimi, 2013).

As illustrated in Figures 4.3 to 4.8, the final $s_{u,cs}$ for each soil increases with increasing D_{rc} while they all lie on a straight line passing through the origin of the stress path plane. The slope of this line indicates the effective friction angle mobilized at the critical state (ϕ'_{cs}). Note that as a result of the strong strain-hardening exhibited during the monotonic shear tests immediately following cyclic shear (approach 1), the mobilized shear strength and friction angles at the end of these tests were greater than $s_{u,cs}$ and ϕ'_{cs} mobilized at the end of approach 2 shearing. The results of the post-cyclic constant-volume monotonic shear tests from approach 2 are summarized in Table 4.2.

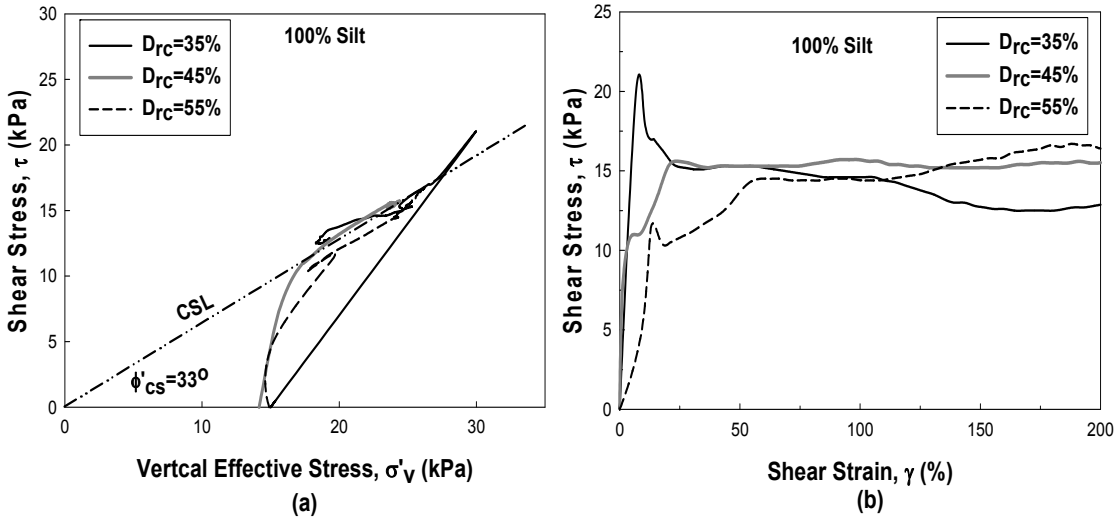

Figure 4.3: Response of pure silt specimens in post-cyclic constant-volume monotonic ring shear tests from Approach 1: (a) stress paths and (b) shear stress-shear strain

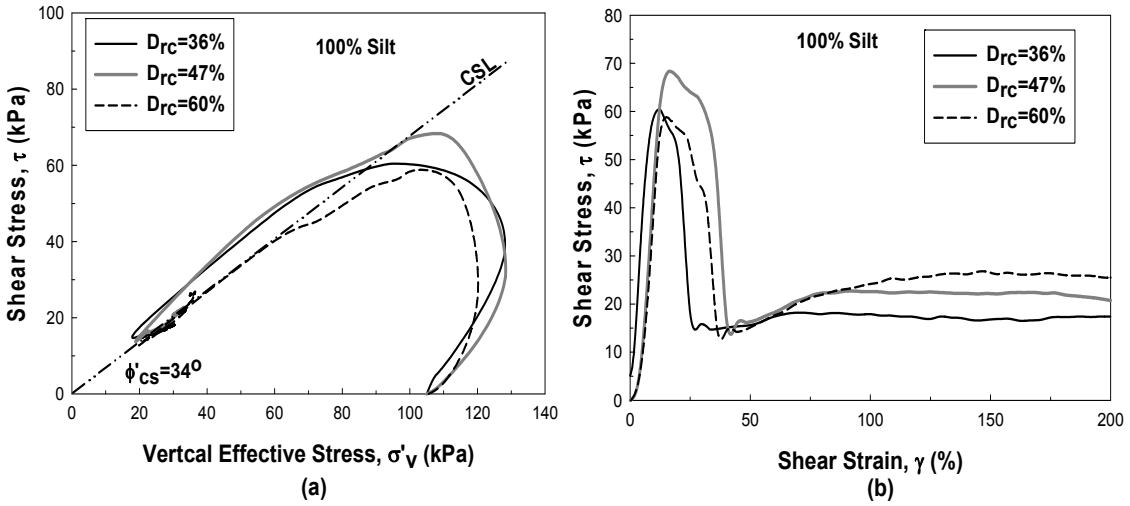

Figure 4.4: (a) stress paths and (b) shear stress - strain response of pure silt specimens in post-cyclic constant-volume monotonic ring shear tests from Approach 2.

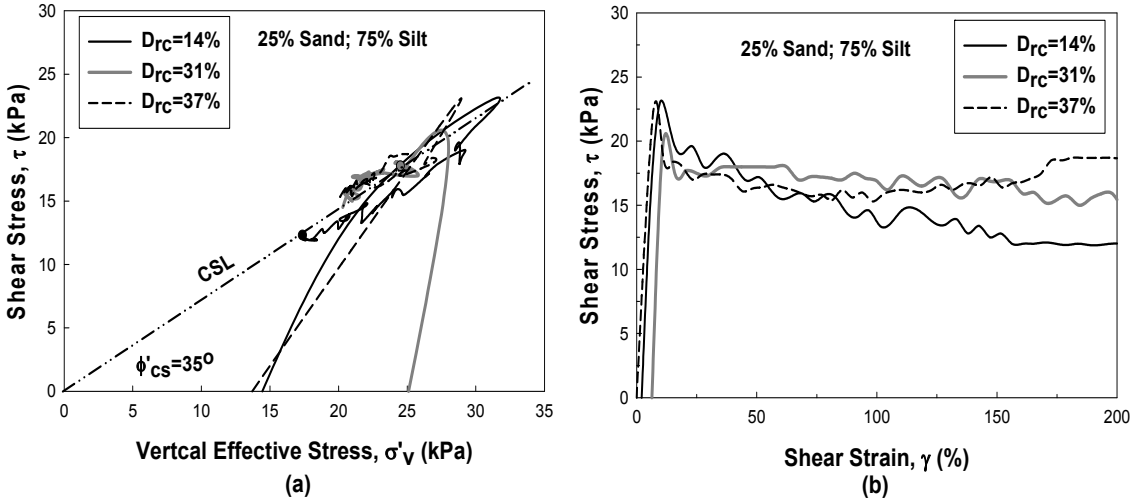

Figure 4.5: (a) stress paths and (b) shear stress - strain responses of sandy silt specimens with 75% silt content in post-cyclic constant-volume monotonic ring shear tests from Approach 1.

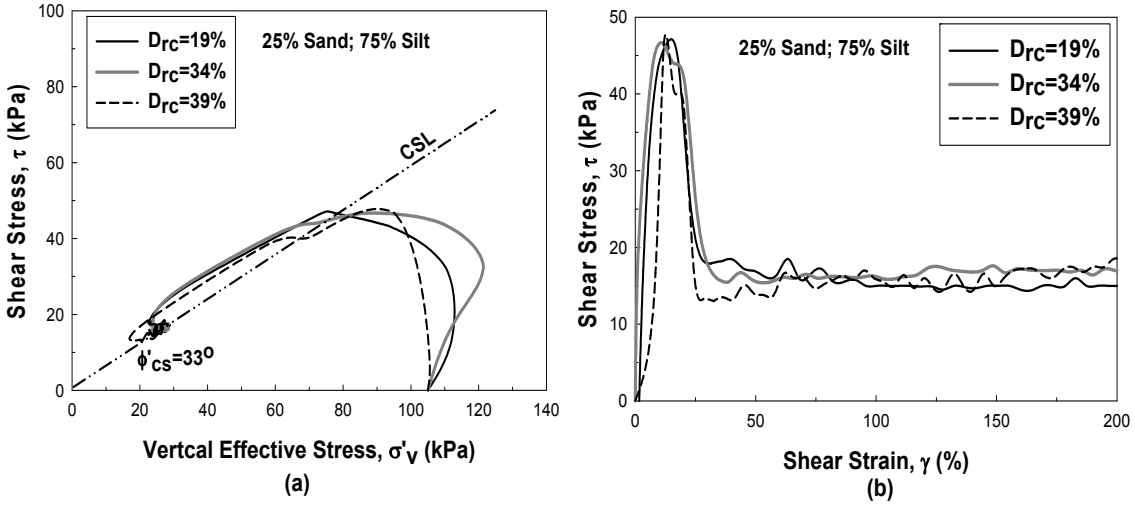

Figure 4.6: (a) stress paths and (b) shear stress - strain responses of sandy silt specimens with 75% silt content in post-cyclic constant-volume monotonic ring shear tests from Approach 2.

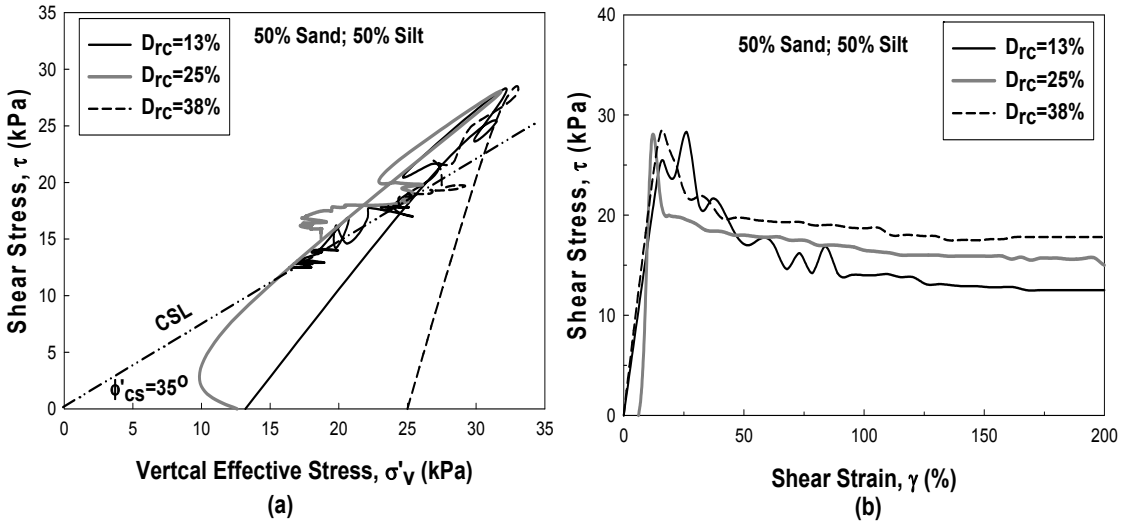

Figure 4.7: (a) stress paths and (b) shear stress - strain responses of sandy silt specimens with 50% silt content in post-cyclic constant-volume monotonic ring shear tests from Approach 1.

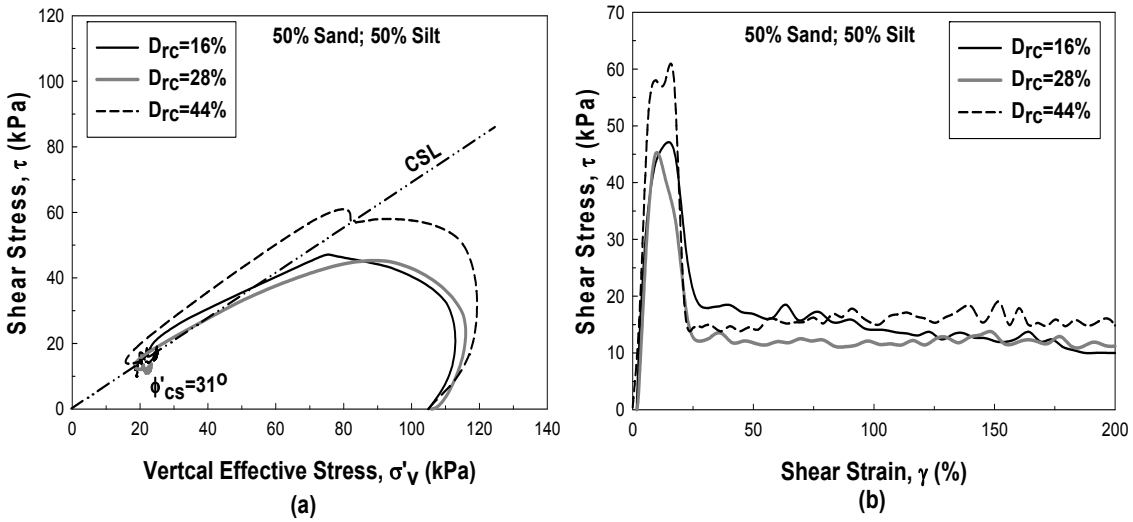

Figure 4.8: (a) stress paths and (b) shear stress - shear strain responses of sandy silt specimens with 50% silt content in post-cyclic constant-volume monotonic ring shear tests from Approach 2.

Table 4.2: Post-cyclic constant-volume monotonic ring shear test results following approach 2 shearing.

Test #	e_c	D_{rc} (%)	$s_{u,cs}$	σ'_{cs}	ϕ'_{cs}	$s_{u,cs}/\sigma'_{vc}$
S100D36M2	1.58	36	17.7	27.2	33.05	0.17
S100D47M2	1.43	47	20.7	30.0	34.6	0.20
S100D60M2	1.24	60	25.5	34.2	36.7	0.25
S75D19M2	1.31	19	14.7	23.5	32.03	0.15
S75D39M2	1.18	39	17.0	27.0	32.19	0.17
S75D37M2	1.13	37	18.4	28.0	33.30	0.18
S50D16M2	1.04	16	11.4	19.2	30.69	0.11
S50D28M2	0.96	28	13.5	22.0	31.53	0.13
S50D44M2	0.85	44	16.1	25.0	32.78	0.16

[a] S and D in test labels indicate the percentage of silt and D_{rc}.

4.5 Critical Strength Ratio

In order to remove the effect of σ'_{vc}, $s_{u,cs}$ is often normalized with respect to σ'_{vc} and presented as a dimensionless critical strength ratio, $s_{u,cs}/\sigma'_{vc}$ (Stark and Mesri 1992; Sadrekarimi and Olson 2011). Figure 4.9 presents the decreasing trends of $s_{u,cs}/\sigma'_{vc}$ with increasing e_c for each soil mix subject to the different loading patterns. Critical strength ratio varies between 0.11 and 0.24 for all soil mixes and increases with increasing silt content and this can be due to the more angular shapes of the silt particles.

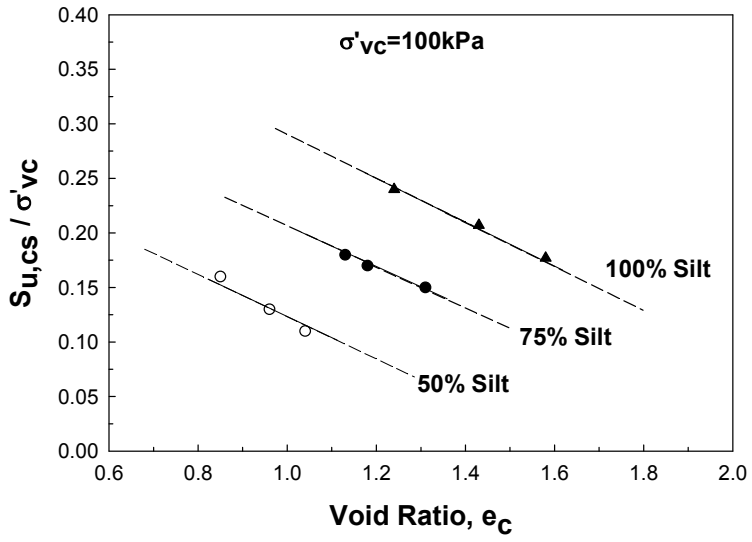

Figure 4.9: Variation of $s_{u,cs}/\sigma'_{vc}$ with e_c following for each soil mix

4.6 Correlation between ($s_{u,cs}/\sigma'_{vc}$) and V_s

Although correlations of CRR with shear wave velocity have been developed in several studies (Andrus and Stokoe 2000, Baxter et al. 2008; Zhou and Chen 2007; Yould et al. 2001), no relationship exists for estimating post-cyclic monotonic shear strength or $s_{u,cs}$ from shear wave velocity measurements. The shear wave velocity (V_s) of samples tested using approach 2 was measured after liquefaction was achieved and σ'_{vc} = 100 kPa was re-established but before the application of the monotonic shear loading. The measurement was made by using a pair of piezoelectric bender elements embedded in the upper and lower platens of the ring shear specimen chamber. Figure 4.10 shows the correlation between the $s_{u,cs}/\sigma'_{vc}$ obtained from approach 2 monotonic shear tests and shear wave velocity (V_s) of different soil specimens. As demonstrated in Figure 4.10 s_{uc}/σ'_{vc} increases with increasing V_s (for each soil) and with increasing silt content (at same V_s).

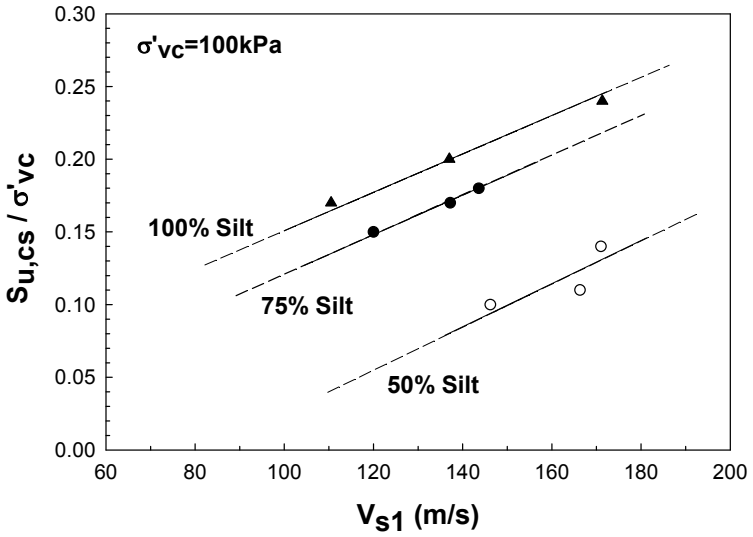

Figure 4.10: Correlations between critical strength ratio obtained from approach 2 and V_s at σ'_{vc} = 100 kPa (V_{s1}).

4.7 e-Log σ'_{cs} Projection of the Critical State Line

Figures 4.11, 4.12, and 4.13 show the critical state lines (CSL), which is the relationship between the void ratio (e) and the vertical effective stress (σ'_{cs}) at the critical state, for the clean silt and sand-silt mixes. This relation is expressed as below:

$$e_{cs} = \Gamma_{cs} - \lambda_{cs} Log\left(\frac{\sigma'_{cs}}{1kPa}\right) \qquad (4.1)$$

Where Γ_{cs} is the critical state void ratio at σ'_{cs} = 1 and λ_{cs} is the slope of the CSL. As illustrated in Figures 4.11 to 4.13, the final states from the monotonic ring shear tests plot within a very narrow range of effective stresses and only reflect the experimental scatter

in the critical states. Many studies have shown that due to the large compressibility of silty soils, CSL is reasonably parallel to the normal compression line, NCL of these soils (Muir Wood 1990; Olson and Stark 2003b; Sadrekarimi 2013). Accordingly, we have assumed that the CSLs of our soils are also parallel to the NCLs and therefore a range of parallel CSLs – encompassing the range of critical states from the tests - are defined. The critical state parameter (ψ) is defined as the difference between e_c and the void ratio on the CSL at the same σ'_{vc} (Been and Jefferies 1985). The ranges of Γ_{cs} and ψ_{cs}, and λ_{cs} for the ranges of the CSLs are summarized in Table 4.3 for each soil mix.

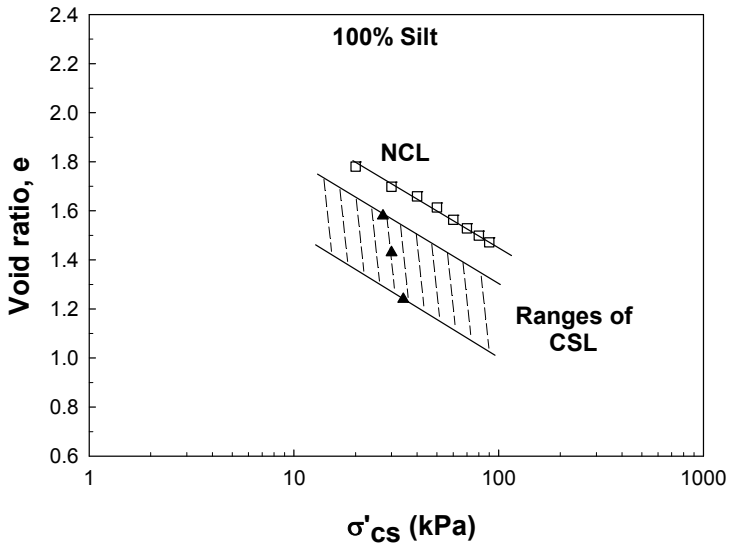

Figure 4.11: CSL and NCL plots for pure silt specimens

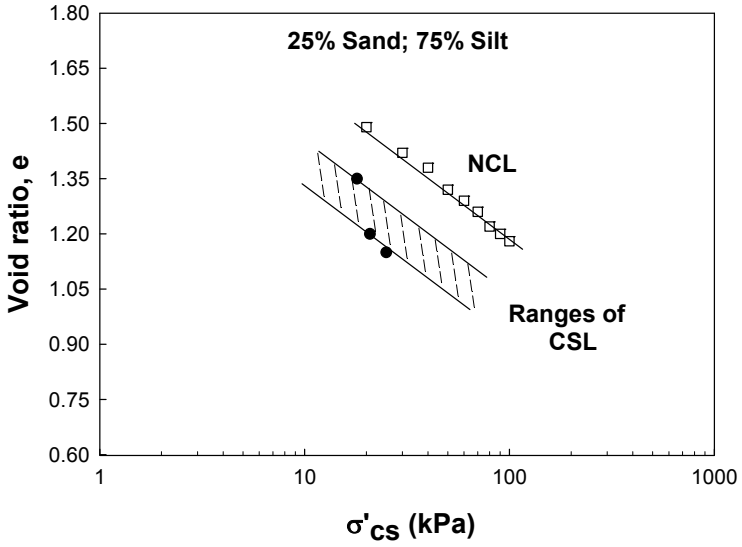

Figure 4.12: CSL and NCL plots for sandy silt specimens with 75% silt content.

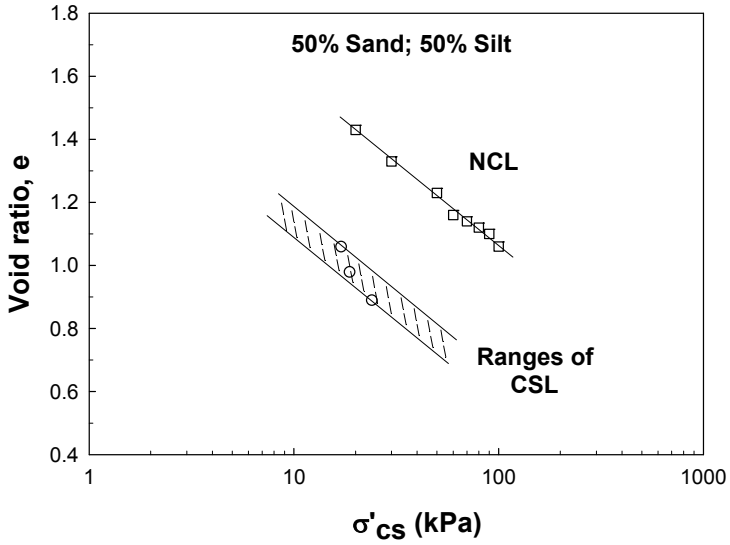

Figure 4.13: CSL and NCL plots for sandy silt specimens with 50% silt content.

Table 4.3: Summary of the upper and lower critical state parameters.

Silt Content (%)	e_c	D_{rc}	λ_{cs}	Γ_{cs}	ψ_{cs}
	1.58	35	-0.473	2.250 - 1.966	0.276 - 0.560
100	1.43	45	-0.473	2.250 - 1.966	0.126 - 0.410
	1.24	55	-0.473	2.250 - 1.966	(-)0.064 - 0.220
	1.31	14	-0.453	1.930 - 1.780	0.286 - 0.436
75	1.18	31	-0.453	1.930 - 1.780	0.156 - 0.306
	1.13	37	-0.453	1.930 - 1.780	0.106 - 0.256
	1.04	13	-0.516	1.700 - 1.570	0.373 - 0.504
50	0.96	25	-0.516	1.700 - 1.570	0.293 - 0.424
	0.85	38	-0.516	1.700 - 1.570	0.183 - 0.314

Figures 4.14 to 4.16 show the ranges of relationships between CRR and the critical state parameter ψ_{cs}. It is clearly demonstrated that CRR for each soil mix decreases with the increase of ψ_{cs}.

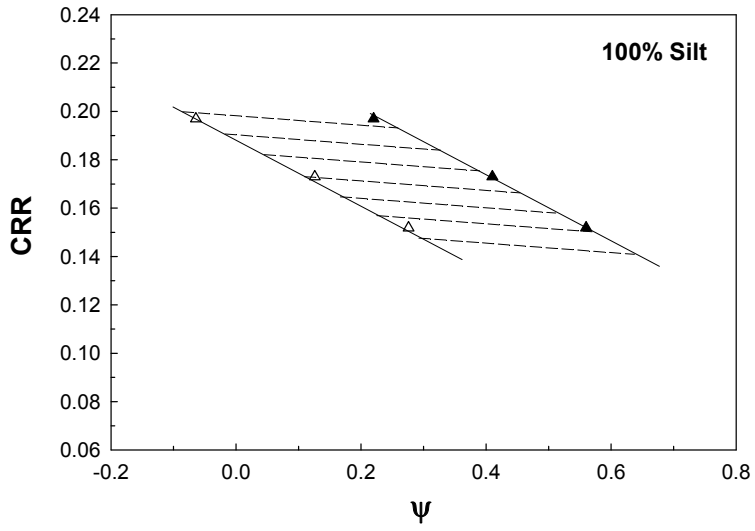

Figure 4.14: Ranges of relationships between CRR and ψ_{cs} for pure silt specimen.

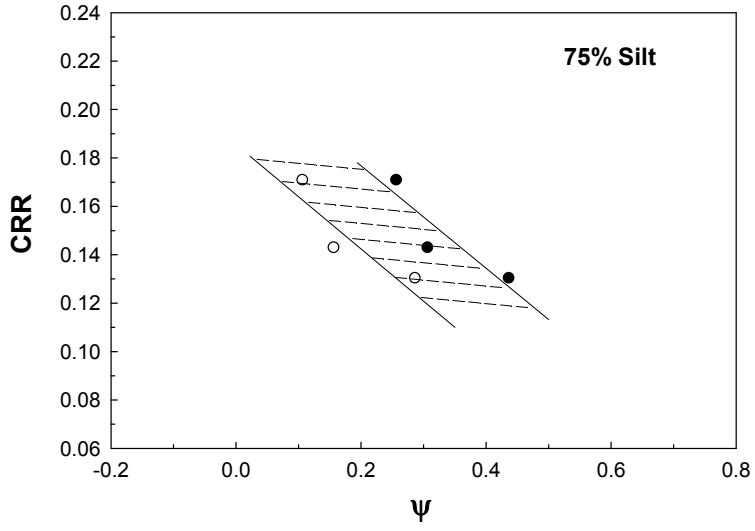

Figure 4.15: Ranges of relationships between CRR and ψ_{cs} for sandy silt specimens with 75% silt content.

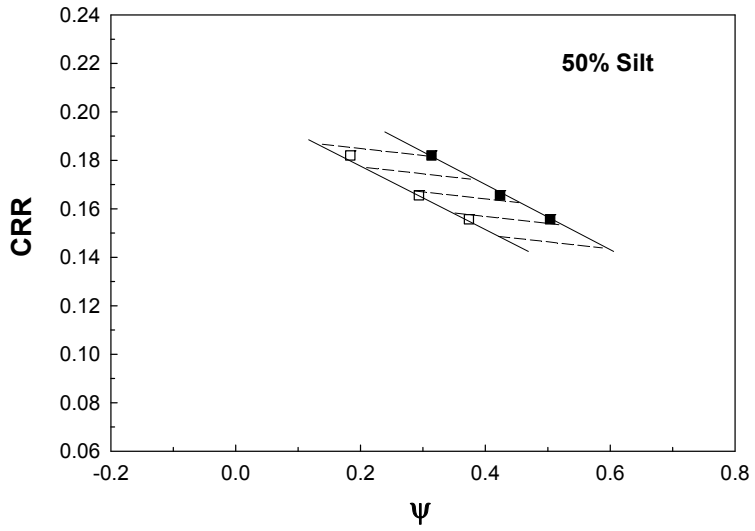

Figure 4.16: Ranges of relationships between CRR and ψ_{cs} for sandy silt specimens with 50% silt content.

Figures 4.17 to 4.19 show the correlation between the critical strength ratio (S_{uc}/ σ'_{vc}) for the ranges of state parameters (Ψ). It can be noticed that S_{uc}/ σ'_{vc} decreases with the increase of Ψ for different mixes of soil. This pattern of variation of S_{uc}/ σ'_{vc} with Ψ is in agreement with previous studies (Dennis 1988; Castro 1969; Been et al.1991)

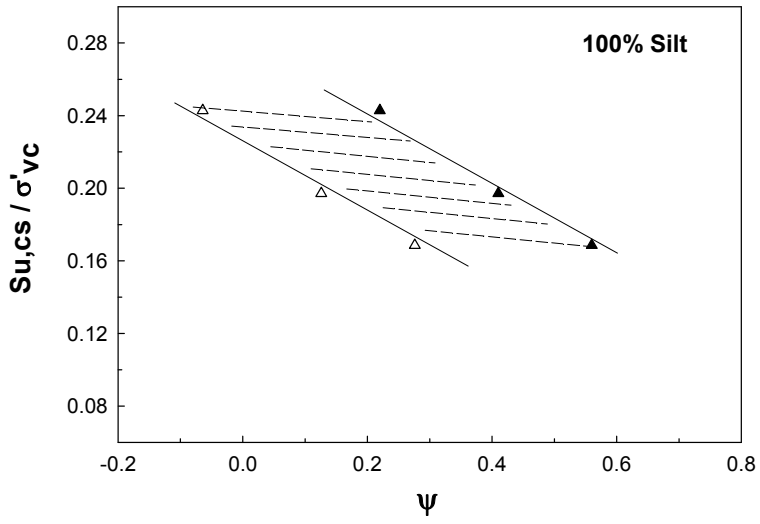

Figure 4.17: Ranges of relationships between critical strength ratio and ψ_{cs} for clean silt specimens

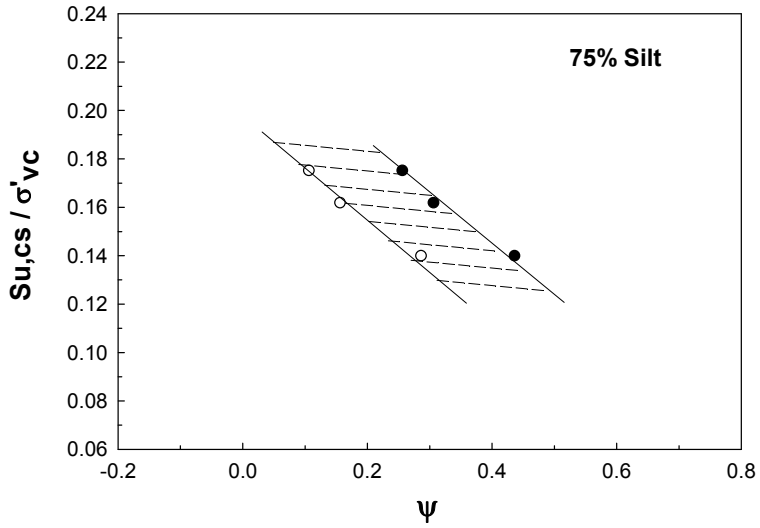

Figure 4.18: Ranges of relationships between critical strength ratio and ψ_{cs} for sandy silt specimens with 75% silt content.

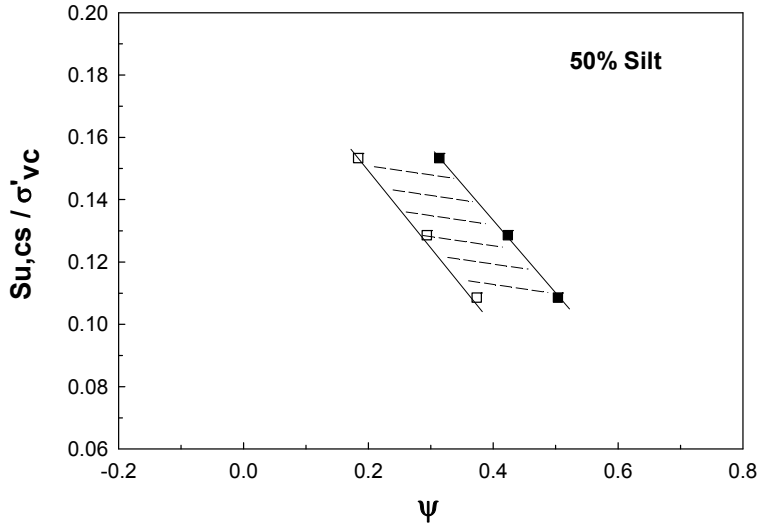

Figure 4.19: Ranges of relationships between critical strength ratio and ψ_{cs} for sandy silt specimens with 50% silt content.

4.8 Summary and Conclusion

Determining the mechanical properties of soils at large shear strains is an important aspect for performing the stability and deformation analysis of geotechnical structures against post-liquefaction failures in landslides, flow slide, during pile driving and cone penetration testing. A series of stress-controlled cyclic ring shear tests followed by displacement-controlled monotonic shearing were carried out using an advanced ring shear testing apparatus along with bender element shear wave velocity measurement to investigate the post-liquefaction undrained shear response of non-plastic pure silt and sand-silt mixes. The results indicate a strong impact of the effective stress on the undrained behavior of silts and sandy silts. It was observed that silt and sandy silt would

exhibit strong strain-hardening post-liquefaction monotonic shearing behavior because of the substantially reduced effective stress immediately following cyclic shear. On the other hand, the same soil could undergo strain-softening and liquefaction following cyclic loading if the pre-cyclic initial stress condition is re-established. Critical state was reached in post-cyclic monotonic shear after about 100 to 150% of shear strain (based on the entire specimen height) and the undrained strength mobilized at this condition increased with decreasing initial void ratio and increasing silt content, despite the looser fabric (higher initial void ratio) of the specimens with higher silt contents. For the first time, correlations are presented between shear wave velocity and the post-cyclic monotonic shear strength ($s_{u,cs}$). These correlations indicated that s_{uc}/σ'_{vc} increases linearly with increasing V_s. The results further indicate that both CRR and s_{uc}/σ'_{vc} decrease with increasing ψ_{cs}.

4.9 References

Amini, Z. and Trandafir, A. Post-Liquefaction Shear Behavior of Bonneville Silty-Sand. Geotechnical Earthquake Engineering and Soil Dynamics IV: 1-9.

Andrus, R. and K. Stokoe II (2000). Liquefaction Resistance of Soils from Shear-Wave Velocity. Journal of Geotechnical and Geoenvironmental Engineering 126(11): 1015-1025.

Ashour, M. Post Liquefaction Response of Liquefiable Soils. Proceeding 37th Engineering Geology and Geotechnical Engineering Symposium, Boise, Idaho, March 2002, pp. 11-26.

Babbitt, D. H., Bennett, W. J. and Hart, R. D. (1983). California's Seismic Reevaluation of Embankment Dams. Procs., ASCE Symp. on Seismic Design of Embankments and Caverns, Philadelphia, PA, May 16-20, 1983, pp. 96-112.

Baxter, C., Bradshaw, A., Green, R., Wang, J. (2008). Correlation between Cyclic Resistance and Shear-Wave Velocity for Providence Silts. Journal of Geotechnical and Geoenvironmental Engineering 134(1): 37-46.

Been K, Jefferies MG, Hachey J. 1991. The critical state of sands. Géotechnique **41**(3): 365-381.

Castro, G., 1969. Liquefaction of Sands. Ph.D. thesis, Harvard Soil Mechanics Series, No. 81, Harvard University, Cambridge, MA.

Dennis, N.D. 1988. Influence of specimen preparation techniques and testing procedures on undrained steady state shear strength. In Advanced triaxial testing of soil and rock. ASTM STP 977. American Society for Testing and Materials, Philadelphia, Pa. pp. 642–654

Escario, V. and Juca, J.F.T. (1989). Strength and Deformation of Partly Saturated Soils, Proc. 12th Int. Conf. on Soil Mechanics and Foundation Engineering, Rio de Janeiro, 1: 43-46.

Huang, Y., H. Zheng, Mao, W. (2012). Triaxial tests on the fluidic behavior of post-liquefaction sand. Environmental Earth Sciences 67(8): 2325-2330.

Idriss, I.M., and Boulanger, R.W. 2008. Soil liquefaction during earthquakes. Earthquake Engineering Research Institute, San Francisco, Calif.

Ishihara, K. 1993. Liquefaction and flow failure during earthquakes. Geotechnique, 43(3): 351–415. doi:10.1680/geot.1993.43.3.351.

Khalili, N., Geiser, F., and Blight, G. E. (2004). Effective stress in unsaturated soils: Review with new evidence. Int. J. Geomech., 4 (2): 115–126

Ladd, R.S. (1978). Preparing Test Specimen Using Undercompacton. Geotechnical Testing Journal 1(1): 16-23.

Lu, N., and Likos, W. J. (2004). Unsaturated soil mechanics, Wiley, NewYork.

Lu, N., Wu, B., P.Tan, C. (2007). Tensile Strength Characteristics of Unsaturated Sands. Journal of Geotechnical and Geoenvironmental Engineering 133 (2): 144-154.

Olson, S.M. and Stark, T.D. (1998). Liquefied shear strength of sands from CPT. Geotechnique, accepted for publication.

Olson, S. and Stark, T. (2003a). Yield Strength Ratio and Liquefaction Analysis of Slopes and Embankments. Journal of Geotechnical and Geoenvironmental Engineering 129(8): 727-737.

Olson, S., and Stark, T. (2003b). Use of laboratory data to confirm yield and liquefied strength ratio concepts. Canadian Geotechnical Journal, **40**: 1164 – 1184.

Pillai, V. S, and Byrne, P. M. (1994). Effect of Overburden Pressure on Liquefaction Resistance of Sands. Canadian Geotechnical Journal, Vol. 31, 1994.

Pillai, V. S. and Salgado, F. M. (1994). Post-liquefaction stability and deformation analysis of Duncan Dam. Canadian Geotechnical Journal 31(6): 967-978.

Sadrekarimi, A. (2013). Influence of state and compressibility on liquefied strength of sands. Canadian Geotechnical Journal 50(10): 1067-1076.

Sadrekarimi, A., and Olson, S. M. (2011). Yield strength ratios, critical strength ratios, and brittleness of sandy soils from laboratory tests. Canadian Geotechnical Journal 48(3): 493-510.

Seed. H. B. (1979). Soil liquefaction and cyclic mobility evaluation for level ground during earthquakes. Journal of Geotechnical Engineering, ASCE. 105(2), 201-255.

Seed, R.B., and Harder, L.F. (1990). SPT-Based analysis of cyclic pore pressure generation and undrained residual strength. In Proceedings of the H. Bolton Seed Memorial Symposium. Edited by J.M. Duncan. pp. 351–376.

Smart, J. D. and Von Thun, J. L. (1983). Seismic Design and Analysis of Embankment Dams-Recent Bureau of Reclamation Experience. Seismic Design of Embankments and Caverns, American Society of Civil Engineers, 1983.

Stark,T.N., and Mesri, G. (1992). Undrained shear strength of liquefied sands for stability analysis. Journal of Geotechnical Engineering., ASCE, 118(11), 1727-1747.

Stark, T.N., Olson, S.M., Kramer, SL., and Youd, T.L. (1998). Shear strength of liquefled soils. Proc., Workshop on Post-Liquefaction Shear Strength of Granular Soils, University of Illinois at Urbana-Champaign, Urbana, Illinois, 288 p.

Sitharam, T., Dash, H., and Jakka, R. (2013). Postliquefaction Undrained Shear Behavior of Sand-Silt Mixtures at Constant Void Ratio. International Journal of Geomechanics 13(4): 421-429.

Sitharam, T. G., Vinod, J. S., and Ravishankar, B. V. (2009). Post-liquefaction undrained monotonic behaviour of sands: experiments and DEM simulations. Geotechnique 59(9); 739–749.

Toan, D. T., Komine, H., Murakami, S. and Duc, D. M. (2013). Grain size and soil suction effect on hydraulic conductivity and shear strength of simulated red river soil. Geotechnical Society of Singapore (GeoSS).

Vaid, Y. P. and Thomas, J. (1995). Liquefaction and Post Liquefaction Behavior of Sand. American Society of Civil Engineers, Journal of Geotechnical Engineering, 121(2): 163-173.

Wijewickreme, D., and Sanin, M. (2010). Postcyclic Reconsolidation Strains in Low-Plastic Fraser River Silt due to Dissipation of Excess Pore-Water Pressures. Journal of Geotechnical and Geoenvironmental Engineering 136(10): 1347-1357.

Wood, D. M. (1990). Soil Behaviour and Critical State Soil Mechanics, Cambridge University Press.

Yamamuro, J. and P. Lade (1998). Steady-State Concepts and Static Liquefaction of Silty Sands. Journal of Geotechnical and Geoenvironmental Engineering 124(9): 868-877.

Youd, T. L., I. M. Idriss, et al. (2001). Liquefaction resistance of soils: Summary report from the 1996 NCEER and 1998 NCEER/NSF Workshops on Evaluation of Liquefaction Resistance of Soils. Journal of Geotechnical and Geoenvironmental Engineering 127(10): 817-833.

Zhou, Y. and Chen, Y. (2007). Laboratory Investigation on Assessing Liquefaction Resistance of Sandy Soils by Shear Wave Velocity. J. Geotech. Geoenviron. Eng., 133(8): 959–972.

Chapter 5

5 Summary and Conclusion

In this study, a series of stress-controlled cyclic ring shear tests followed by strain-controlled monotonic shear tests were carried out in an advanced ring shear apparatus to investigate the cyclic and post-cyclic undrained shear response of pure silt and sandy silts mixes with 25% and 50% sands. All specimens were initially consolidated to a vertical pressure of 100 kPa and then subjected to a cyclic shear load with cyclic shear stress ratio (CSR) values between 0.075 and 0.225. The shear wave velocity (V_s) traveling through the soil specimen was measured before the application of the cyclic shear loading by a pair of piezoelectric bender elements embedded in the upper and lower platens of the specimen chamber.

In another set of experiments, the elastic soil behavior at very small shear strains ($\gamma < 10^{-4}\%$) was investigated through shear wave velocity measurements using bender elements at vertical stresses ranging from 50 to 300 kPa while strain-controlled constant volume cyclic ring shear tests were conducted to establish shear modulus (G) and damping ratio (D) at larger shear strain amplitudes ($\gamma > 0.01\%$) and to investigate the influence of silt content and γ on these parameters.

The experimental results lead to the following conclusions:

- Silts are found to be susceptible to liquefaction and their cyclic response is very similar to sand in terms of strain and excess pore water pressure development.

- An increase in the cyclic load amplitude accelerated excess pore water pressure development in the samples and decreased the number of cycles needed to reach failure.
- Liquefaction and strain-softening occurred at excess pore water pressure ratios (r_u) between 0.6 and 0.7 associated with cumulative shear strains (γ) of 4% to 6%, after which cyclic mobility failure ensued with very large shear strains and excess pore water pressure ratio ($r_u > 0.9$).
- Cyclic resistance ratio (CRR) was defined as the cyclic stress ratio needed to trigger liquefaction at $r_u = r_{u,th}$ in 15 cycles of uniform shear stress and it was observed that CRR decreased with increasing initial void ratio, while at the same void ratio CRR increased with increasing silt content.
- The existing field CRR-V_{s1} correlations could underestimate the liquefaction resistance of soils with FC $\geq$ 50%.
- Vs and the maximum shear modulus (G_o) significantly decrease with increasing void ratio.
- V_s is also found to vary with the effective overburden stress to the power of 0.31 - 0.34 for all silt and sandy silt mixes.
- G decreases with increasing γ, D increases with increasing γ only up to $\gamma < 1\%$, beyond which it exhibits a decreasing trend.
- Post-cyclic undrained shear strength is mainly affected by the relative density (D_{rc}) or void ratio of tested soils.

- Effective stress has a strong impact on the undrained post-cyclic behavior of silts and sandy silts. It was observed that silt and sandy silt would exhibit strong strain-hardening post-liquefaction monotonic shearing behavior because of the substantially reduced effective stress immediately following cyclic shear. On the other hand, the same soil could undergo strain-softening and liquefaction following cyclic loading if the pre-cyclic initial stress condition is re-established.
- $s_{u,cs}/\sigma'_{vc}$ increases linearly with increasing V_s. The results further indicate that both CRR and $s_{u,cs}/\sigma'_{vc}$ decrease with increasing ψ_{cs}.

Appendix A

(a)

(b)

Figure A - 1: Pictures of bender elements (a) Bender element embedded in the upper loading platen (b) Bender element embedded in the lower platen.

Figure A - 2: Picture of the ring shear machine (SRS-150) and the suction control panel.

Appendix B

Appendix A includes the results of the stress-controlled cyclic ring shear tests of silt and sandy silt soils. The results show the pore water pressure, shear strain, stress path, and hysteresis loops variation with the cyclic shear load.

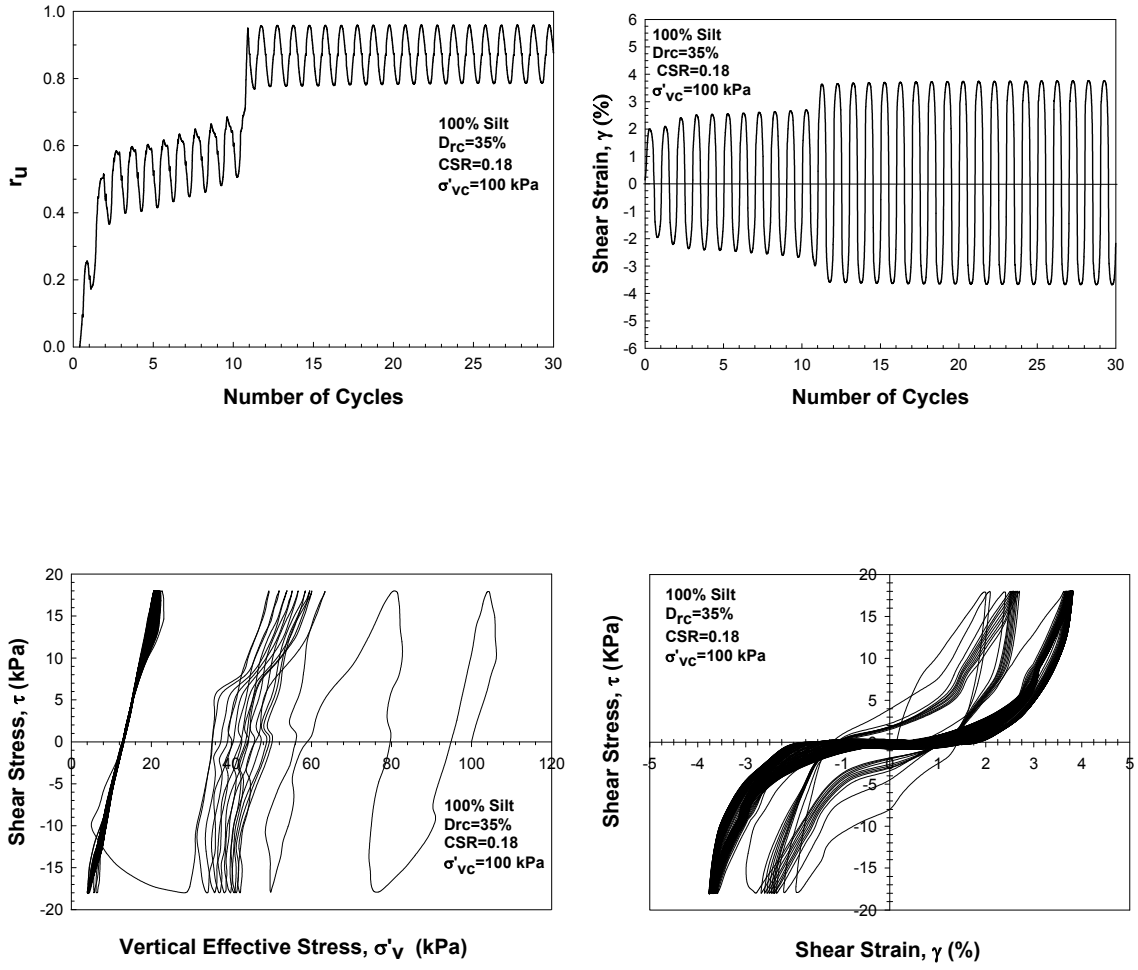

Figure B-1: Response of a pure silt specimen in a constant volume cyclic ring shear test (D_{rc} = 35%, CSR = 0.18, σ'_{vc} = 100 kPa).

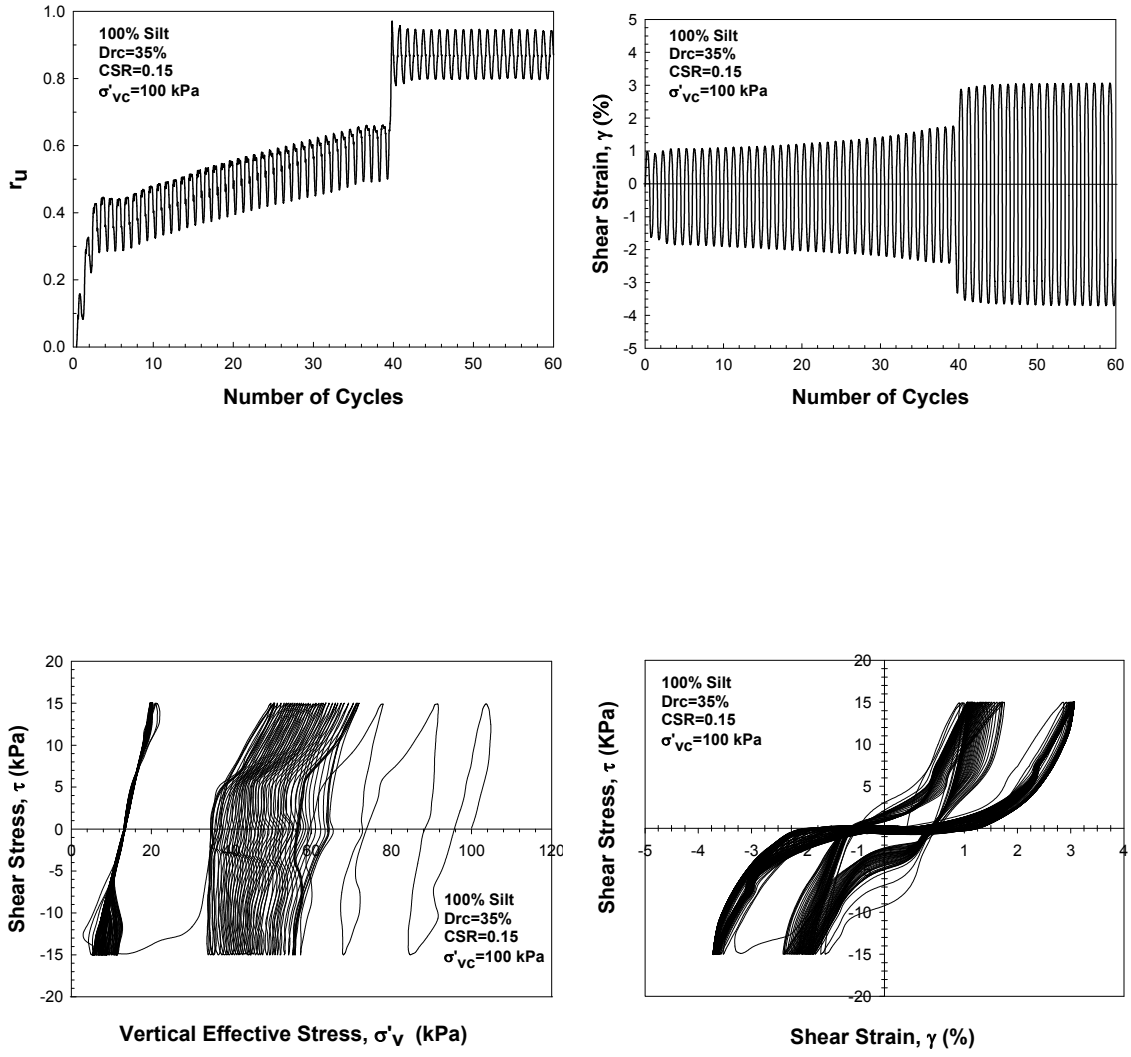

Figure B-2: Response of a pure silt specimen in a constant volume cyclic ring shear test (D_{rc} = 35%, CSR = 0.15, σ'_{vc} = 100 kPa).

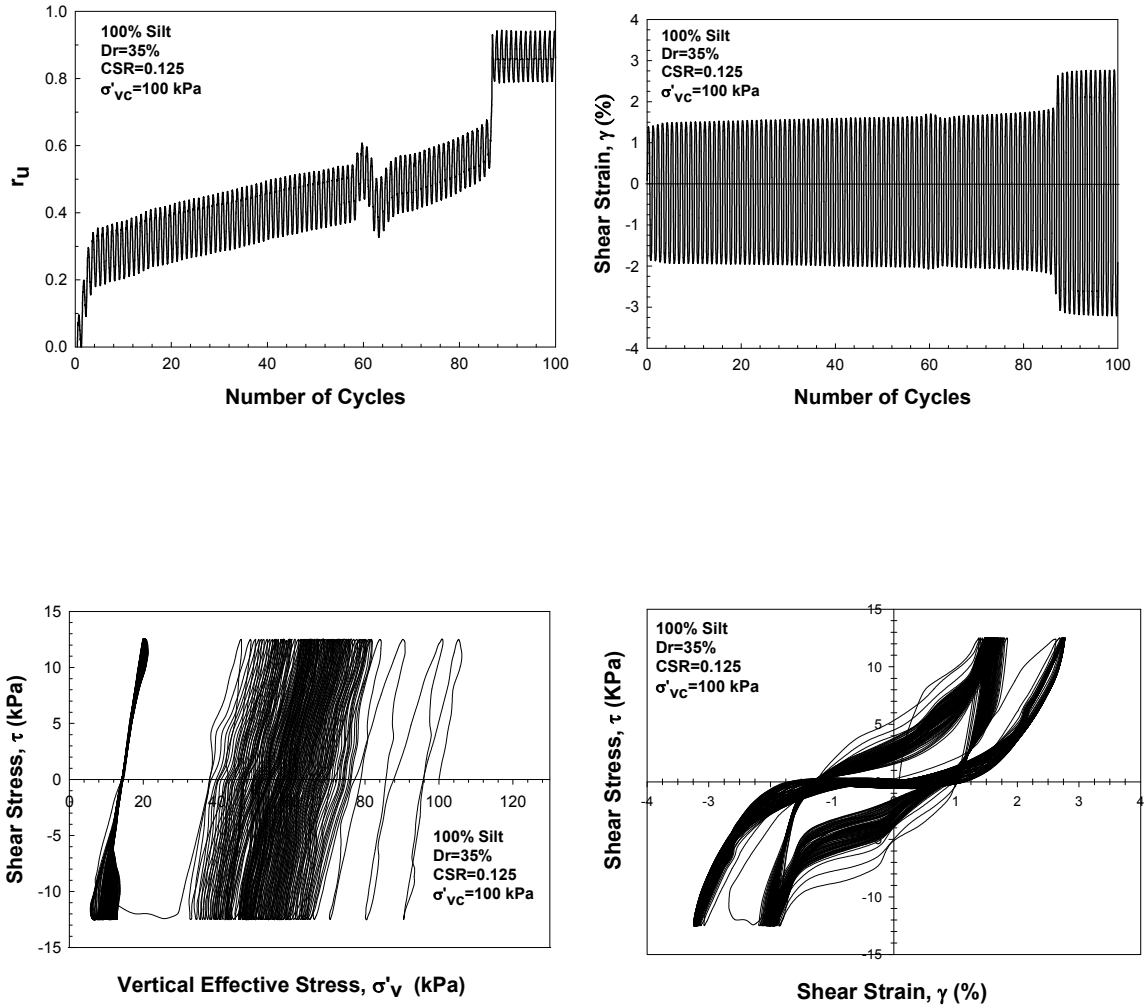

Figure B-3: Response of a pure silt specimen in a constant volume cyclic ring shear test (D_{rc} = 35%, CSR = 0.125, σ'_{vc} = 100 kPa).

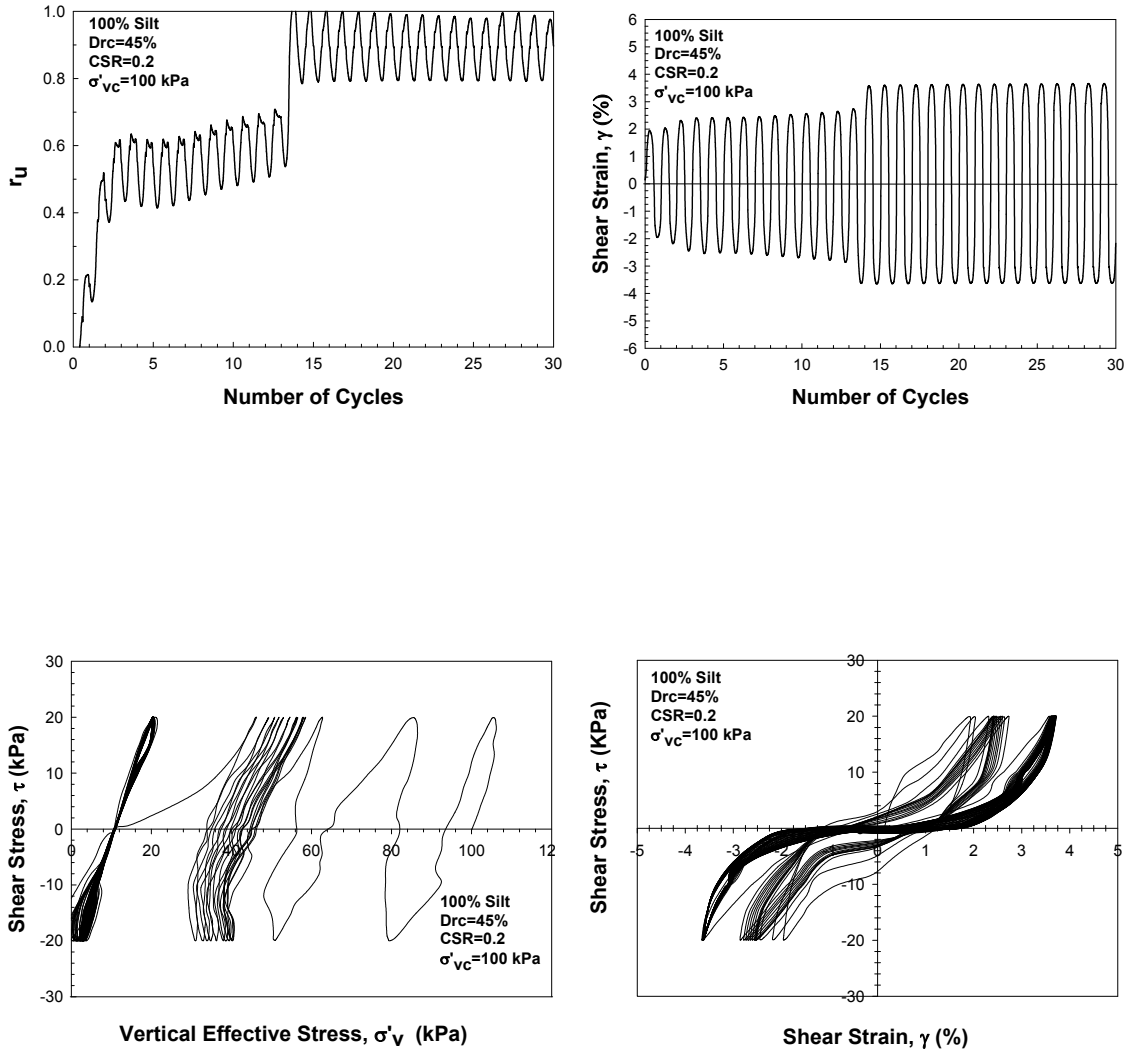

Figure B-4: Response of a pure silt specimen in a constant volume cyclic ring shear test (D_{rc} = 45%, CSR = 0.2, σ'_{vc} = 100 kPa).

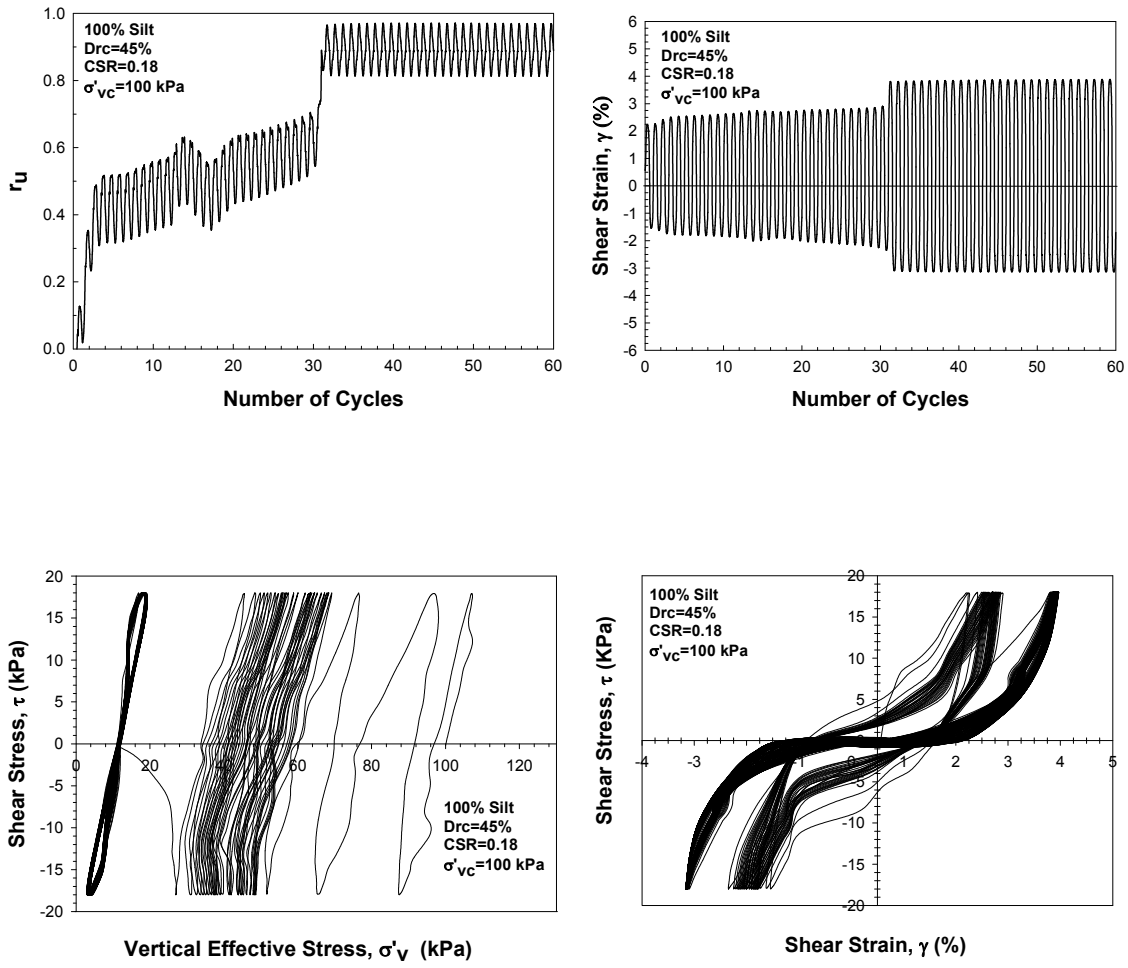

Figure B-5: Response of a pure silt specimen in a constant volume cyclic ring shear test (D_{rc} = 45%, CSR = 0.18, σ'_{vc} = 100 kPa).

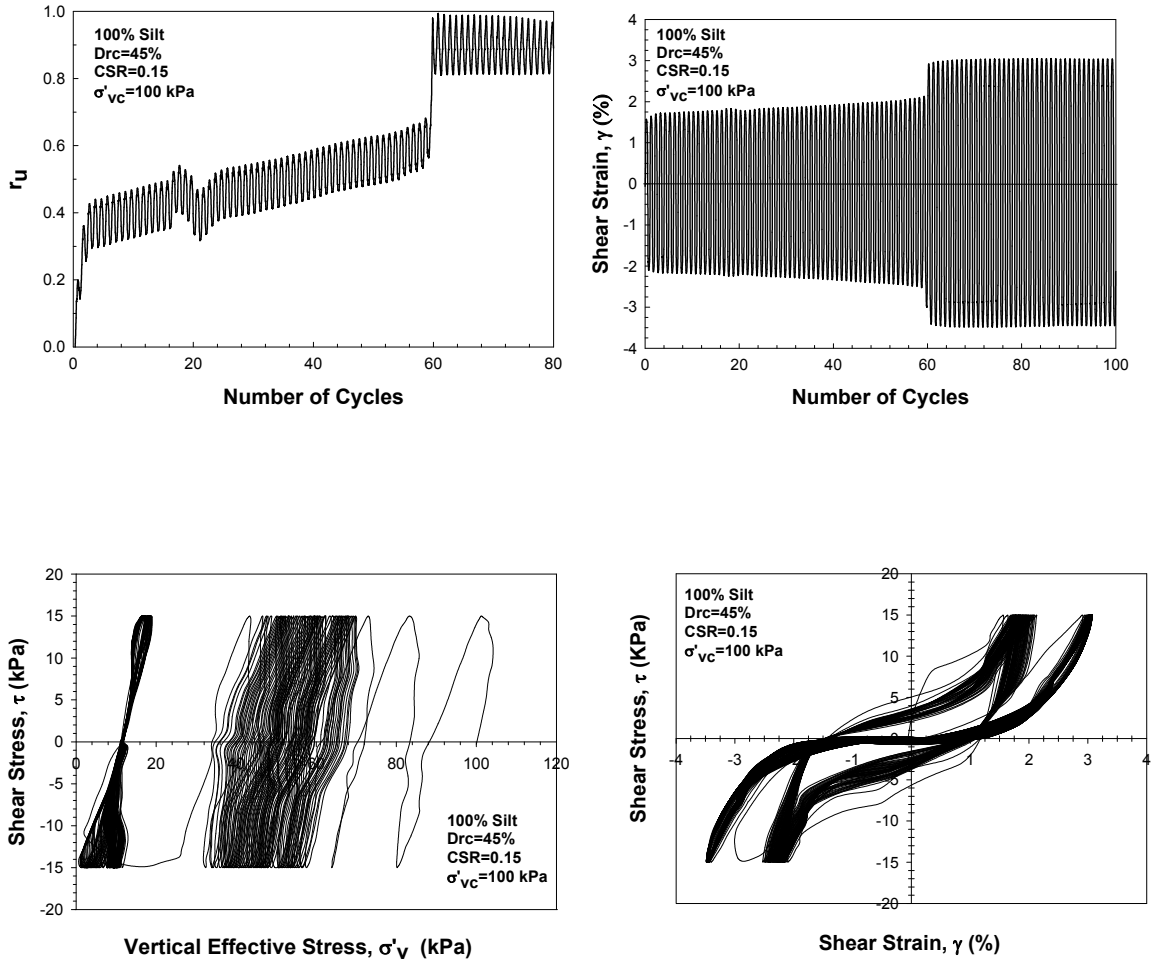

Figure B-6: Response of a pure silt specimen in a constant volume cyclic ring shear test (D_{rc} = 45%, CSR = 0.15, σ'_{vc} = 100 kPa).

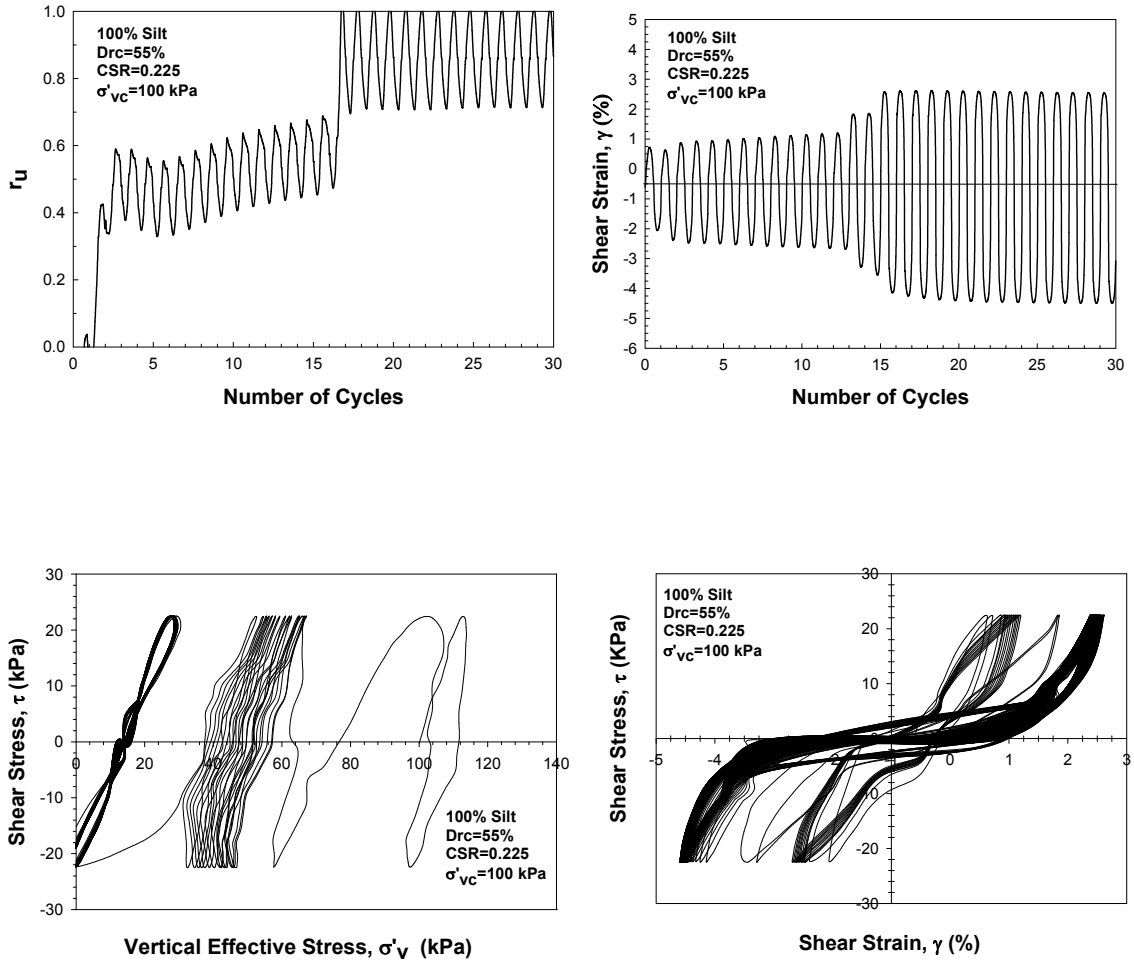

Figure B-7: Response of a pure silt specimen in a constant volume cyclic ring shear test (D_{rc} = 55%, CSR = 0.225, σ'_{vc} = 100 kPa).

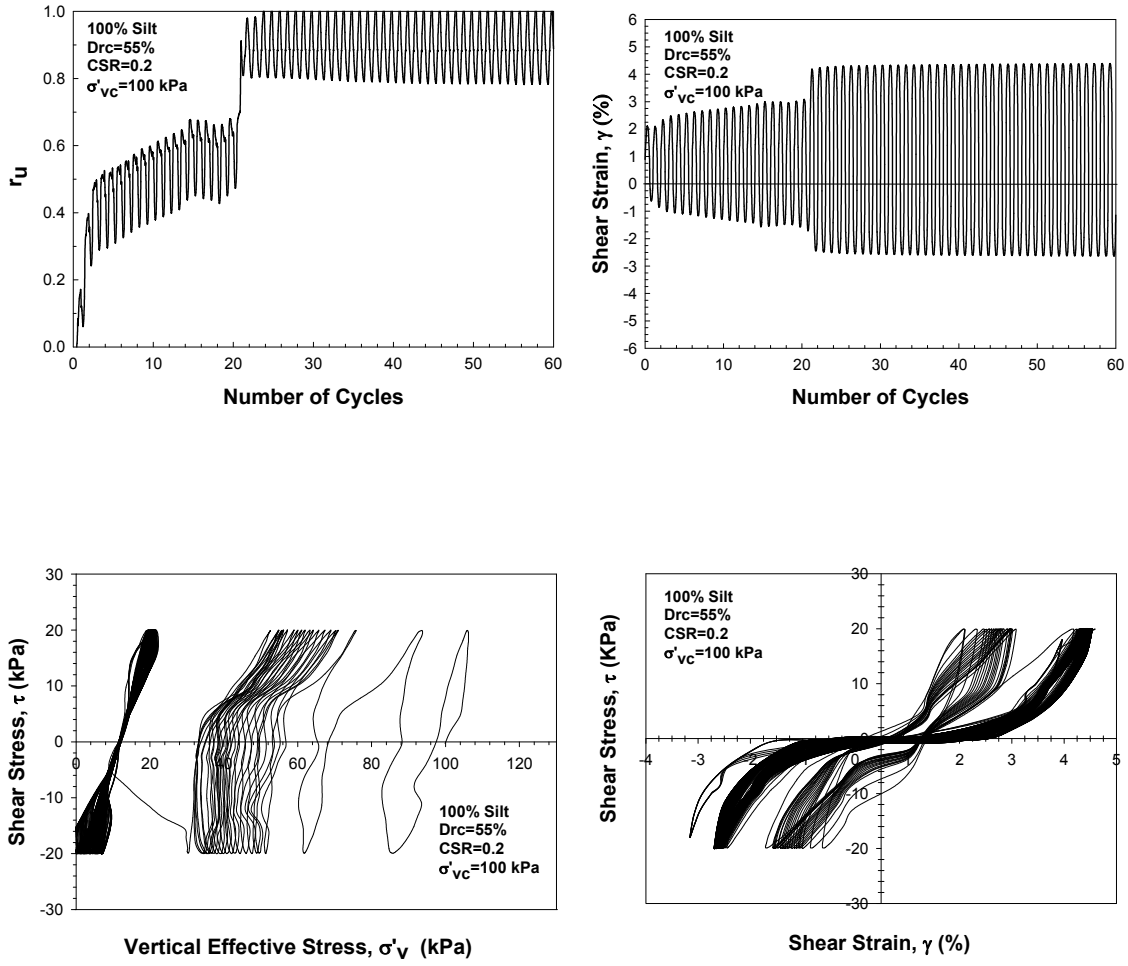

Figure B-8: Response of a pure silt specimen in a constant volume cyclic ring shear test (D_{rc} = 55%, CSR = 0.2, σ'_{vc} = 100 kPa).

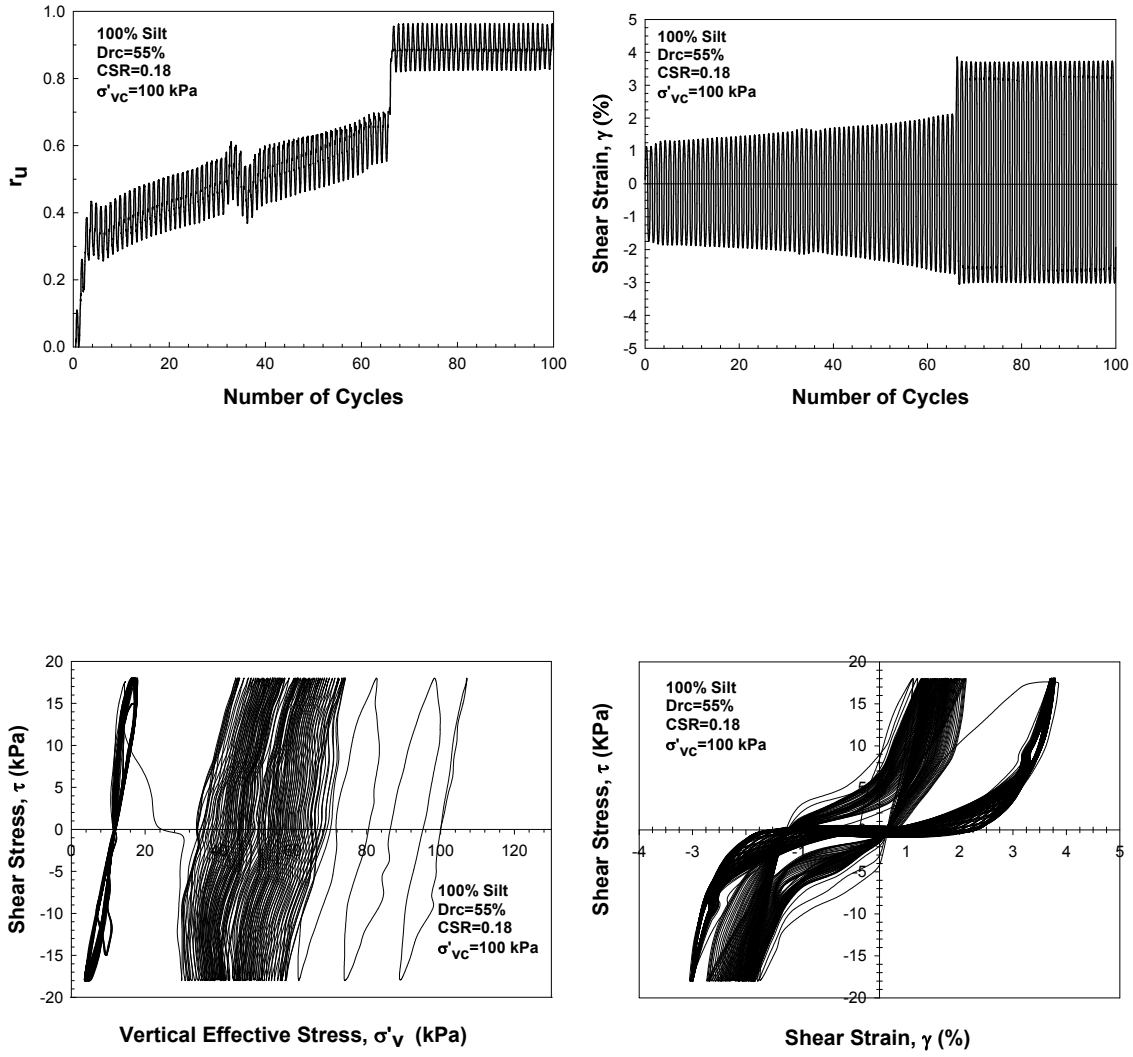

Figure B-9: Response of a pure silt specimen in a constant volume cyclic ring shear test (D_{rc} = 55%, CSR = 0.18, σ'_{vc} = 100 kPa).

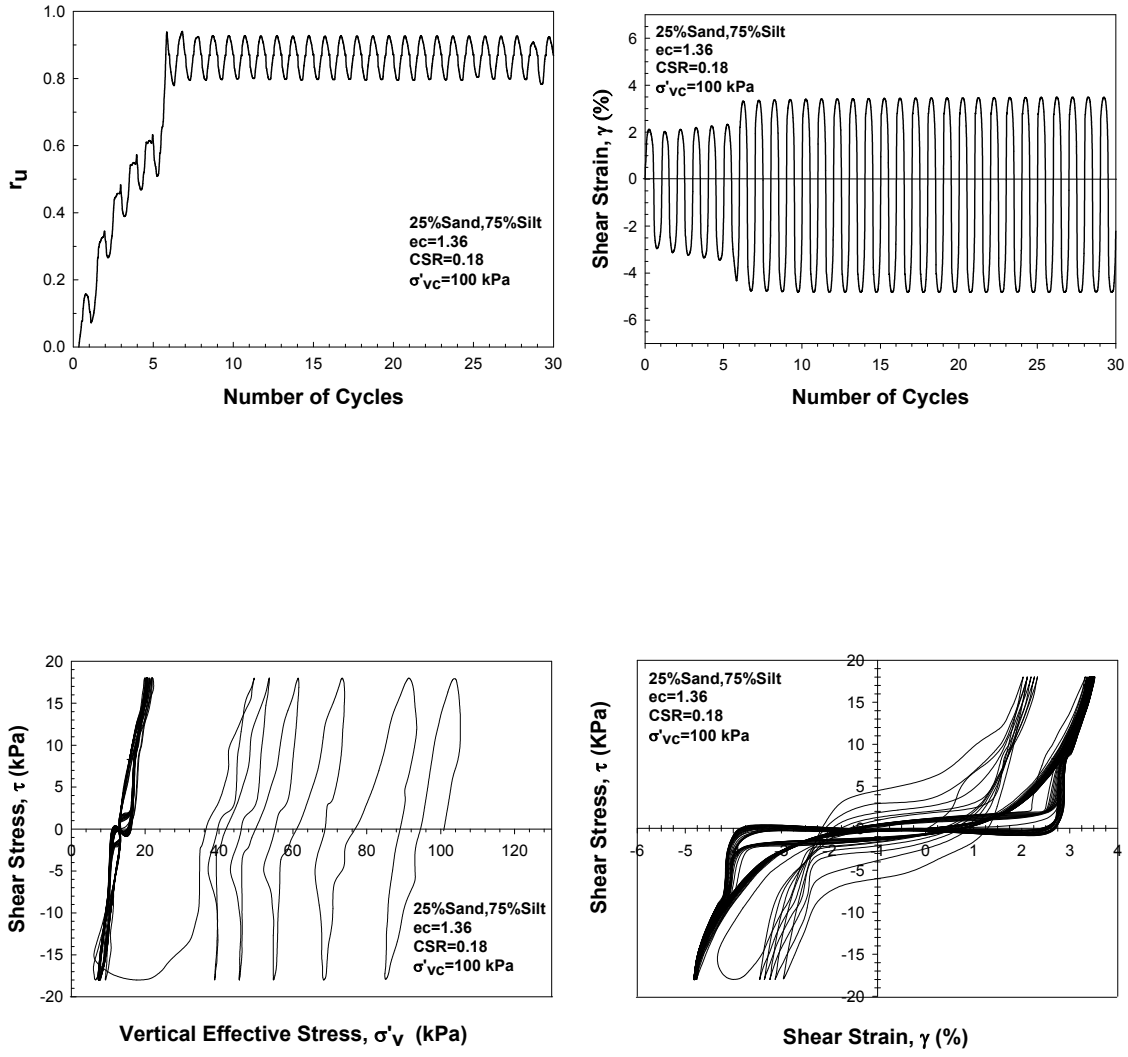

Figure B-10: Response of a sandy silt specimen with 75% silt a content in constant volume cyclic ring shear test (D_{rc} = 14%, CSR = 0.18, σ'_{vc} = 100 kPa).

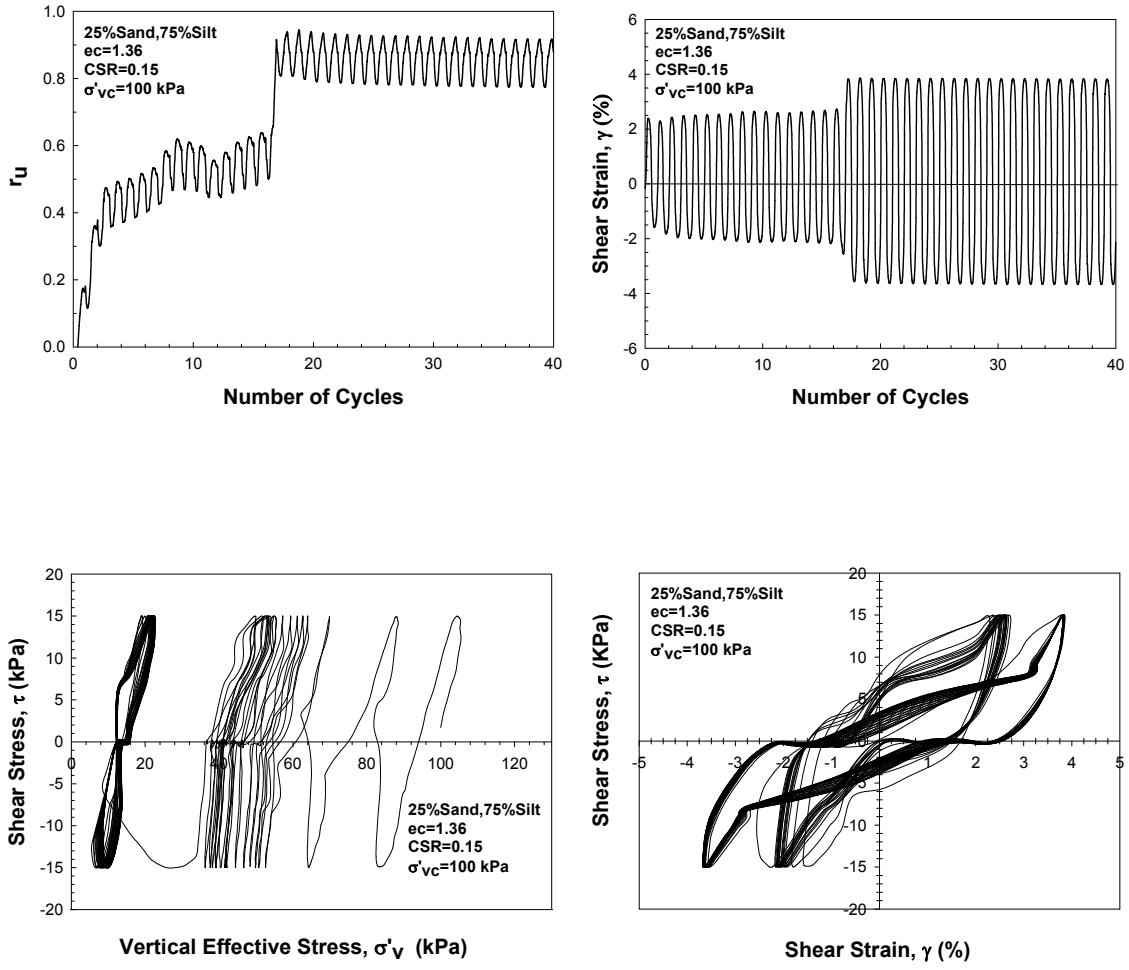

Figure B-11: Response of a sandy silt specimen with 75% silt a content in constant volume cyclic ring shear test (D_{rc} = 14%, CSR = 0.15, σ'_{vc} = 100 kPa).

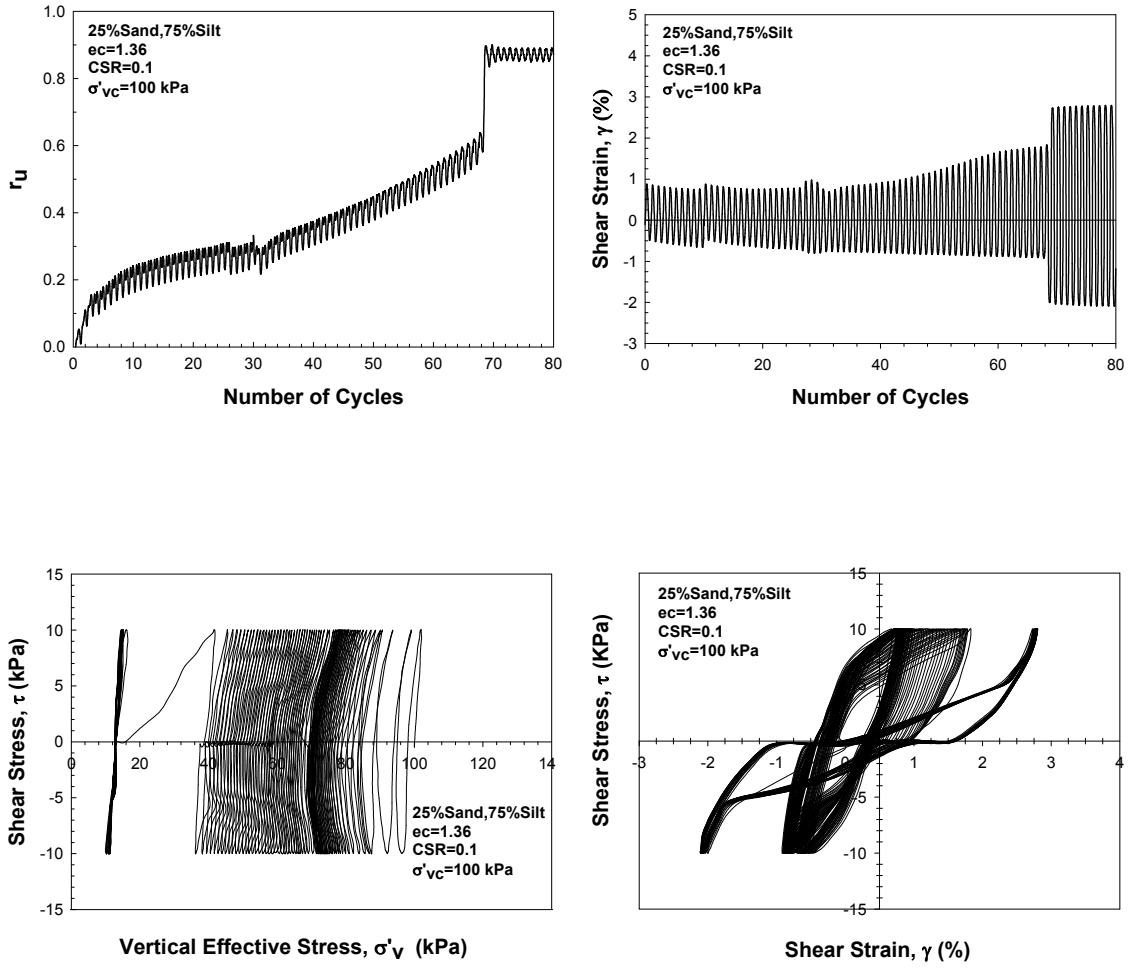

Figure B-12: Response of a sandy silt specimen with 75% silt a content in constant volume cyclic ring shear test (D_{rc} = 14%, CSR = 0.1, σ'_{vc} = 100 kPa).

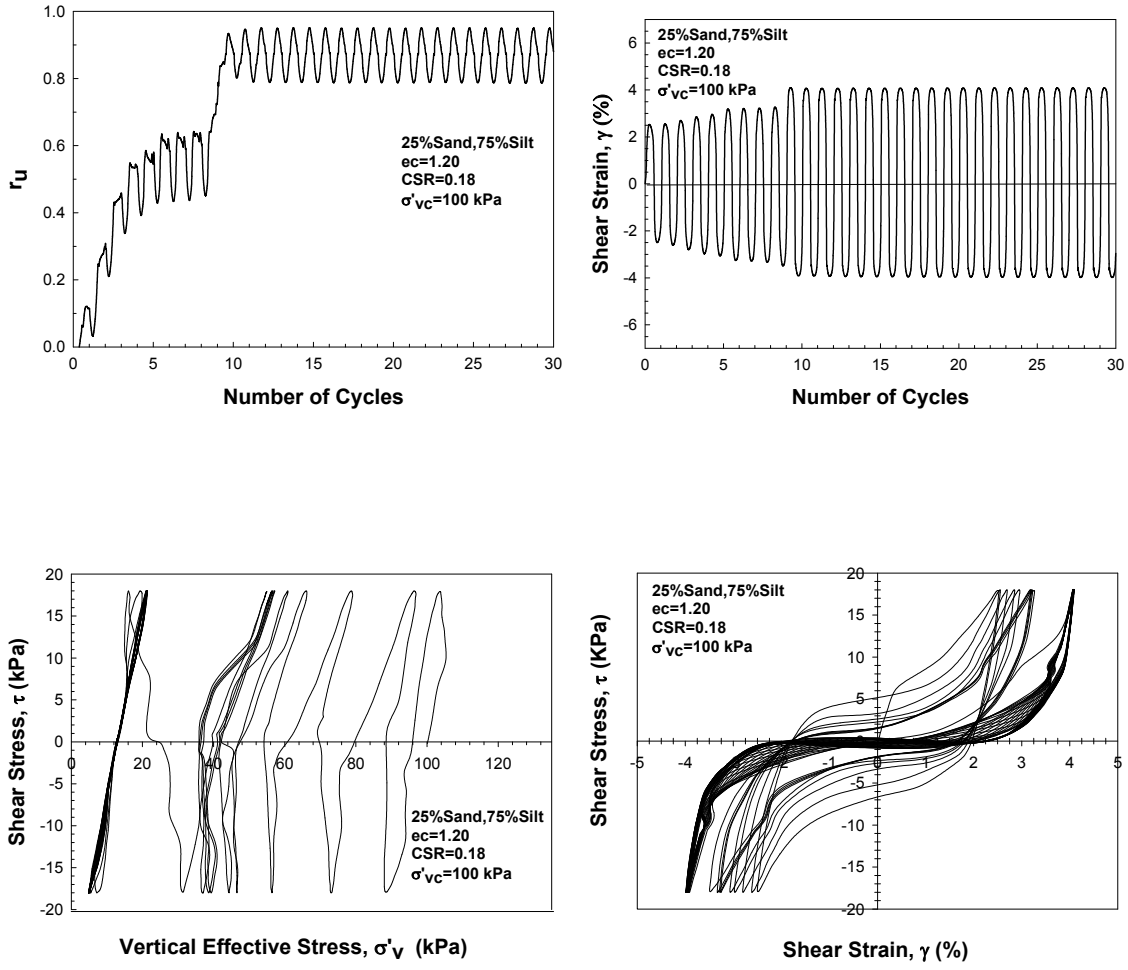

Figure B-13: Response of a sandy silt specimen with 75% silt a content in constant volume cyclic ring shear test (D_{rc} = 31%, CSR = 0.18, σ'_{vc} = 100 kPa).

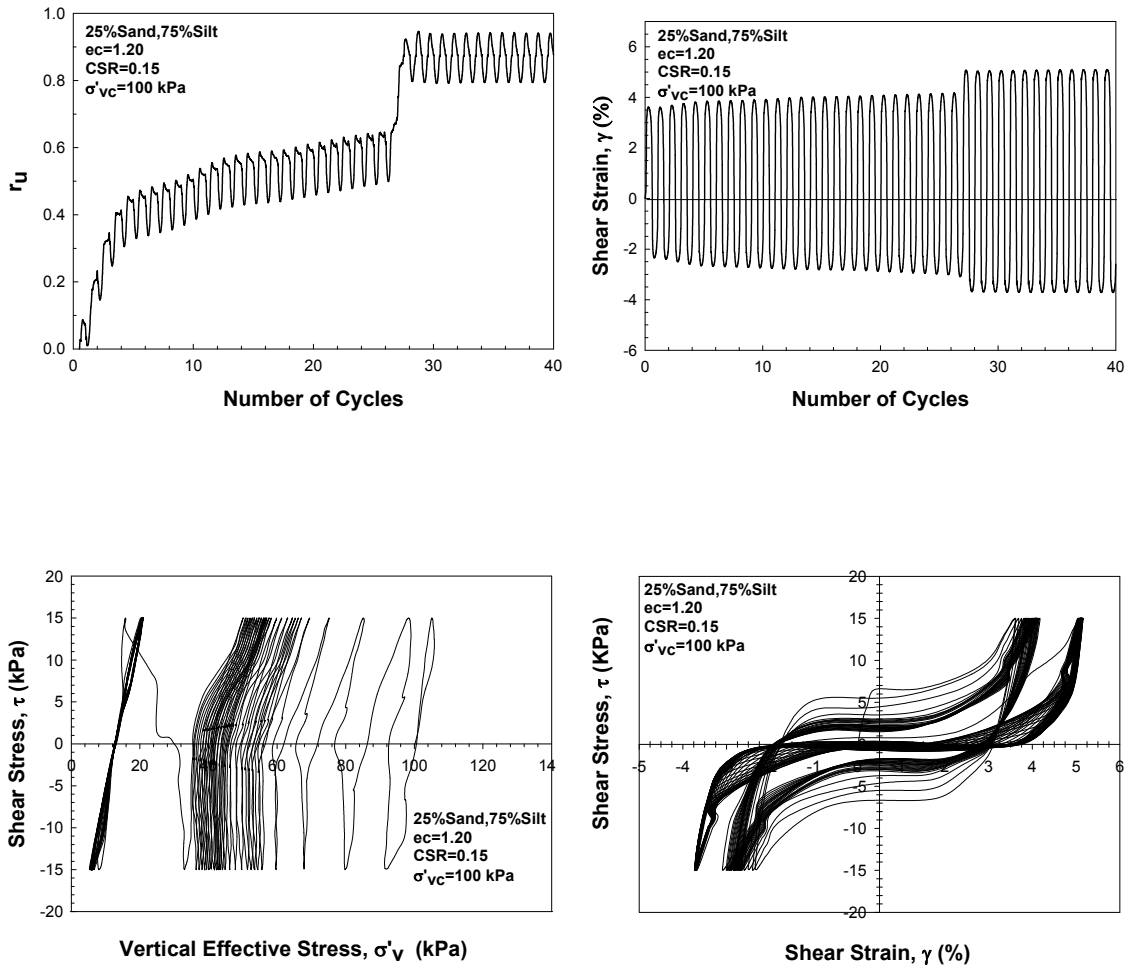

Figure B-14: Response of a sandy silt specimen with 75% silt a content in constant volume cyclic ring shear test (D_{rc} = 31%, CSR = 0.15, σ'_{vc} = 100 kPa).

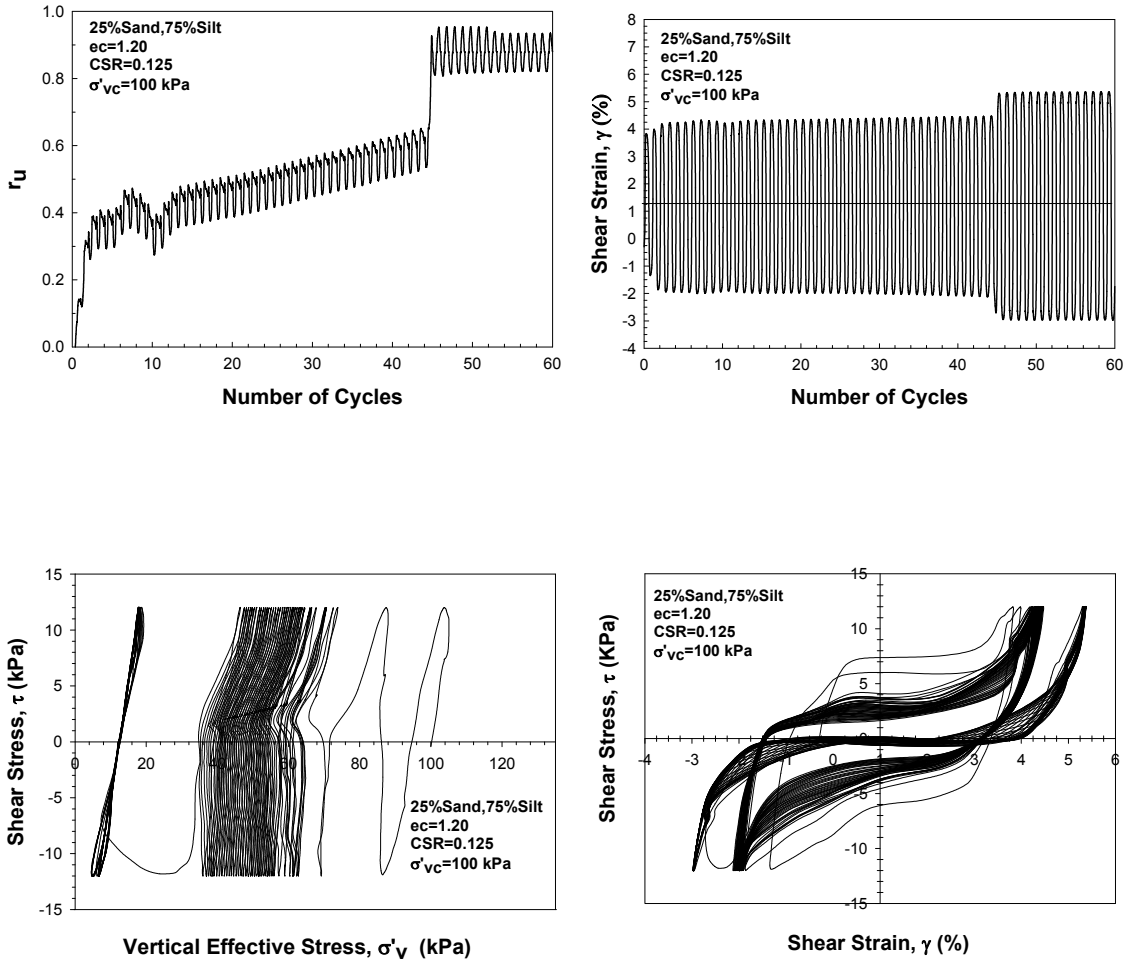

Figure B-15: Response of a sandy silt specimen with 75% silt a content in constant volume cyclic ring shear test (D_{rc} = 31%, CSR = 0.125, σ'_{vc} = 100 kPa).

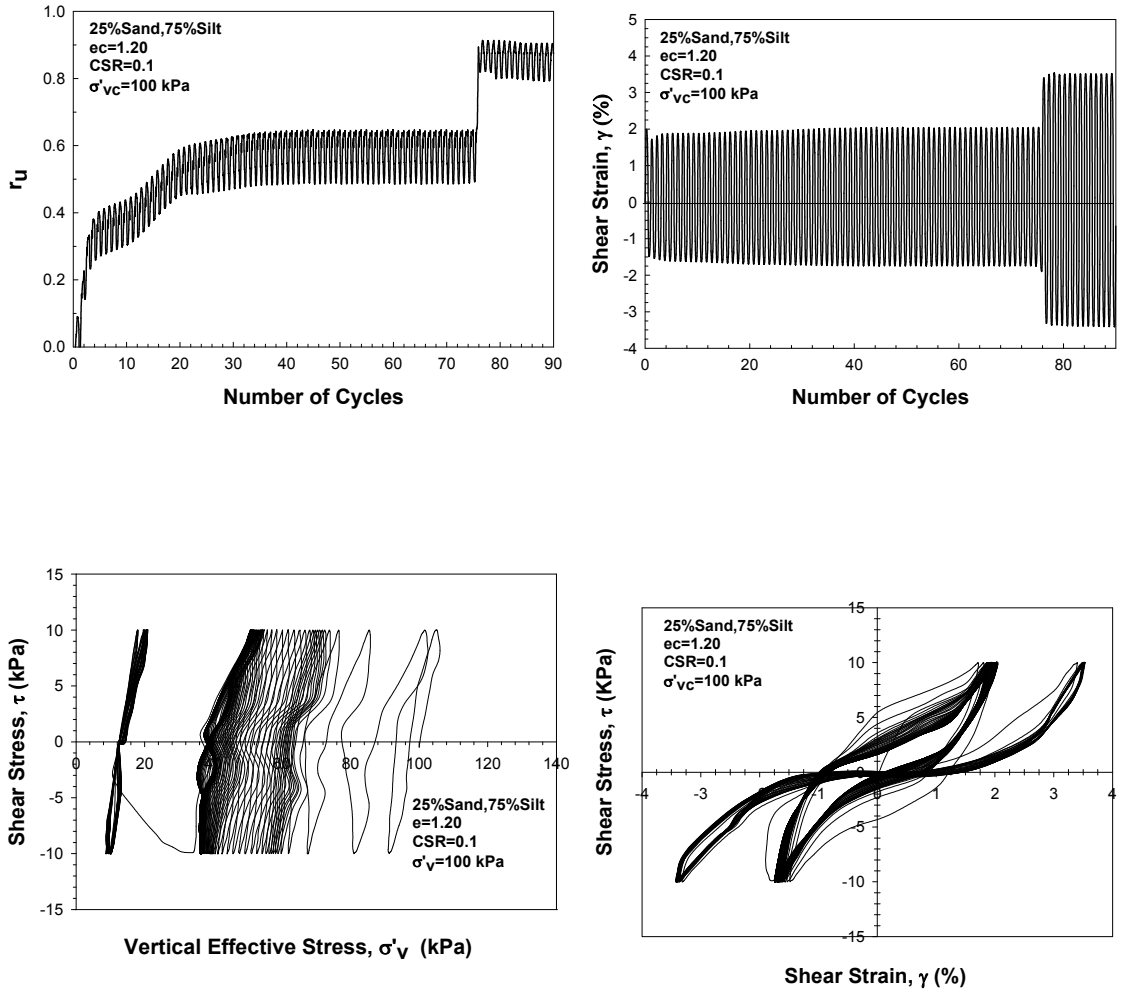

Figure B-16: Response of a sandy silt specimen with 75% silt a content in constant volume cyclic ring shear test (D_{rc} = 31%, CSR = 0.1, σ'_{vc} = 100 kPa).

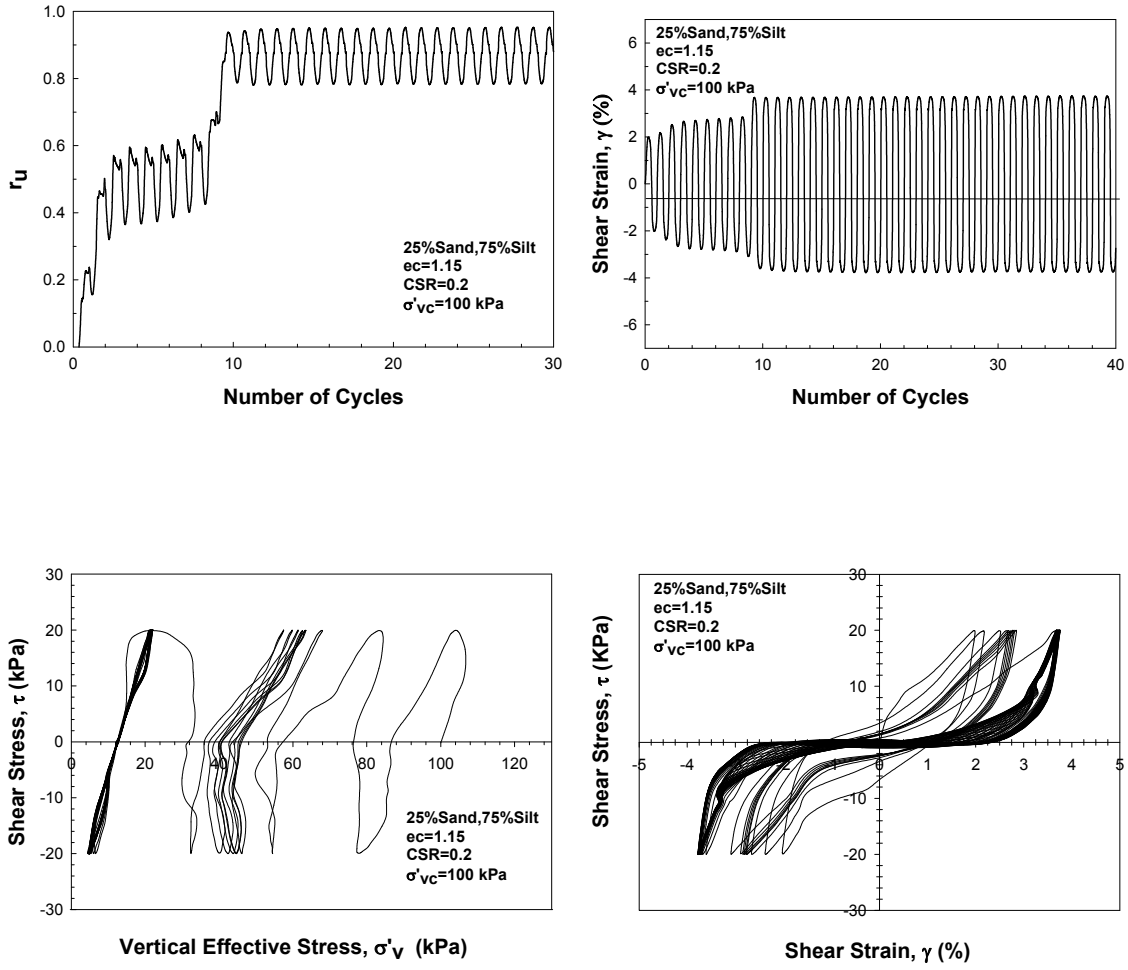

Figure B-17: Response of a sandy silt specimen with 75% silt a content in constant volume cyclic ring shear test (D_{rc} = 37%, CSR = 0.2, σ'_{vc} = 100 kPa).

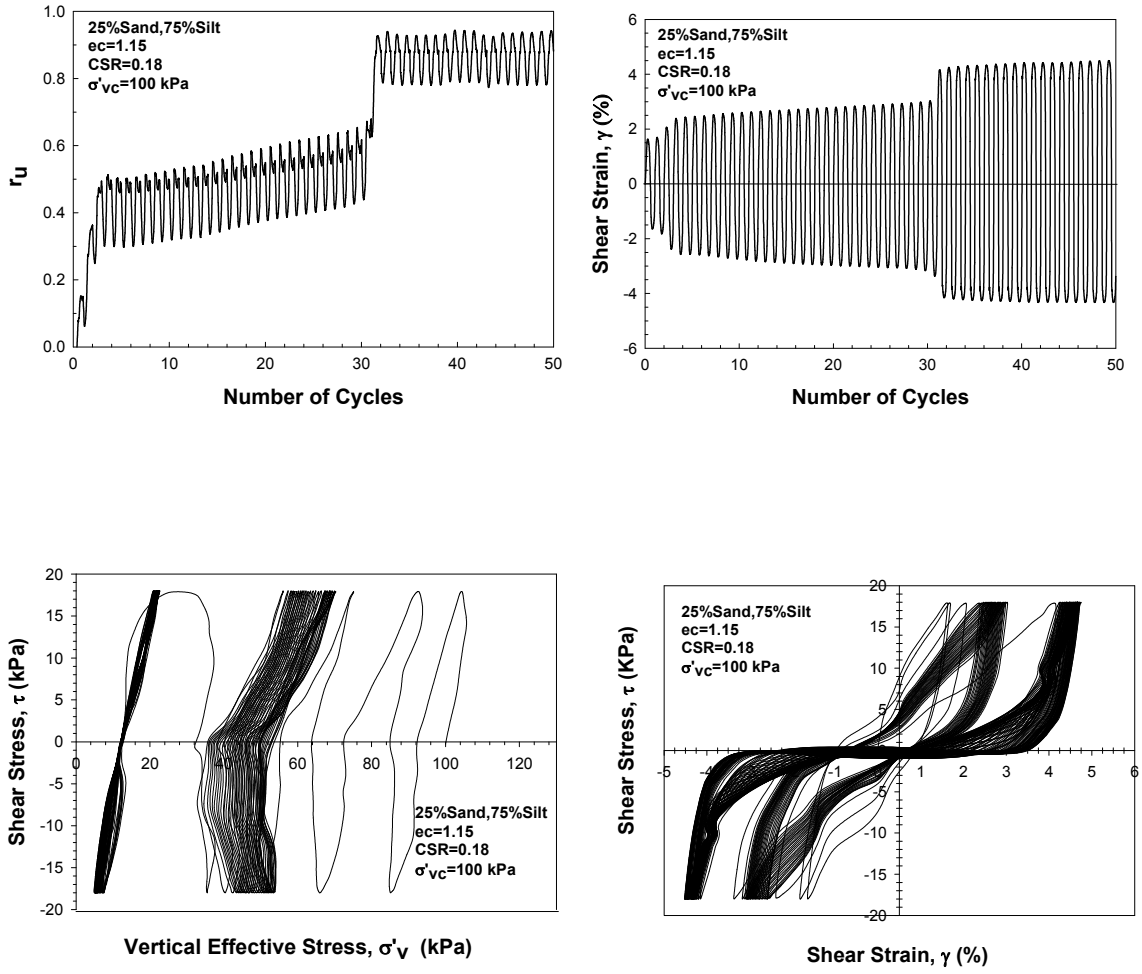

Figure B-18: Response of a sandy silt specimen with 75% silt a content in constant volume cyclic ring shear test (D_{rc} = 37%, CSR = 0.18, σ'_{vc} = 100 kPa).

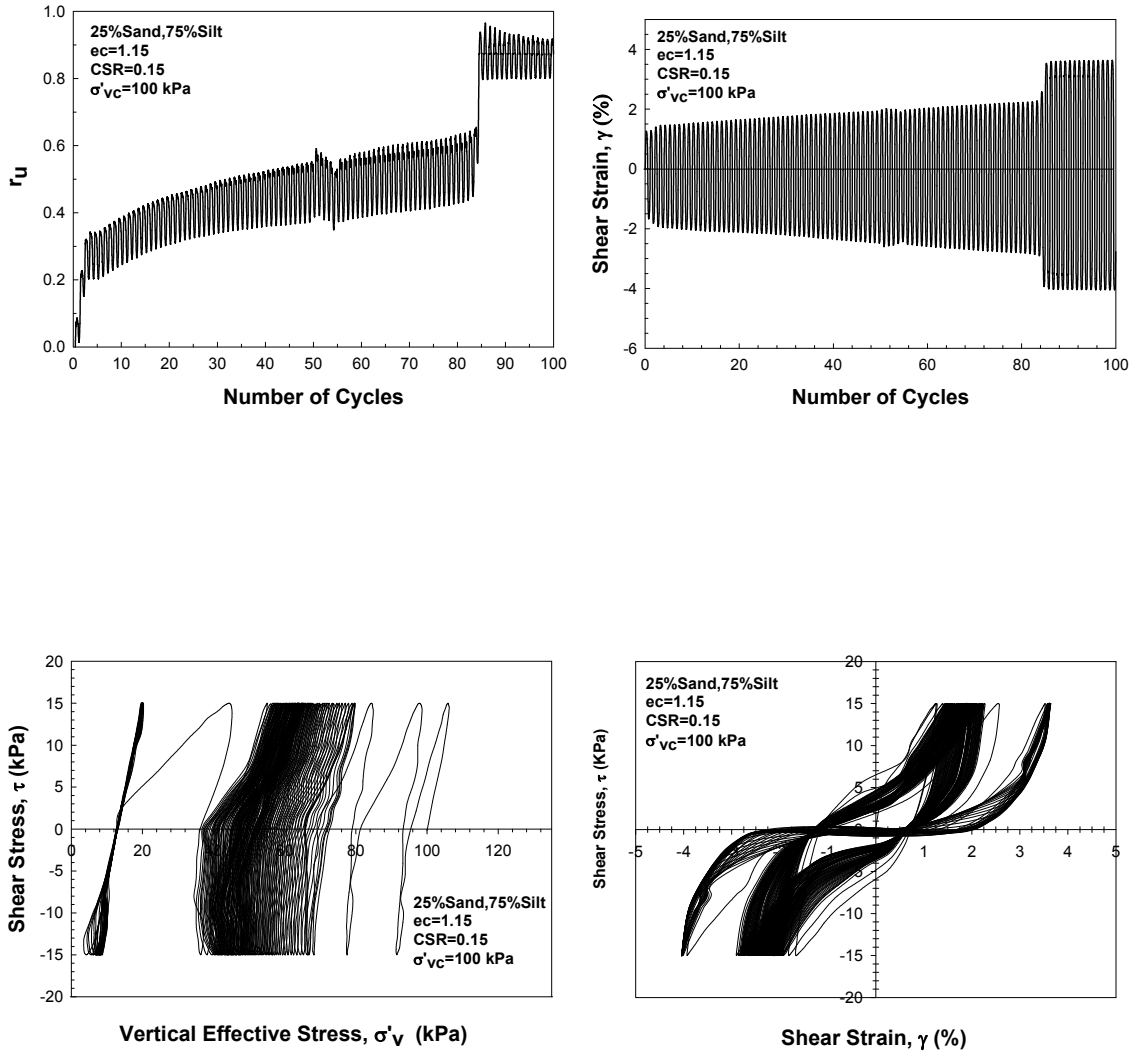

Figure B-19: Response of a sandy silt specimen with 75% silt a content in constant volume cyclic ring shear test (D_{rc} = 37%, CSR = 0.15, σ'_{vc} = 100 kPa).

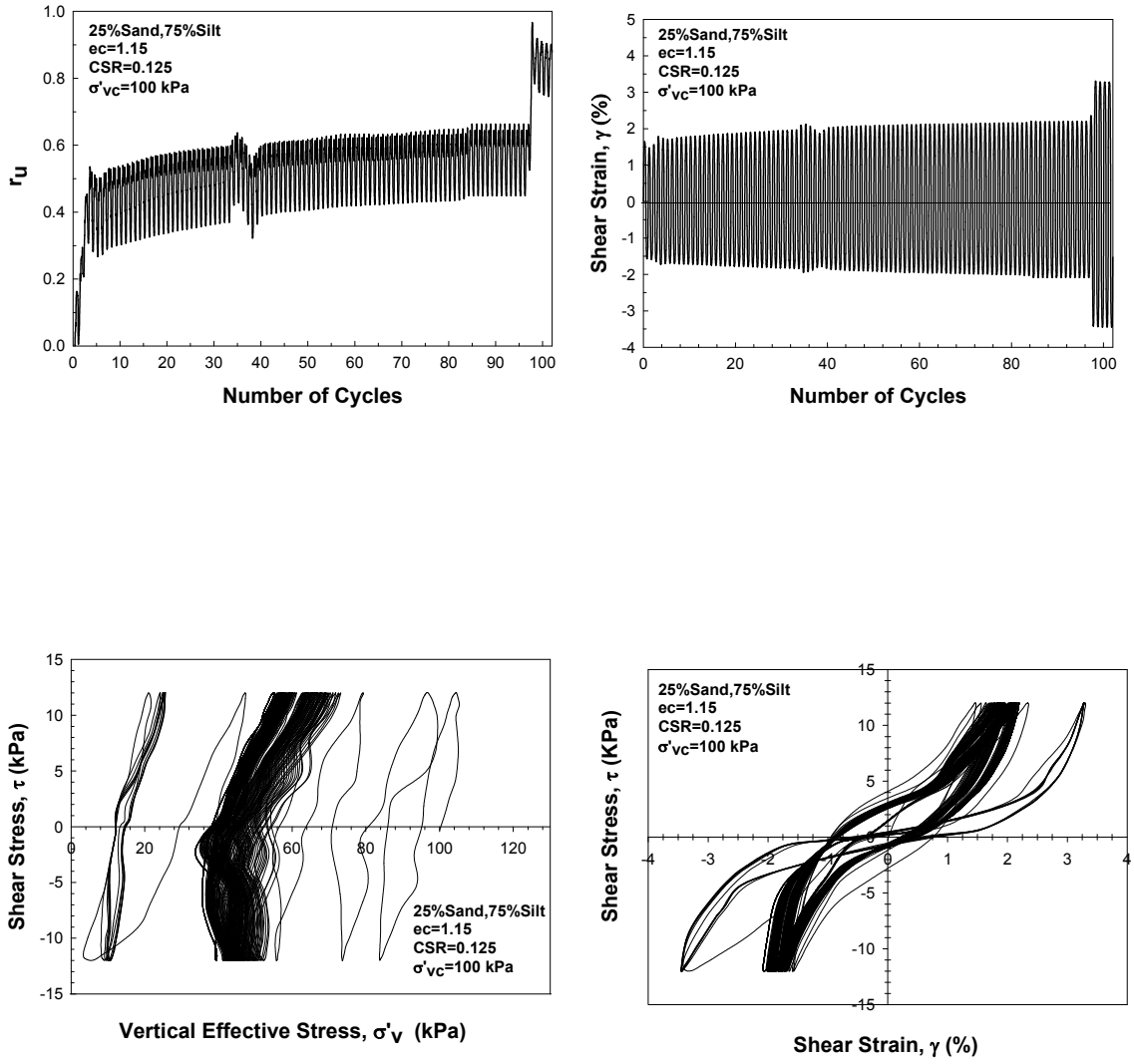

Figure B-20: Response of a sandy silt specimen with 75% silt a content in constant volume cyclic ring shear test (D_{rc} = 37%, CSR = 0.125, σ'_{vc} = 100 kPa).

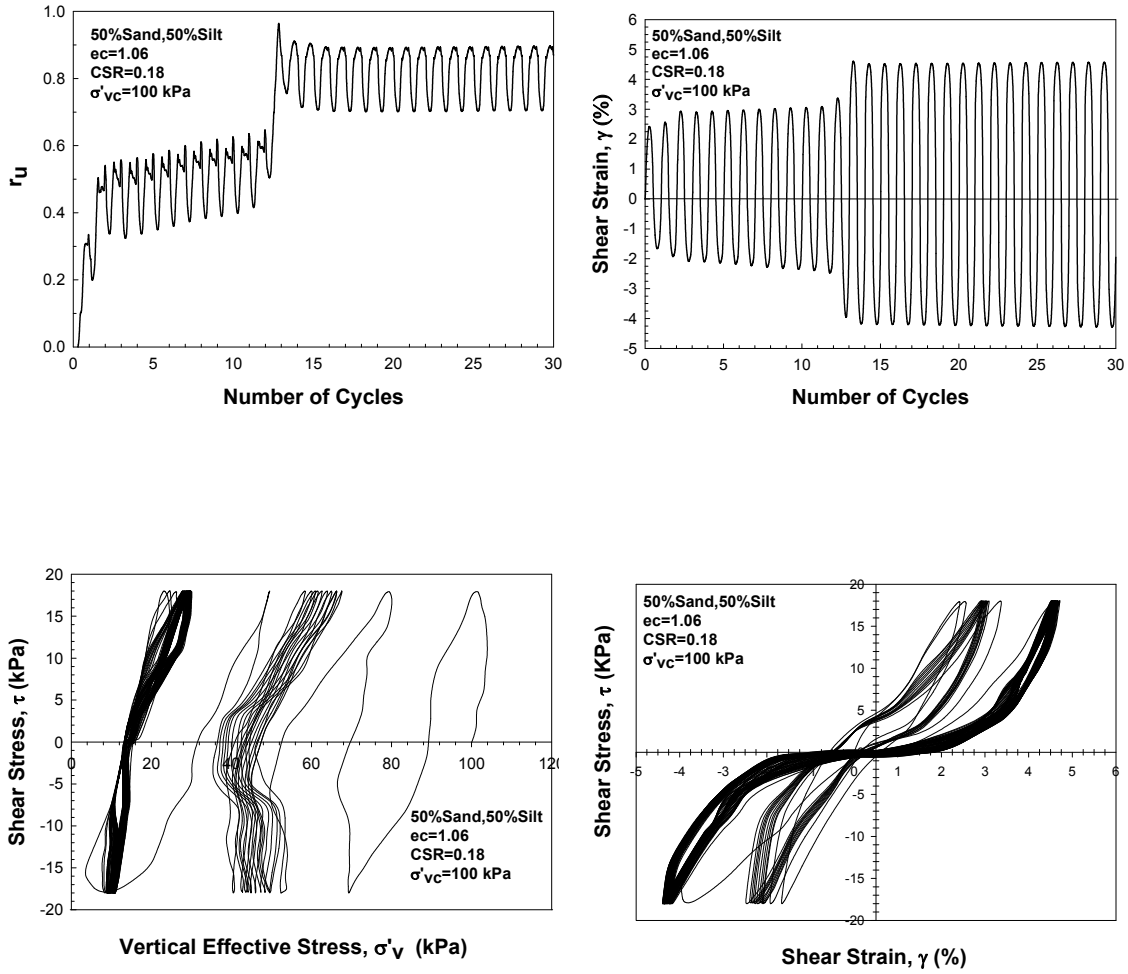

Figure B-21: Response of a sandy silt specimen with 50% silt a content in constant volume cyclic ring shear test (D_{rc} = 13%, CSR = 0.18, σ'_{vc} = 100 kPa).

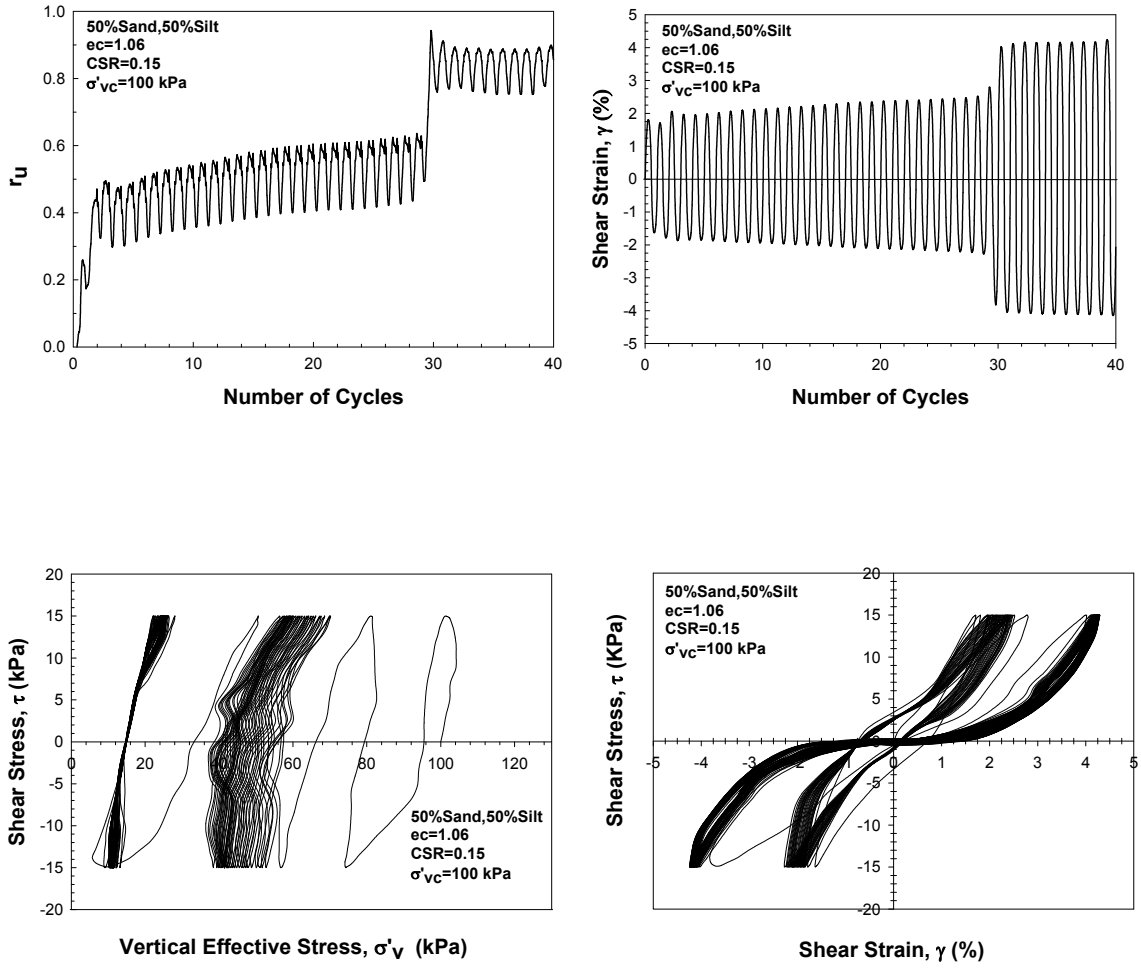

Figure B-22: Response of a sandy silt specimen with 50% silt a content in constant volume cyclic ring shear test (D_{rc} = 13%, CSR = 0.15, σ'_{vc} = 100 kPa).

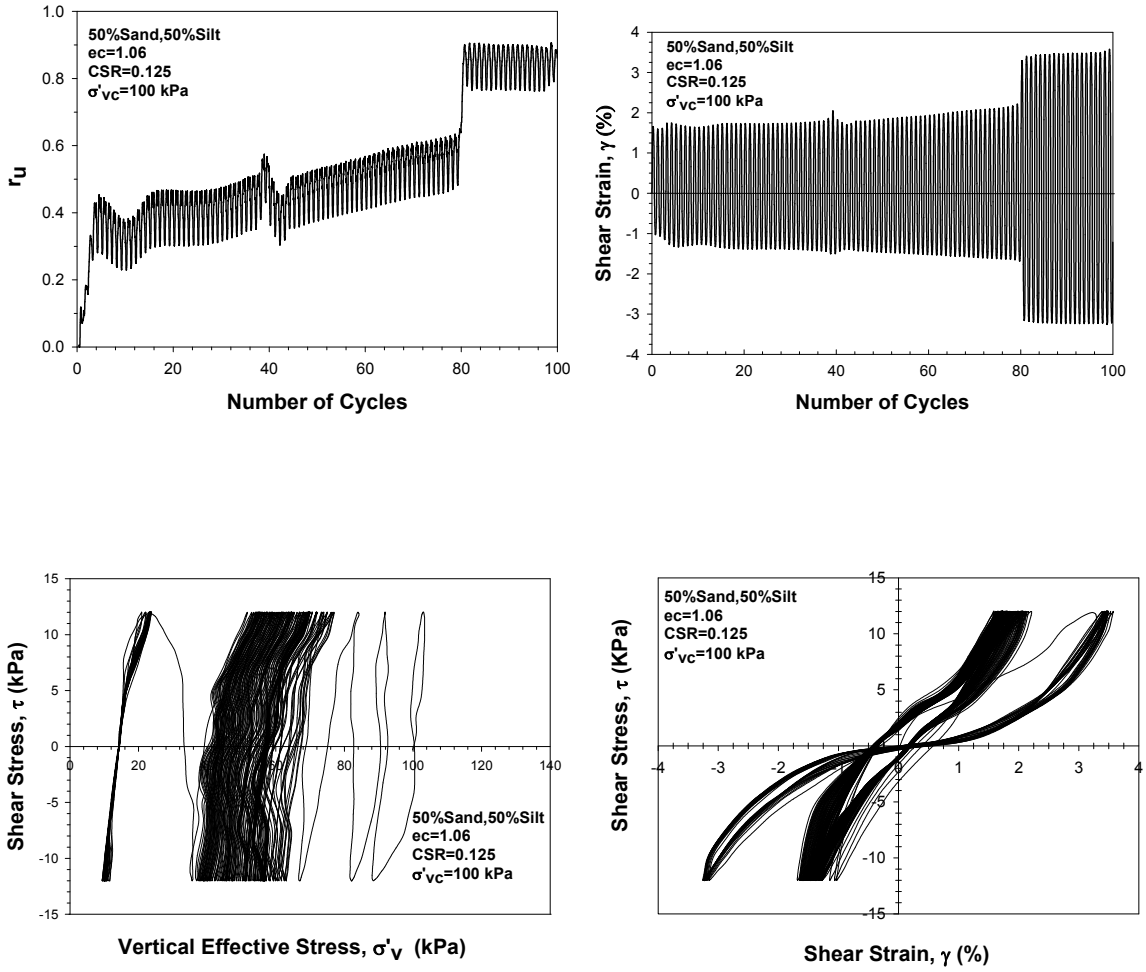

Figure B-23: Response of a sandy silt specimen with 50% silt a content in constant volume cyclic ring shear test (D_{rc} = 13%, CSR = 0.125, σ'_{vc} = 100 kPa).

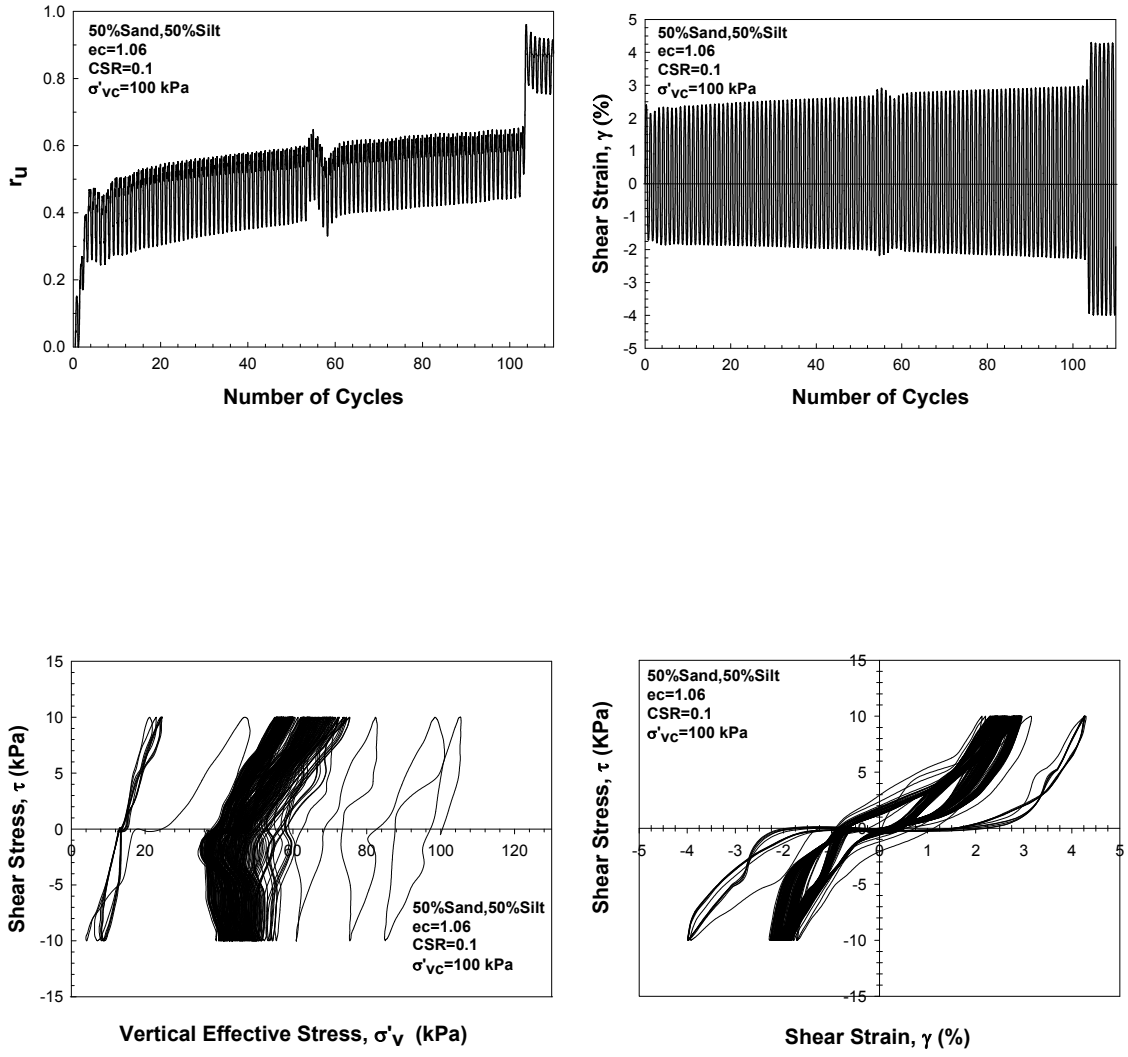

Figure B-24: Response of a sandy silt specimen with 50% silt a content in constant volume cyclic ring shear test (D_{rc} = 13%, CSR = 0.1, σ'_{vc} = 100 kPa).

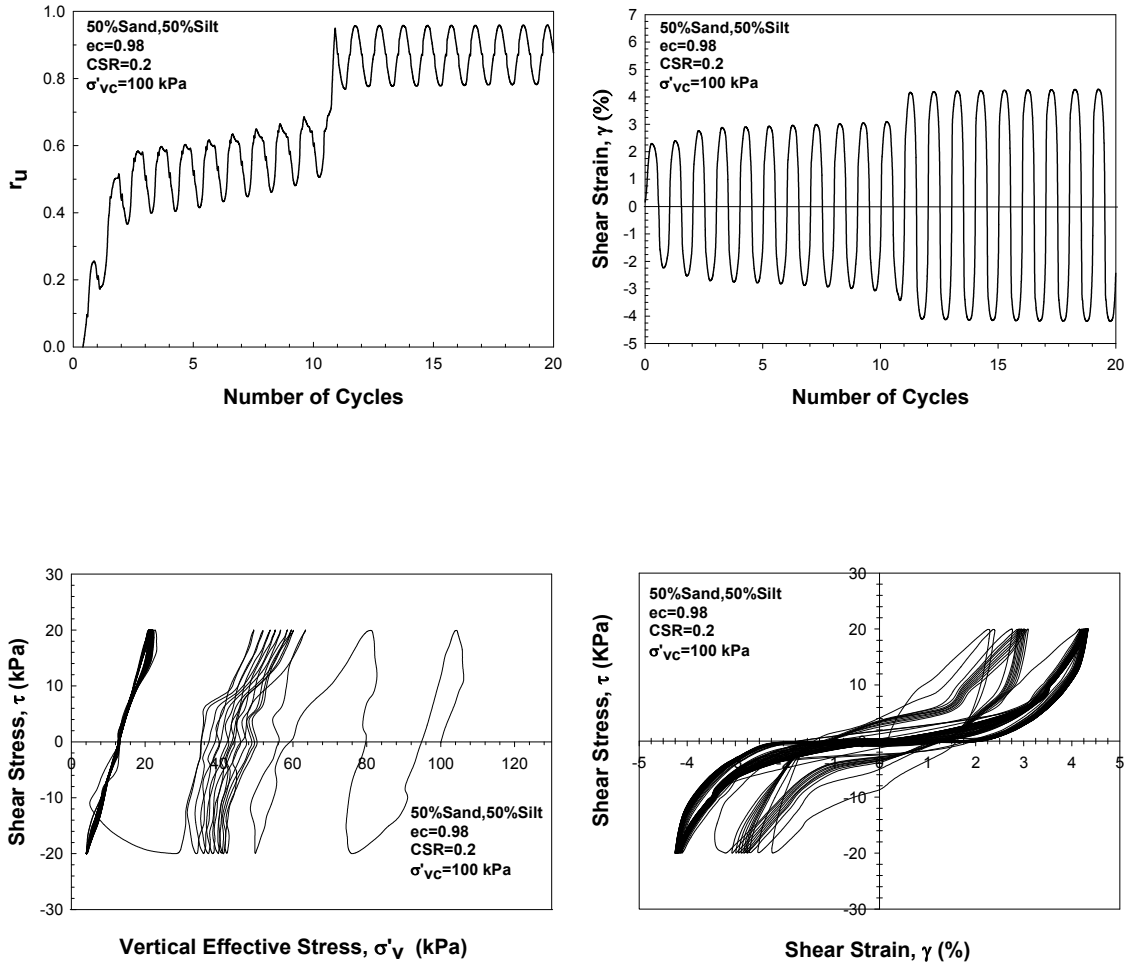

Figure B-25: Response of a sandy silt specimen with 50% silt a content in constant volume cyclic ring shear test (D_{rc} = 25%, CSR = 0.2, σ'_{vc} = 100 kPa).

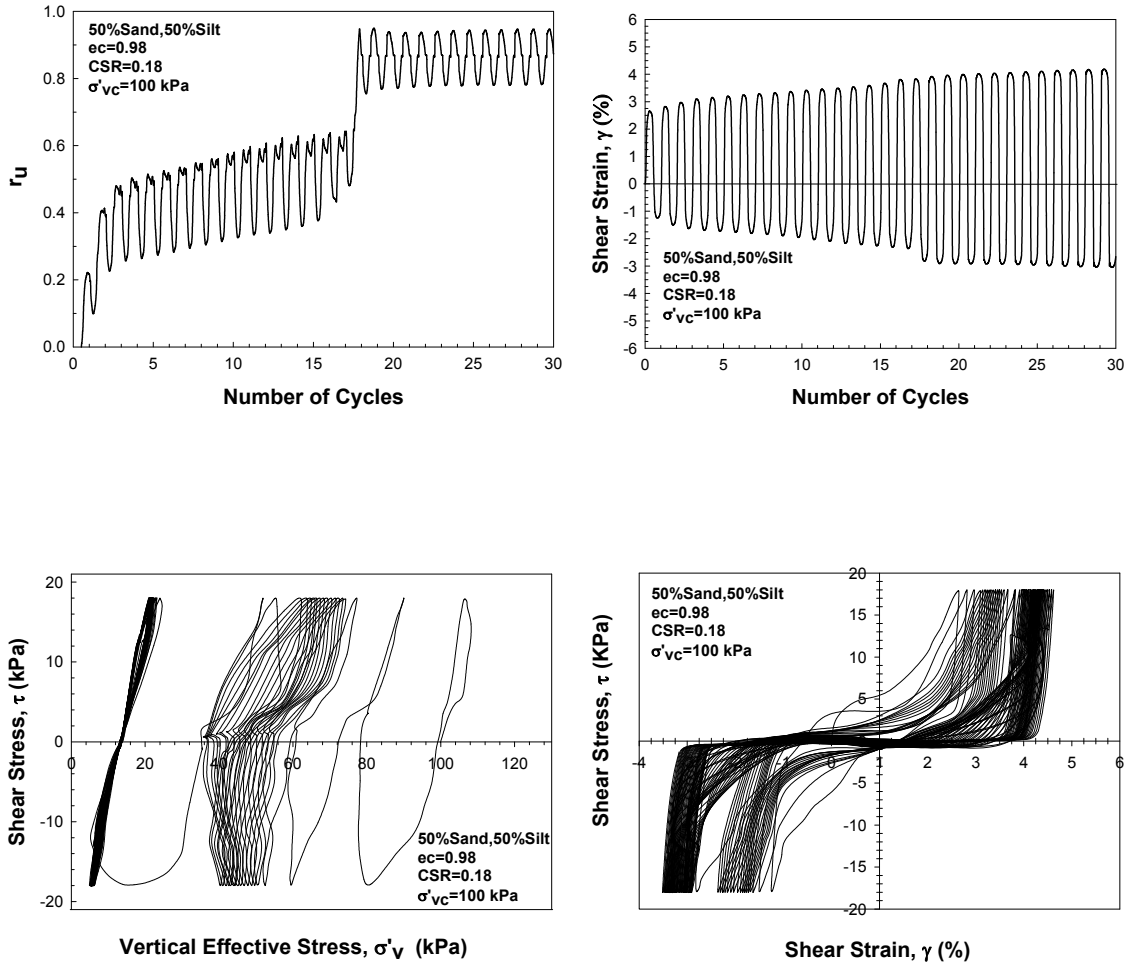

Figure B-26: Response of a sandy silt specimen with 50% silt a content in constant volume cyclic ring shear test (D_{rc} = 25%, CSR = 0.18, σ'_{vc} = 100 kPa).

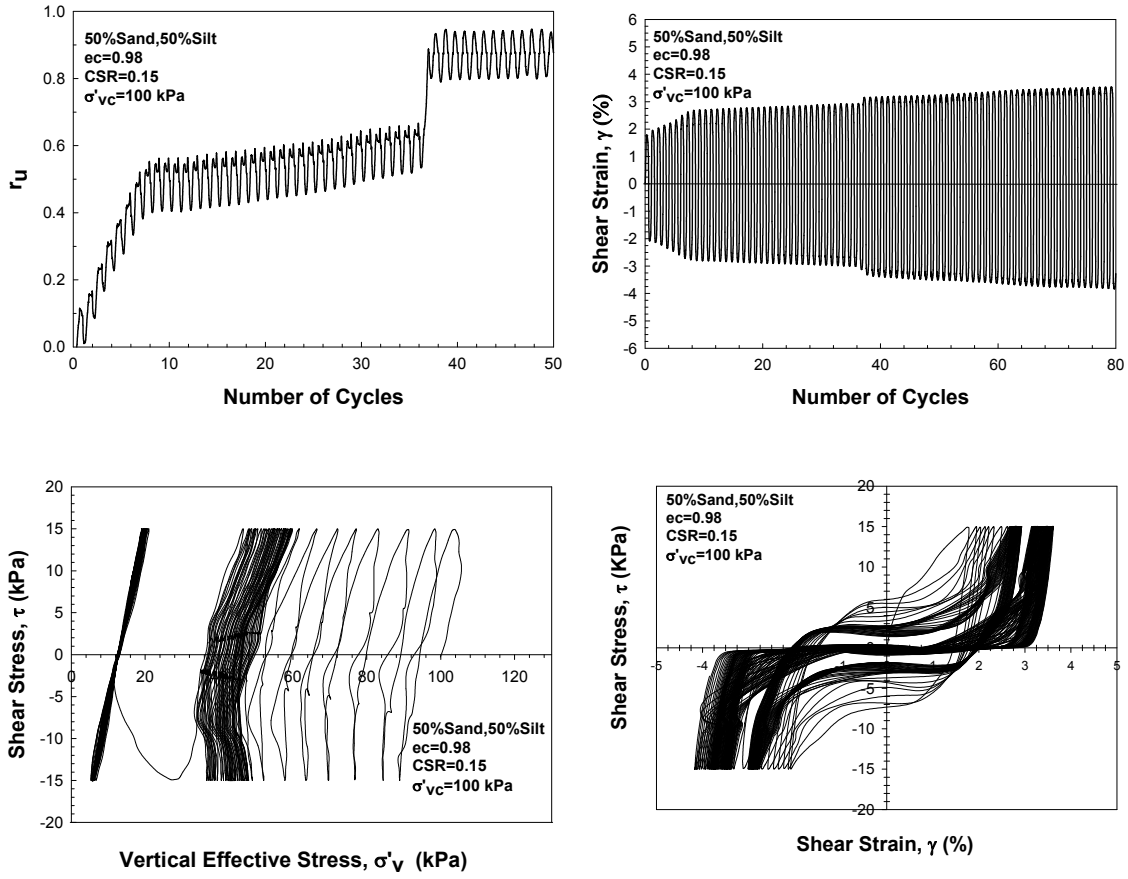

Figure B-27: Response of a sandy silt specimen with 50% silt a content in constant volume cyclic ring shear test (D_{rc} = 25%, CSR = 0.15, σ'_{vc} = 100 kPa).

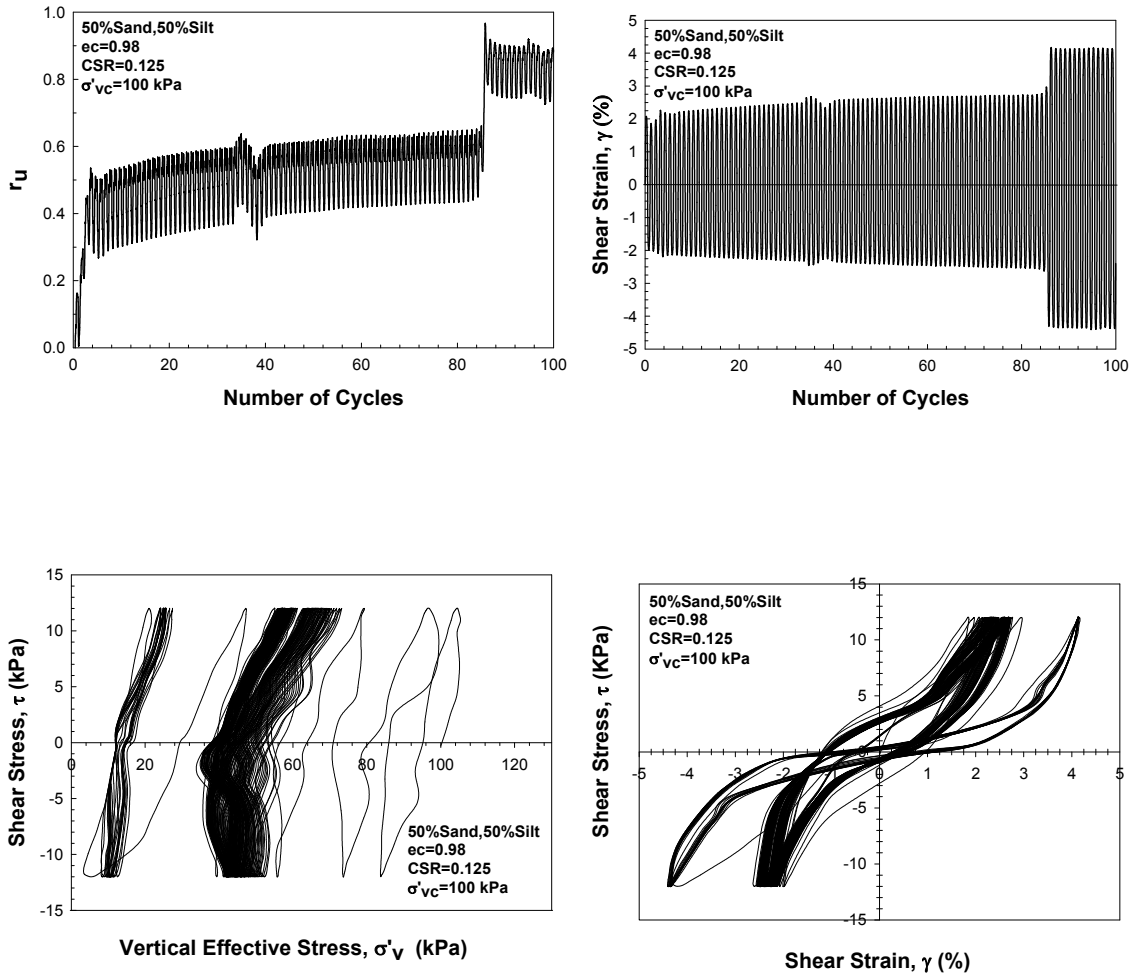

Figure B-28: Response of a sandy silt specimen with 50% silt a content in constant volume cyclic ring shear test (D_{rc} = 25%, CSR = 0.125, σ'_{vc} = 100 kPa).

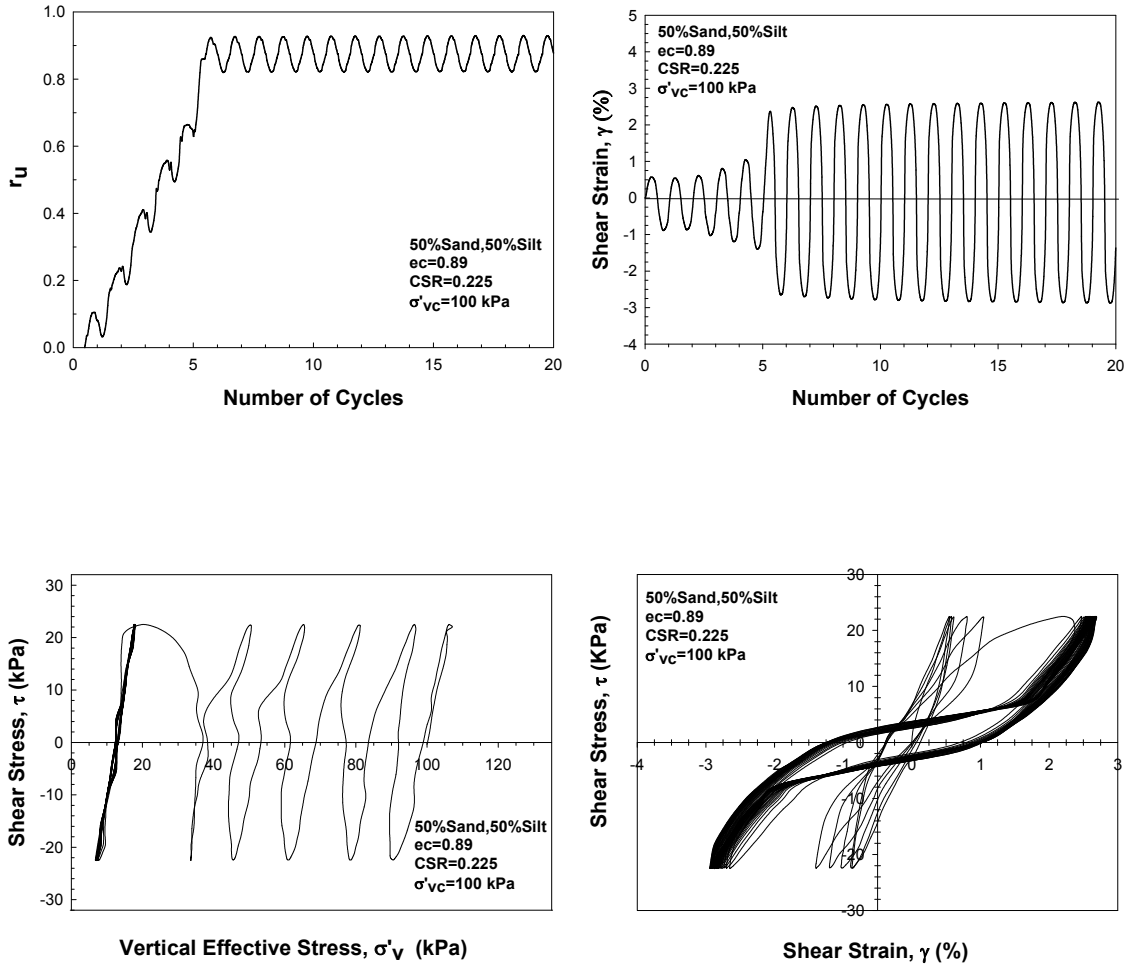

Figure B-29: Response of a sandy silt specimen with 50% silt a content in constant volume cyclic ring shear test (D_{rc} = 38%, CSR = 0.225, σ'_{vc} = 100 kPa).

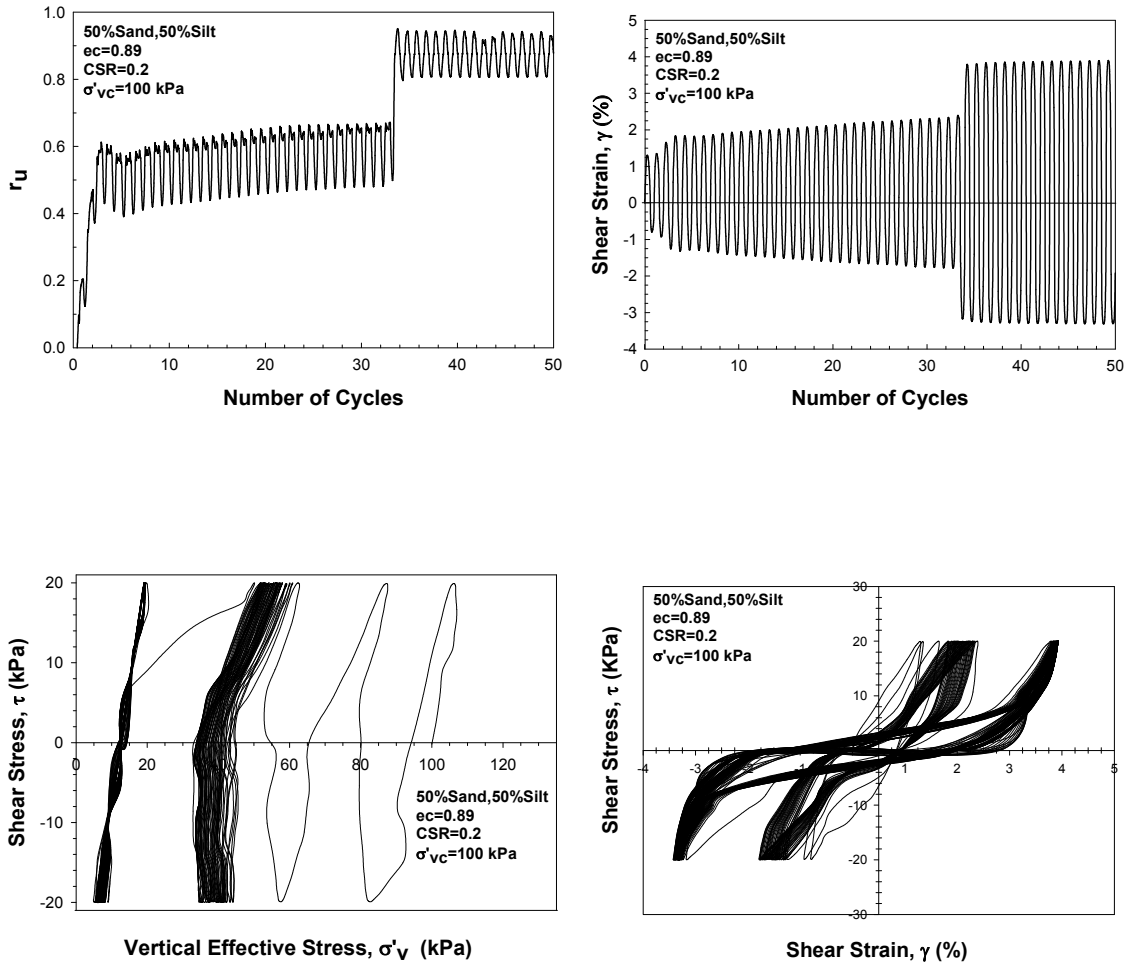

Figure B-30: Response of a sandy silt specimen with 50% silt a content in constant volume cyclic ring shear test (D_{rc} = 38%, CSR = 0.2, σ'_{vc} = 100 kPa).

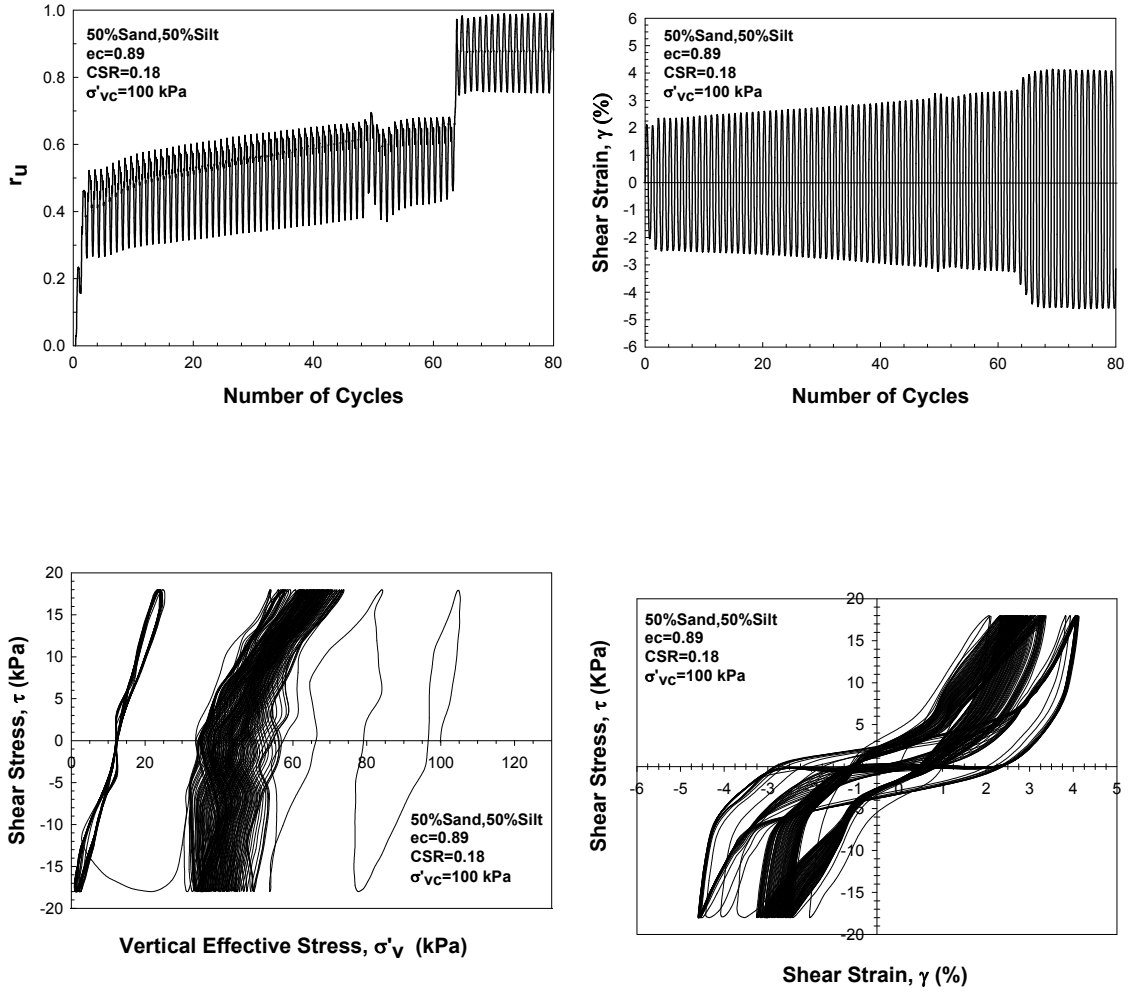

Figure B-31: Response of a sandy silt specimen with 50% silt a content in constant volume cyclic ring shear test (D_{rc} = 38%, CSR = 0.18, σ'_{vc} = 100 kPa).

Appendix C

Appendix C includes the shear wave velocity readings and measurements captured by bender elements. The measurements have been conducted on silt and sandy silt specimens of different relative densities (Drc) at a vertical effective stress (σ′vc) ranging from 50 to 300 kPa, in 50 kPa increments.

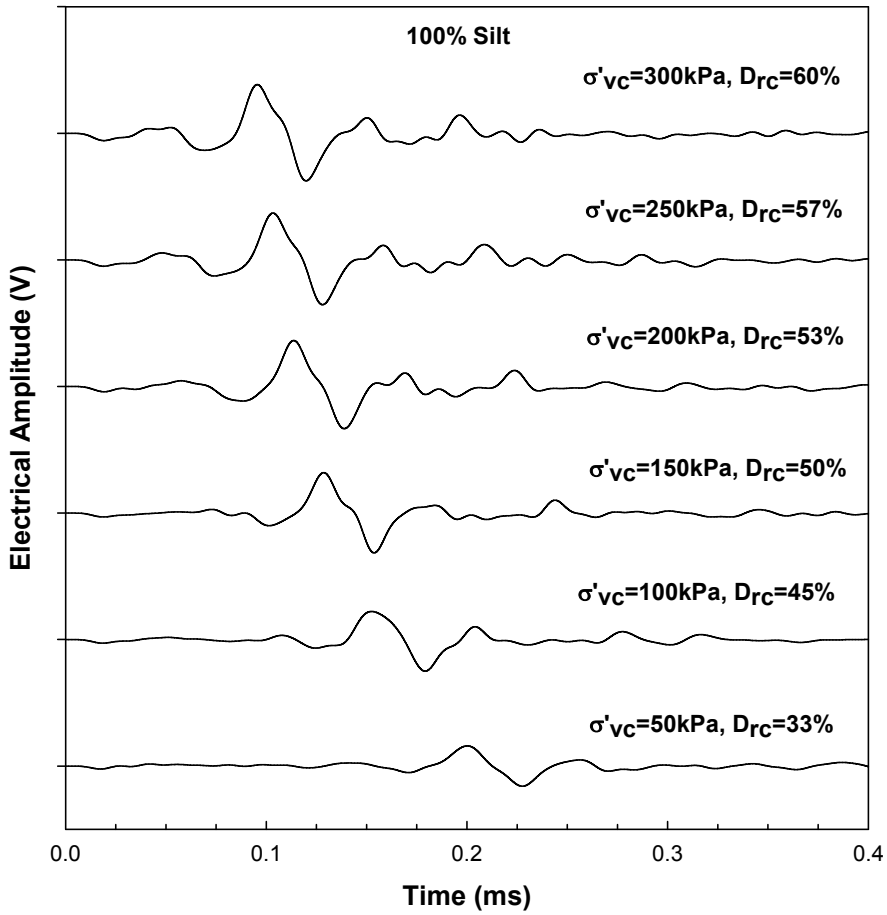

Figure C - 2: Electrical wave signals captured by the bender element over a range of σ'_{vc} = 50 - 300 kPa in pure silt specimen.

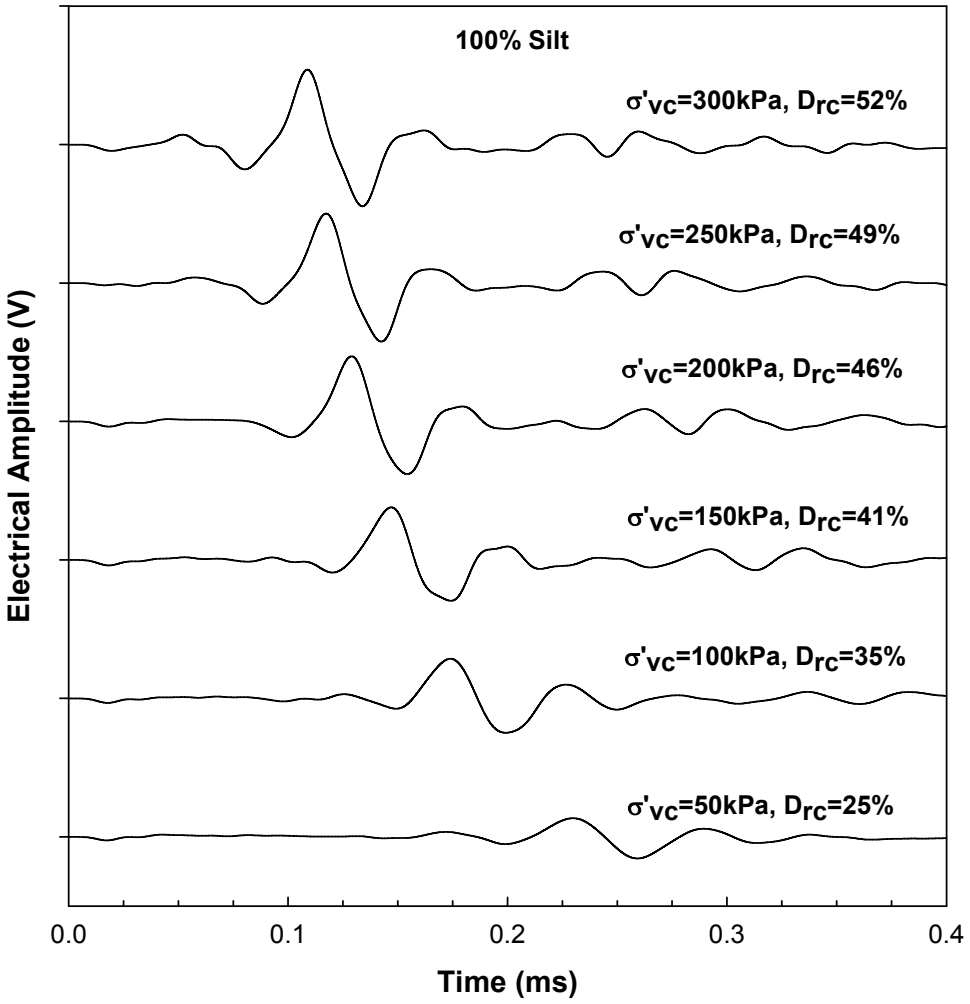

Figure C - 3: Electrical wave signals captured by the bender element over a range of σ'_{vc} = 50 - 300 kPa in pure silt specimen.

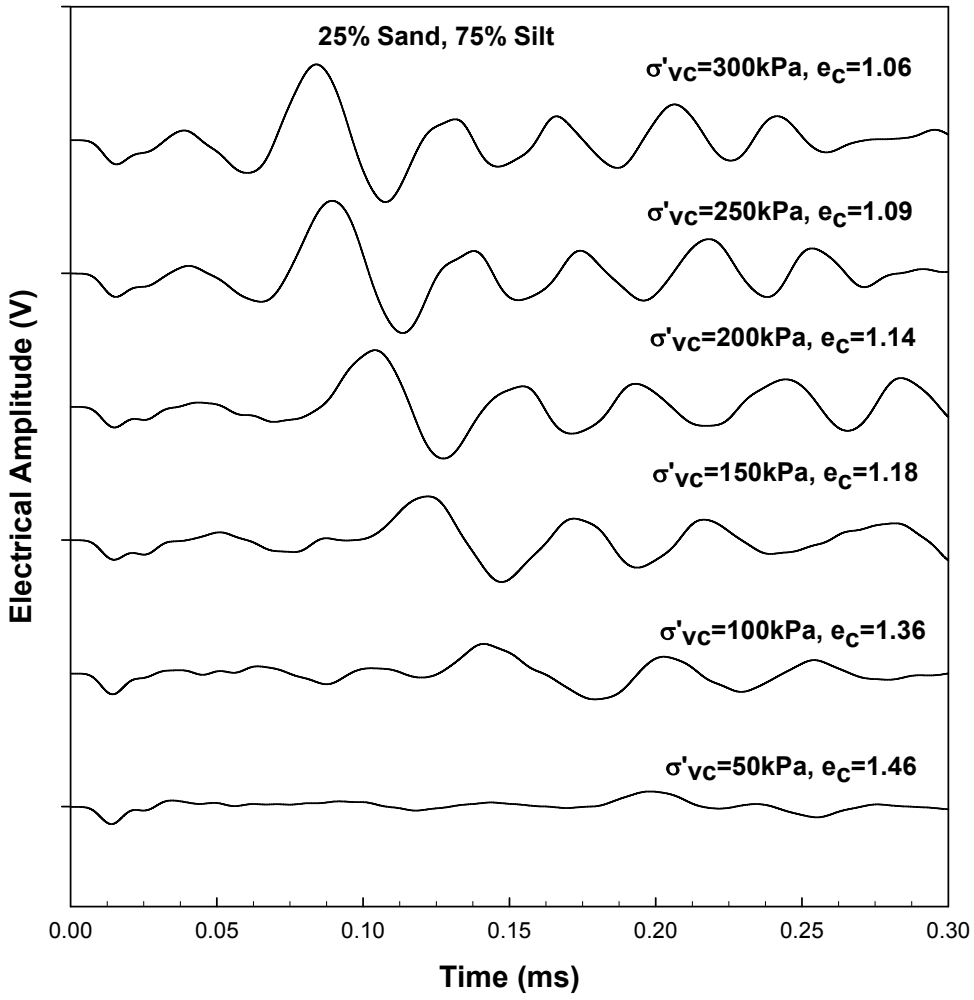

Figure C - 4: Electrical wave signals captured by the bender element and over a range of σ'_{vc} = 50 - 300 kPa in specimens of 75% silt content.

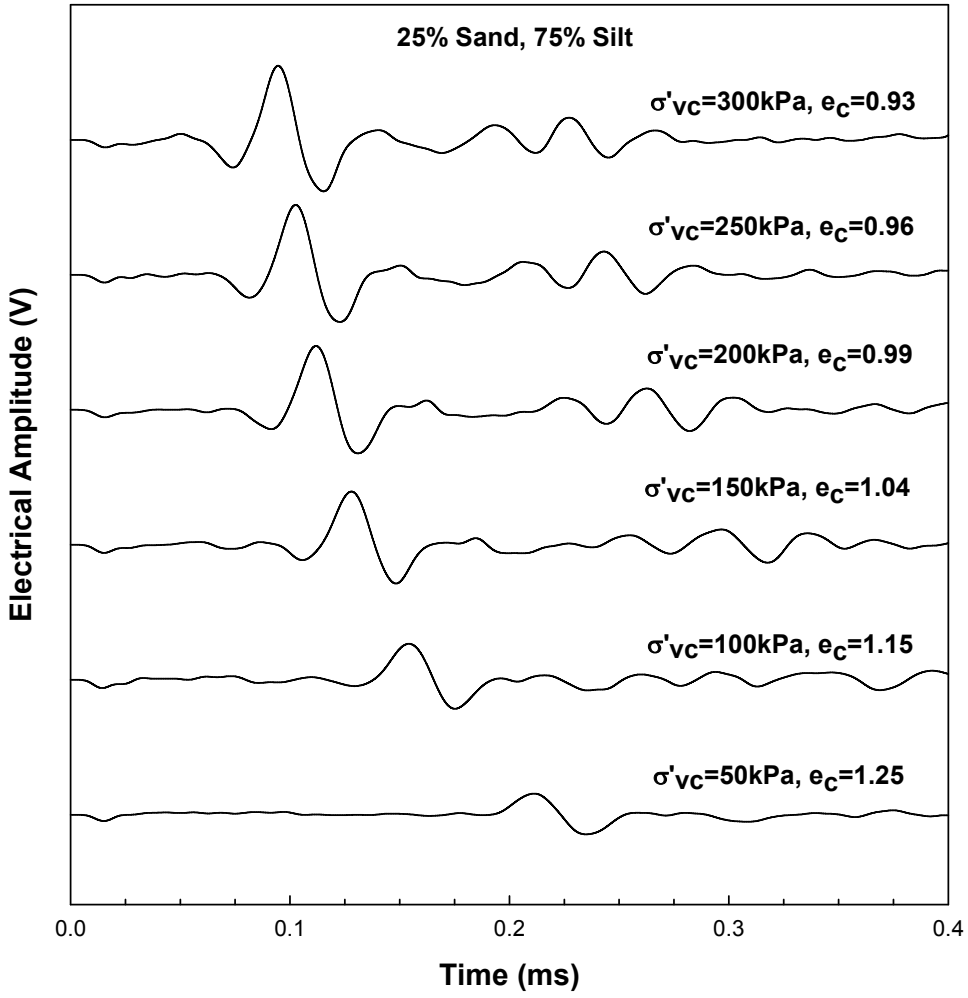

Figure C - 5: Electrical wave signals captured by the bender element and over a range of σ'_{vc} = 50 - 300 kPa in specimens of 75% silt content.

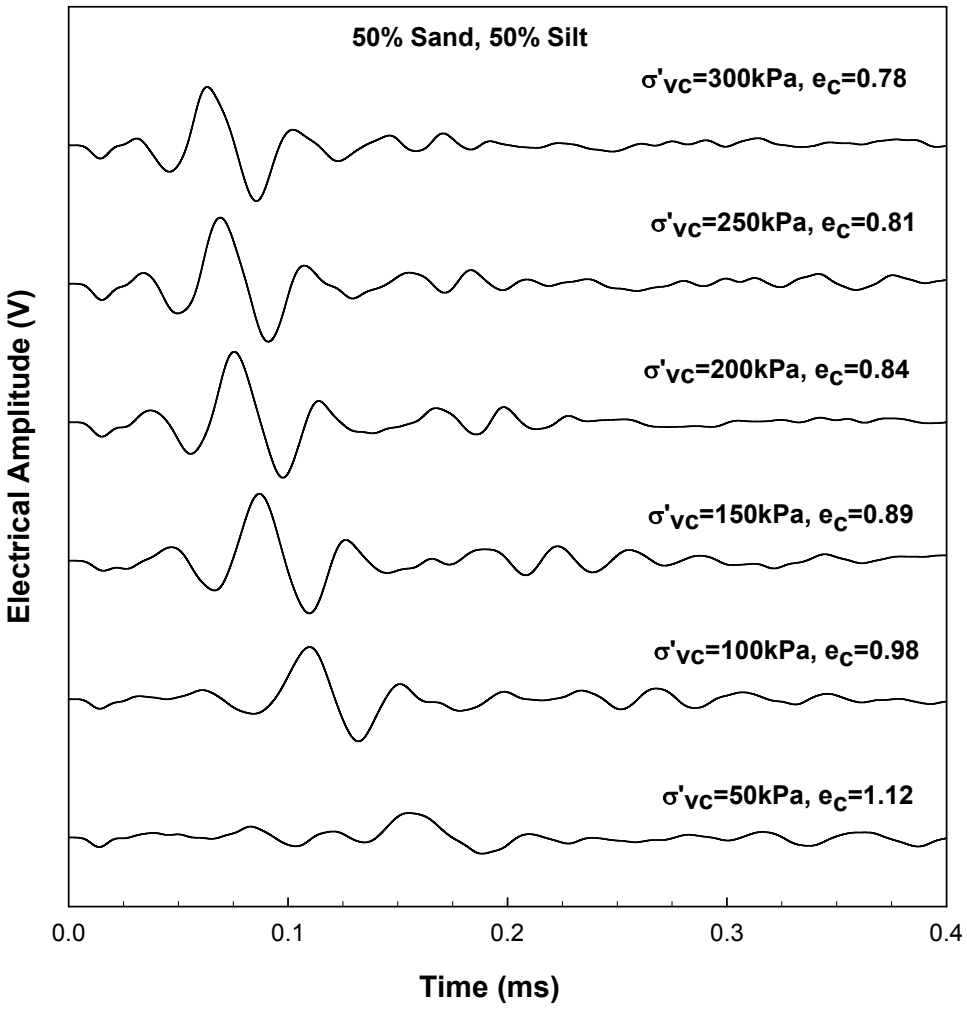

Figure C - 6: Electrical wave signals captured by the bender element and over a range of σ'_{vc} = 50 - 300 kPa in specimens of 50% silt content.

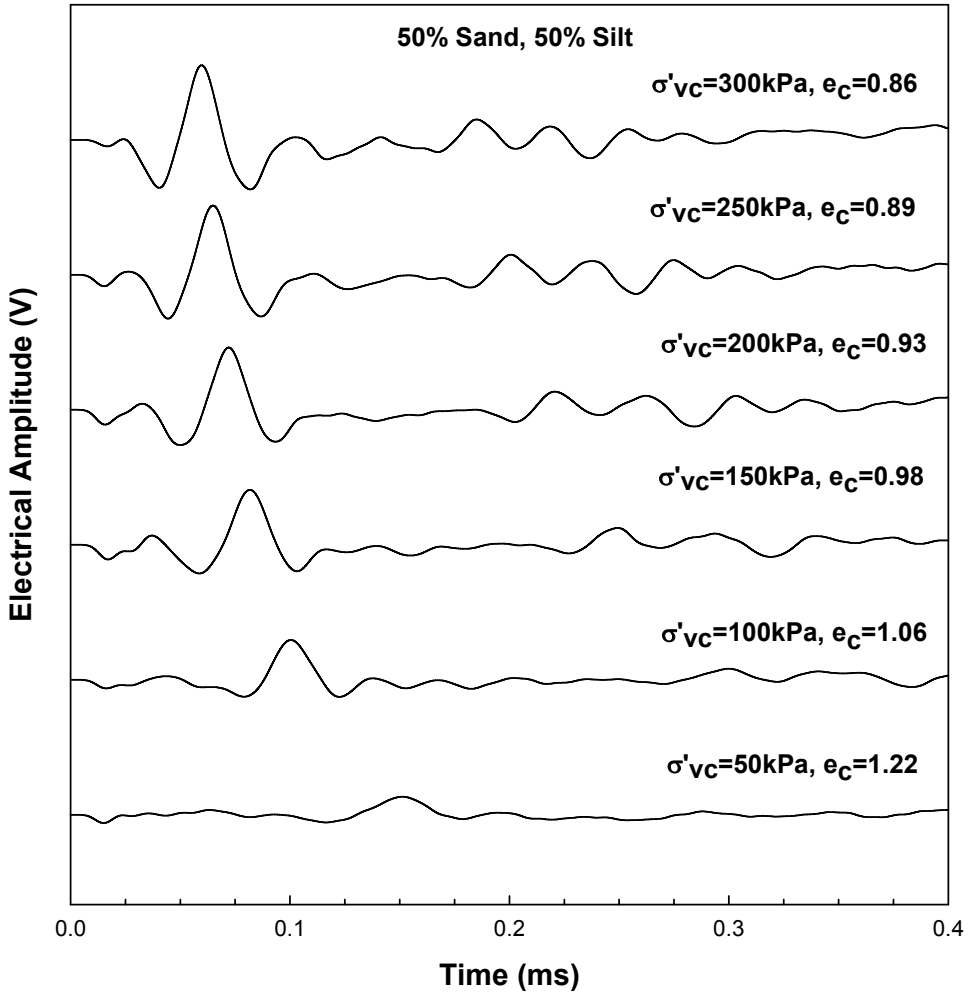

Figure C - 7: Electrical wave signals captured by the bender element and over a range of σ'_{vc} = 50 - 300 kPa in specimens of 50% silt content.

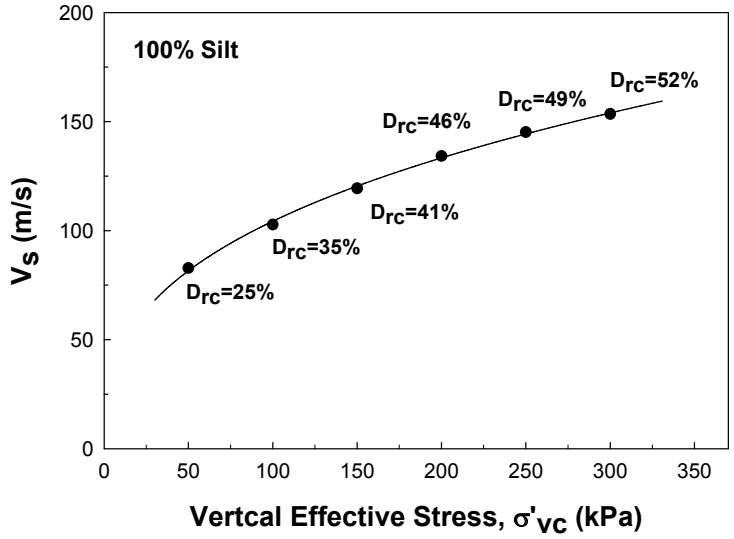

Figure C - 8: Shear wave velocity versus σ'_{vc} over a range of σ'_{vc} = 50 - 300 kPa in specimens of pure silt specimen.

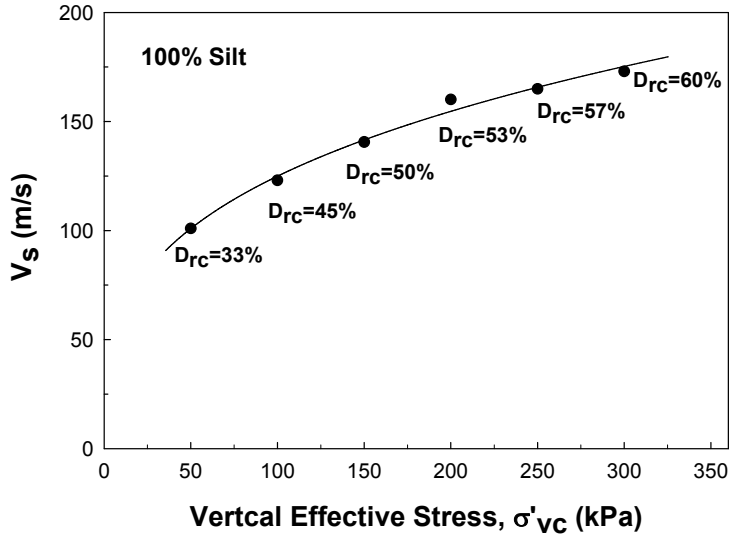

Figure C - 9: Shear wave velocity versus σ'_{vc} over a range of σ'_{vc} = 50 - 300 kPa in specimens of pure silt specimen.

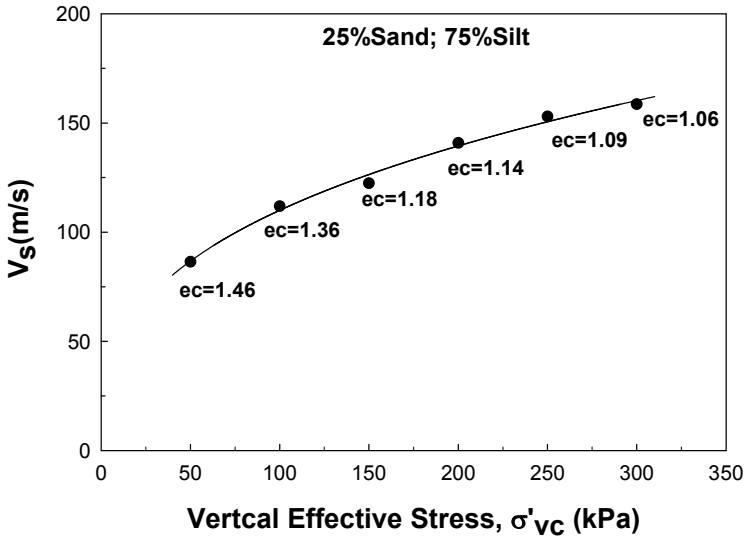

Figure C - 10: Shear wave velocity versus σ'_{vc} over a range of σ'_{vc} = 50 - 300 kPa in specimens of 75% silt content.

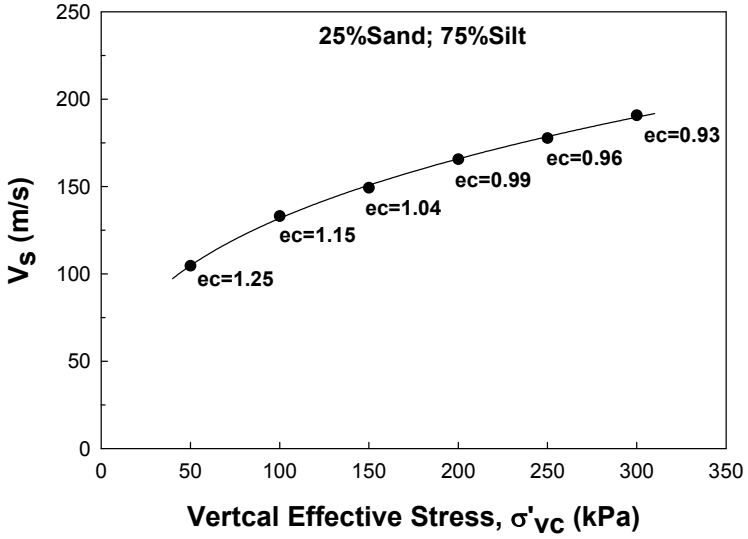

Figure C - 11: Shear wave velocity versus σ'_{vc} over a range of σ'_{vc} = 50 - 300 kPa in specimens of 75% silt content.

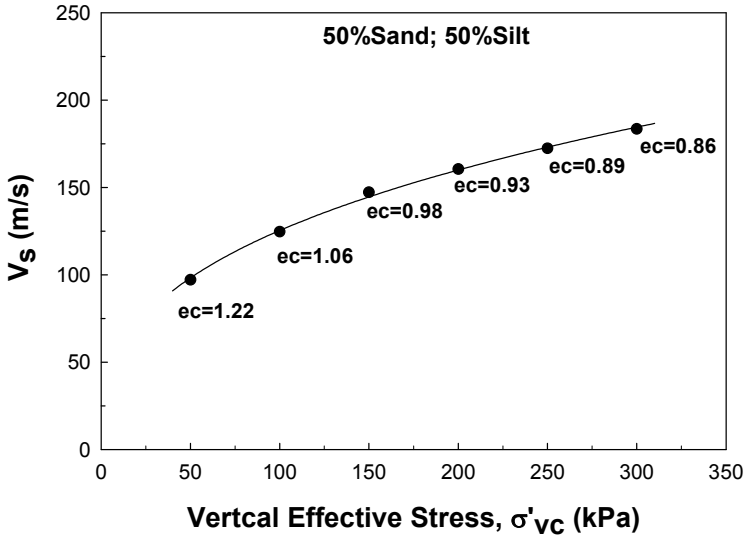

Figure C - 12: Shear wave velocity versus σ'_{vc} over a range of σ'_{vc} = 50 - 300 kPa in specimens of 50% silt content.

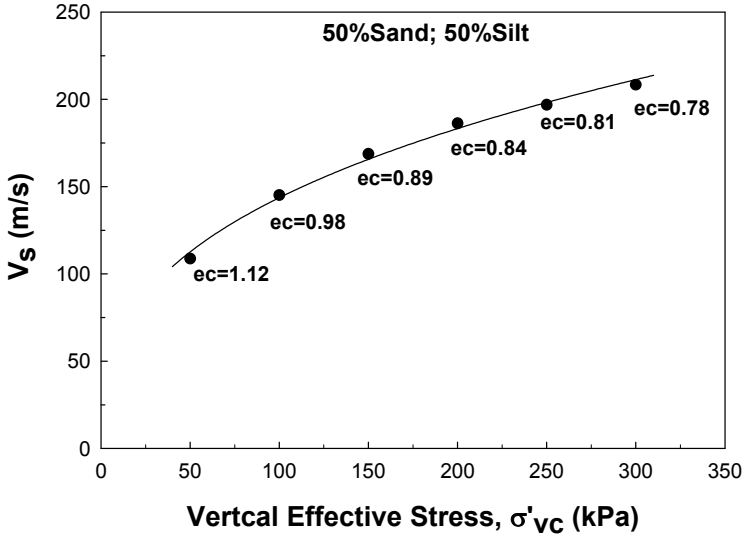

Figure C - 13: Shear wave velocity versus σ'_{vc} over a range of σ'_{vc} = 50 - 300 kPa in specimens of 50% silt content.

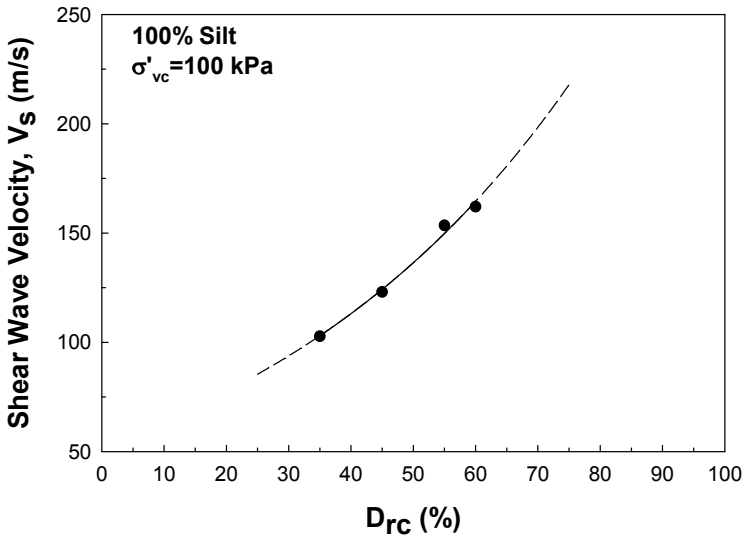

Figure C - 14: Correlation between shear wave velocity and relative density for clean silt specimen at vertical effective stress (σ'_{vc}) of 100 kPa.

Curriculum Vitae

Name: Ali El Takch

Post-secondary Education and Degrees:

- **Bachelor of Engineering Science, 2006 - 2011**
  Civil Engineering
  Lebanese University, Faculty of Engineering, Beirut, Lebanon

- **Master of Engineering Science, 2011 - 2013**
  Geotechnical and Geo-Environmental Engineering
  Western University, London, ON

Scholarships and Awards:

- **Western Graduate Research Scholarship (WGRS), 2012-2013**
  Western University, London, ON
- **Nominated for the Graduate Teaching Assistant Award, 2013**
  Western University, London, ON
- **Milos Novak Memorial Award, 2013**
  Geotechnical Research Center, Western University, London, ON

Related Work Experience

- **Research Assistant, 2011 - 2013**
  Civil and Environmental Engineering Department, Western University, London, ON
- **Teaching Assistant, 2011 - 2013**
  Civil and Environmental Engineering Department, Western University, London, ON